UCLouvain

École polytechnique de Louvain

Titanium Implant Coatings Composed of Chitosan and Heparin to Promote Osseointegration

Author: **Romain HARDY**
Supervisor: **Christine DUPONT**
Readers: **Sophie DEMOUSTIER, Anne DES RIEUX, Christine DUPONT**
Academic year 2018–2019
Master [120] in Biomedical Engineering

Acknowledgements

During the last year, I have had the chance to be surrounded by people without whom the realisation of this master thesis would not have been possible. I would like to take this opportunity to thank them all.

The first person I would like to express my gratitude to is my promoter, Prof. Christine Dupont-Gillain, who welcomed me to her laboratory and gave me the opportunity to write this master thesis. Her help and insight on some problems was of crucial importance to carry out this project successfully.

Then, I would like to thank Cédric Vranckx, my supervisor, for his guidance, daily help, explanations and great advice in all moments. His support was essential to make this master thesis a successful work. I would also like to thank Cédric for his continuous coaching and for showing me what the real laboratory life looks like.

Thank you to the entire laboratory team that were always eager to help me. More precisely I would like to thank my direct colleagues that made this an unforgettable experience. I would like to particularly mention Vincent Delmez and Thibaut Huybrechts that allowed me to work in a positive atmosphere.

A special thanks goes to all the people that helped me work with laboratory devices; Yasmine Adriaens, Cédric Vranckx, Pierre Eloy, Loïc Germain, Marine Delsaute and especially Damien Lefèvre who taught me all there was to know about cell culture and even took care of my cells when I could not do it.

I would also like to thank Prof. Sophie Demoustier and Prof. Anne des Rieux to be part of the jury of my master thesis.

Finally, I would like to thank my family who always stood behind me in difficult moments for the love, joy and time they gave me. A special thanks goes to my girlfriend, Stiene Vandergucht, who was always there for me throughout this stage of my life.

I would like to thank everyone who will take the time to read this work. I hope you will enjoy reading it as much as I did writing it.

Abstract

Total hip arthroplasty (THA) is a surgical procedure in which the hip joint of the patient is replaced by a hip prosthesis. Aseptic loosening and prosthetic joint infection (PJI) are the two most significant causes of prosthetic implant failure. In such cases, revision surgery is required and the implant must be replaced. To prevent such interventions, the ideal implant should be able to promote osseointegration and prevent bacterial adhesion.

In this master thesis, a coating is developed to improve the performances of titanium prostheses. This coating will be based on chitosan and heparin, two polysaccharides, that each have a specific action; repel bacteria and attract bone cells respectively. The coating is constructed using a technique called *layer-by-layer* self-assembly in which layers of the two polyelectrolytes are alternately deposited on titanium coupons owing to electrostatic interactions. Films were created with different number of layers or according to different deposition protocols, in order to analyse the effect of their composition.

The different obtained layers were characterised using a combination of surface analysis techniques. The static water contact angle (WCA) technique is first used to collect information about the wettability of the layers. The adhesion of both polyelectrolytes could be confirmed with the WCA as a saw-tooth pattern was identified when alternately adding chitosan and heparin. The contact angle of the final condition made of 3 bilayers of chitosan and heparin, $(CHI/HEP)_3$, was equal to $40.5° \pm 7.5$, 5 days after layer deposition on the samples. After that, the chemical composition of the surface of the samples was determined by X-ray photoelectron spectroscopy (XPS). The results showed the chemical signature of chitosan and heparin, reinforcing the hypothesis that layers are adequately formed on the titanium coupons. Also, the surface molar fraction of titanium decreased from approximately 10% to 2% for the condition $(CHI/HEP)_3$, showing that the coating screens the original titanium. Finally, the layer thickness was measured using the quartz-crystal microbalance, and a thickness of approximately 13 nm was found for the $(CHI/HEP)_3$ multilayer.
Thereafter, cell viability and proliferation were investigated on the previously characterised layers. To quantify cell viability, the AlamarBlue assay was used. Proliferation was monitored using a DNA assay and fluorescence microscopy. Taken together, the results suggest that the developed coatings present no cytotoxicity and could be used as a basis to design a more complex coating.

To conclude, it is shown in this work that heparin and chitosan can be successfully assembled on titanium coupons using the layer-by-layer method, with a certain degree of control on the physicochemical properties of the obtained coatings according to the number of deposited layers. The developed systems are shown to be suitable for bone cell-related applications.

This master thesis contributes to the development of antibacterial coatings prepared for metal prostheses and could be developed further to prevent the formation of biofilms while promoting osseointegration.

List of abbreviations

AFM	Atomic Force Microscopy
BAI	Biomaterial-Associated Infection
CHI	Chitosan
DA	Degree of Acetylation
DDA	Degree of DeAcetylation
ELI	Extra Low Interstitial
FBS	Fetal Bovine Serum
HEP	Heparin
HOb	Human Osteoblast
LbL	Layer by Layer
MEM	Minimum Essential Medium
OI	OsseoIntegration
TCPS	Tissue Culture grade PolyStyrene
THA	Total Hip Arthroplasty
PJI	Prosthetic Joint Infection
QCM-d	Quartz Crystal Microbalance with dissipation
SFM	Serum-Free Media
WCA	Water Contact Angle
XPS	X-ray Photoelectron Spectroscopy

Contents

1 Introduction

1.1 Context of research

According to the annual report of Orthopride in 2017, more than 36000 total hip arthroplasties (THA; *"Surgery in which the diseased ball and socket of the hip joint are completely removed and replaced with artificial materials"* (Shiel, 2018)) were performed in 2016 in Belgium (Orthopride, 2017). An amount of 76% of these THA were performed on elderly people ($\geq$ 60 years) as shown on Figure 1. As reported by StratBel, the Belgian population increased by 6.6% between 2008 and 2018 as well as the percentage of elderly people (from 22.5% in 2008 to 24.2% in 2018 are older than 60 (Statbel, 2019)). Along with these increases comes an augmentation of the amount of THA surgeries per year.

The problem is that hip prostheses are not safe for a lifetime. Over time, hip replacements can fail for several reasons. In 2016, almost 5000 hip prosthesis revisions were performed and according to Orthopride, the ratio of revised implants to newly implanted prostheses is 13.5% per year (Belgica, 2018). The three main causes for such revisions are: aseptic loosening (37.5% of the revisions), instability (15% of the revisions) and infections, called prosthetic joint infections (PJI; 13% of the revisions). Other less frequent reasons are also possible like pain, periprosthetic fracture (fracture of the bone near the prosthesis) or recurrent dislocations of the "ball-and-socket" structure (Orthopride, 2017). In case of such complications, *Revision total hip replacement* (hip revision) is required. Even though both procedures (primary and revision THA) have the same purpose, revision surgery is a longer and more complex procedure and is also heavier for the patient.

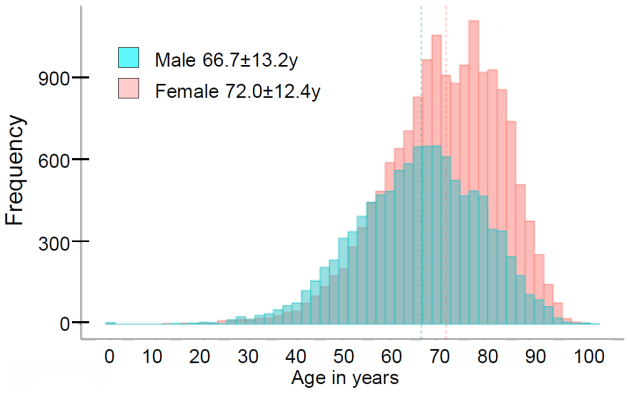

Figure 1: Age distribution of patients with primary THA in Belgium (Modified from Belgica, 2018)

The procedure for revision goes as follows; the surgeon opens the patient following the first incision made for the primary THA. The surgeon then examines the prosthesis and adjacent tissues for infections (bacterial) or inflammations due to metal erosion. The old prosthesis is removed and the site of implant is prepared for the new prosthesis. The new prosthesis is often bigger and longer because of significant bone loss in the femur (Micheal et al., 2017).

This procedure is not only tough for the patient but also costly. According to Mutualité Chrétienne, the mean price payed by the patient in Belgium for a THA is 954€ (Béthune et al., 2015) while the total price for the surgery lies around 6770 - 7070€ (Baetens et al., 2018). For revision, the price is even higher. The main reason for this price increase is the duration of the hospital stay. According to Klouche et al in 2009, the hospital stay for THA was 7.5 ± 1.5 days. In the case of revision surgery due to aseptic loosening, the stay increased to 8.9 ± 2.2 days (price: 12 409 ± 2059 €) and for PJI it increased even more to 30.6 ± 14.9 days (price: 25 151 ± 7447 €) (Klouche et al., 2009).

In order to minimise the amount of revisions and consequently the money and time lost by patients and insurances, a solution has to be found. Several solutions are already being investigated (Table 1). To this end, this work is dedicated to find a solution to drastically decrease the failure rate of hip prostheses due to PJI.

Table 1: Problems with hip prosthesis and investigated solutions

Problem	Solution
Aseptic loosening (*"is the failure of the bond between an implant and bone in the absence of infection"* (Cedars-Sinai, 2019))	Promoting osseointegration: - Surface coating (hydroxyapatite (John et al., 2016), etc) - Porous surface (Vasconcellos et al., 2010) - etc
Instability (dislocations, etc)	- Thorough planning of the intervention - Patient optimisation (reducing BMI, smoking) - Choice of implant, surgeon experience (Werner et al., 2018) - etc
Prosthesis Joint Infection (PJI)	Prophylactic administration of antibiotics in a systemic or local way - Surface modification (Orapiriyakul et al., 2018) - Coatings made of antibacterial agents (chitosan, metal ions, antibiotics) (J. Fu et al., 2005) - etc

This master thesis is part of a broader research project, a PhD thesis, aimed at developing an antibacterial coating for metal orthopaedic prostheses, based on the use of antimicrobial peptides. The PhD thesis is realised by Cédric Vranckx. The basis of the coating in his thesis is a film made using a technique called *Layer-by-Layer* assembly. This work aims to characterise this assembly which will allow the subsequent incorporation of the antimicrobial peptide.

1.2 Hip prosthesis

As stated in Subsection 1.1, a hip prosthesis is a prosthetic implant that will replace the hip joint. The surgeon can choose between several approaches (type of incision) when it comes to hip surgery. These approaches can be antero-lateral, postero-lateral, anterior or posterior with regard to the gluteus medius (Appendix A, Figure 44). The choice is left to the surgeon, depending on his preferences. After the surgeon made the initial incision and exposed the hip, he removes the acetabulum and femoral head of the patient. Then, he inserts the different parts of the prosthesis in the femoral bone and in the acetabulum's socket to finally put the different parts together. The distinct steps are seen on Figure 2.

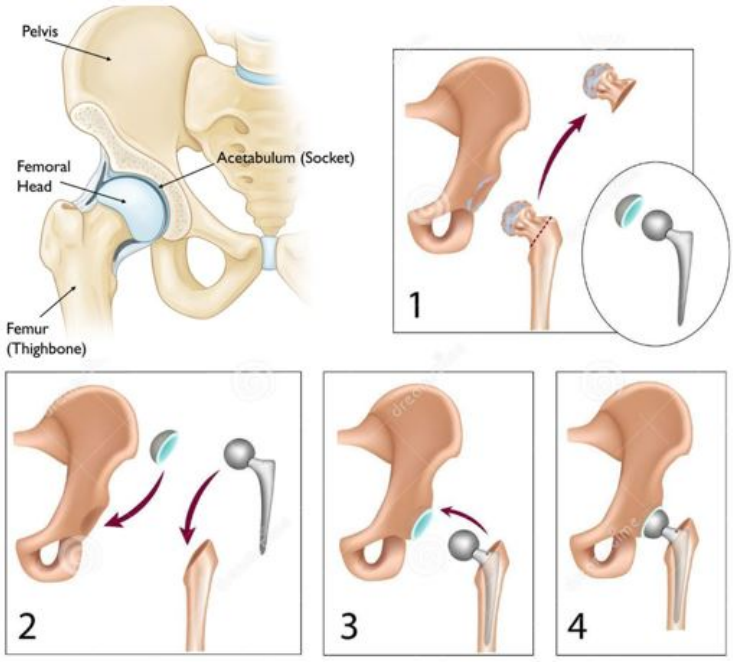

Figure 2: Upper left: representation of the hip anatomy. (1) removal of the acetabulum and femoral head (2) insertion of the hip prosthesis' components (3) and (4) connection of the different components (LMHHealt, 2019); Micheal et al., 2017

Typical hip prostheses are made out of 4 different components. The first component is the **femoral stem** that is inserted in the hollow part of the femur. This femoral stem can either be cemented or *press-fit* into the femur. The cemented approach uses a fast-drying cement to fix the prosthesis at the right place while the *press-fit* approach is where the prosthesis is designed in such a way that it allows bone to grow onto the prosthesis and adhere to it over time (called *osseointegration*). Both methods have pros and cons that are listed in Table 2.

The second component of a hip prosthesis is a **ball** that replaces the femoral head and is attached on top of the stem. The third component is the **acetabular cup** which is placed inside of the hip and the last component, the **liner**, is fixed inside of the cup. The liner plays the role of articulation together with the ball. All these components can be seen on Figure 3.

Table 2: Pros and cons of cemented and *press-fit* prostheses (Sood, 2014)

	Pros	Cons
Cemented	- Allows to treat patients with bad bone condition (osteoporosis) - Possibility to add anti-bacterial substances to the cement - Cement dries within 10 minutes assuring fast adhesion	- Cement can break down leading to loosening of the prosthesis - Cement debris can lead to inflammation of surrounding soft tissue due to irritations - Debris can also enter the bloodstream and end in the lungs leading to life-threatening conditions (very rare)
Press-fit	- Better for long-term adhesion between bone and prosthesis - Eliminates the worry of cement breakdown	- Requires healthy bones from the patient (no low bone-density called osteoporosis) - It can take up to 3 months for a proper bone-prosthesis interaction

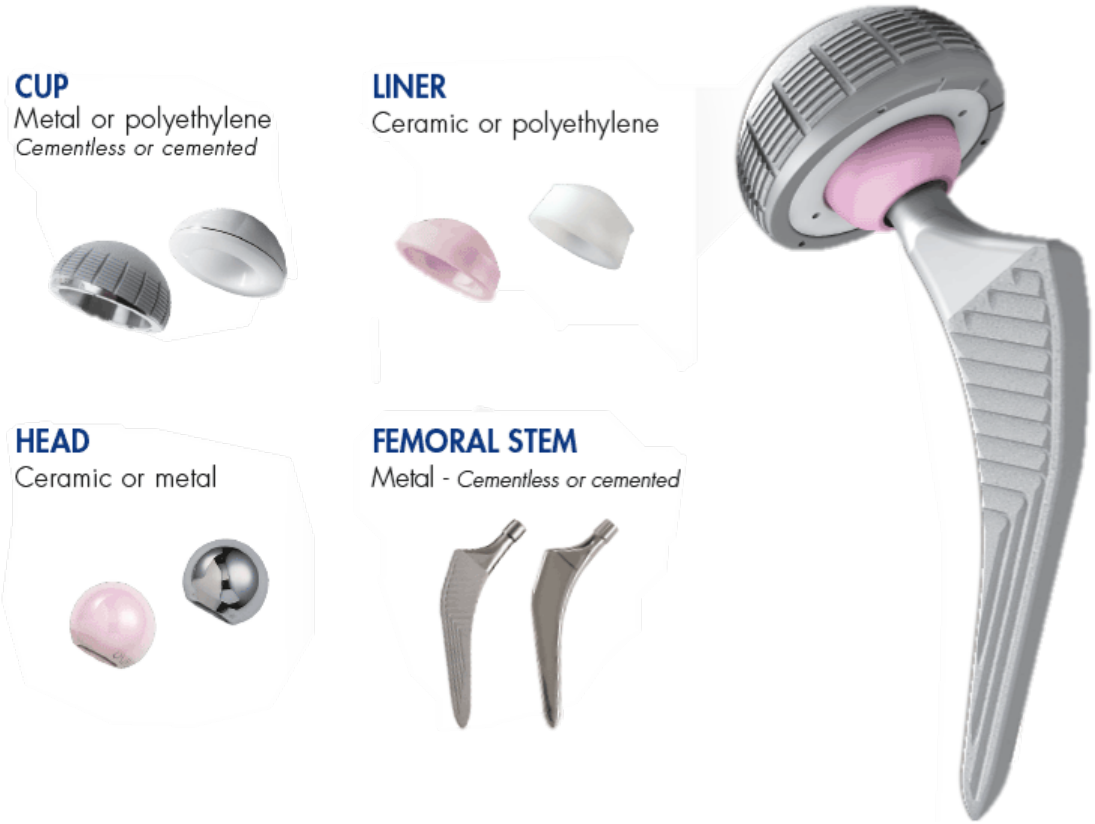

Figure 3: Different components of hip prostheses (Medacta International, 2018)

Another important element that can be seen on Figure 3 is that prostheses can be made of different materials and combinations of these materials are also possible. The main combinations for the ball–liner junction are: ceramic on ceramic (58.9%) which is the most common combination in Belgium, followed by ceramic on polyethylene (31.5%) and metal on polyethylene (6.9%) (Orthopride, 2017). In this master thesis, research is done on a titanium plate (Ti-6Al-4V Extra Low Interstitial (ELI)) which is an α-β-alloy of titanium and is usually used for titanium prostheses.
Titanium is often the favoured metal used for implants, especially its α-β-alloy, Ti-6Al-4V. It is composed of 6 wt.% of aluminium (α-phase stabiliser) and 4 wt.% of vanadium (β-phase stabiliser). The β-phase titanium is more ductile while the α-phase is stronger yet the α-β-alloy's properties lie in between both (Hanson, 1995). The reason why this alloy is often favoured is because it has a higher biocompatibility, a good strength to density ratio, it is corrosion resistant and has a lower Young's modulus ($\sim$110 GPa) compared to other titanium alloys (Apostu et al., 2017; ASM Handbook, 1990). The Young's modulus of the prosthesis should be as close as possible to that of bone ($\sim$ 10-30 GPa). This allows to avoid stress shielding which results in an increased bone resorption and thus increasing aseptic loosening (Apostu et al., 2017).

According to Apostu et al., the ideal features of an implant should be: high biocompatibility, high strength, lightweight, corrosion resistant, non-toxic, cost efficient and a Young elasticity modulus similar to that of bone (Apostu et al., 2017).

However, since the ideal prosthesis does not yet exist, problems can arise. The two following subsections will explain what the two main problems of prostheses are and how they could be treated or countered.

1.3 Prosthetic joint infections

As mentioned in Subsection 1.1, more THA surgeries are executed every year and therefore, more prosthetic failures occur. As stated, one of the main reasons for failure are *Prosthetic Joint Infections* (PJI) or *Biomaterial-Associated Infection* (BAI) (2-5% of all prostheses). The cause of such infections can be various. In trauma, skin bacteria such as *Staphylococcus aureus* (*S. aureus*) and *Staphylococcus epidermidis* (*S. epidermidis*) are the most common pathogens and can easily enter the site of wound. Contamination from the surrounding environment at the time of injury is also possible, introducing a wide range of bacteria to the soft tissue or biomaterial.
Infections can also occur during surgery. Here again, the most common infecting bacteria are *S. aureus* and *S. epidermidis* as well as Gram-negative organisms (Orapiriyaku et al., 2018).
Infections diagnosed within 3 months after surgery are classified as "early postoperative infection", between 3 to 24 months we speak of "delayed infection" and after more than 24 months they are classified as "late infections".

Bacterial adhesion to the surface

For bacterial infection to develop, bacteria must attach to the surface of the implant. This happens in a two-phase approach.
The first phase is defined by the initial, instantaneous and reversible (unspecific) attachment of bacteria to the surface. This starts with attraction of the bacteria to the surface and is followed by cell adsorption to the surface of the implant. Movement of bacteria is governed by physical interaction such as Brownian motion or Van der Waals' and gravitational forces.
The second phase of bacterial adhesion to a surface is defined by specific and irreversible attachment and is time-dependent (Arciola et al., 2018; Orapiriyaku et al., 2018).

Biofilm formation

Once bacteria have adhered to the surface, the biofilm formation starts. A biofilm is defined as *"a structured group of bacteria that cover themselves in an extracellular polymeric substance, which results in firm adhesion on the implant"* (Orapiriyaku et al., 2018). The formation of such a biofilm follows **four distinct phases**. First, as mentioned above, bacteria **adhere** to the surface of the implant in two sub-phases. Then, bacteria **aggregate** on the surface by forming micro-colonies where they can proliferate and make intercellular adhesion. While doing so, bacteria produce *Extracellular Polymeric Substances* (EPS). These EPS are the main components of the biofilm and provide three important advantages to the cells residing in the biofilm. First, it can trap the external nutrients required for cell sustenance and growth. Second, the EPS helps with nutrient circulation to the cells, needed for cell growth. Third, encapsulated cells are protected from external environmental stresses (Veerachamy et al., 2014).

The third step of biofilm formation is the development of the biofilm and its **maturation**. Bacteria proliferate and the biofilm grows in size (tower-like structure: macrocolony) until the biofilm reaches the fourth phase, biofilm **dispersal**. During this last step, the biofilm disperses cells from the surface because of the depletion in nutrient. These bacteria detach from the structure and spread around to restart this cycle somewhere else on the implant or on neighbouring tissue. This detachment could also be caused by shear stresses or by fluidic interactions. These four steps are depicted on Figure 4. Note that within the EPS matrix, cells can interact using *Quorum Sensing* (QS). Quorum sensing is defined as *"the regulation of gene expression in response to fluctuations in cell-population density."* Bacteria produce and release chemical signal molecules called autoinducers and communicate via these autoinducers within and between bacterial species. Quorum sensing allows bacteria to coordinate the gene expression, and therefore the behaviour, of the entire community (Miller et al., 2001; Veerachamy et al., 2014).

Biofilm formation is very problematic because the EPS protects bacteria. Antibiotic treatments do not have the desirable effect because the biofilm does not disappear. In such cases, a surgical intervention is needed where the surgeon washes the implant site and often replaces the prosthesis (revision surgery).

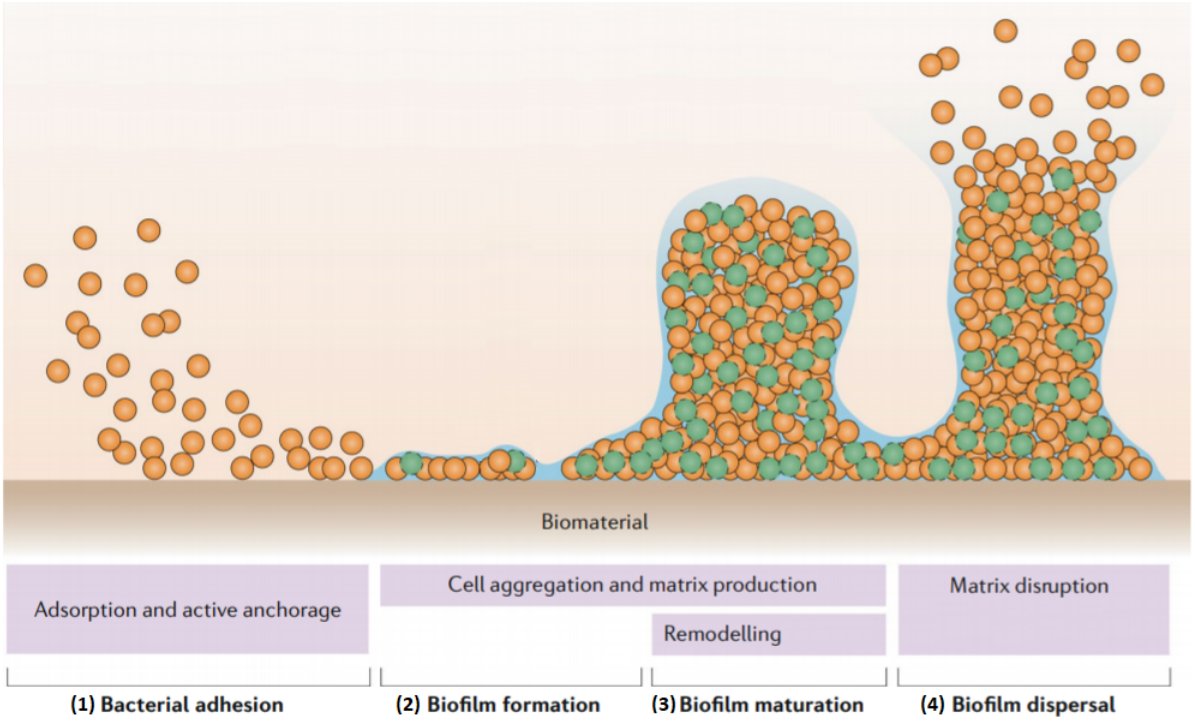

Figure 4: Different stages of biofilm formation: (1) bacterial adhesion (2) biofilm formation/aggregation (3) biofilm maturation (4) biofilm dispersion (modified from Arciola et al., 2018)

Removal of the biofilm

A first method to remove the biofilm is to use an intensive and long-term, local, antibiotic treatment such as polymethylmethacrylate (PMMA) antibiotic beads (Klemm, 1979) or using a high-dose antibiotic-impregnated cement spacer (Springer et al., 2004). Unfortunately, such treatments are often disappointing because of the low penetration of antibiotics inside the biofilm due to the EPS. Antibiotic treatment, used to suppress the infection, is often linked with a revision surgery to completely treat and heal the patient. Remember that this intervention is very tough on the patient and should be avoided at all costs. Also, bacteria can develop, over time, a resistance to certain antibiotics. *S. epidermidis* for example is known as the most frequent cause of nosocomial infections (contracted in hospitals) and often resists antibiotic treatment due to a reservoir in resistance genes (Otto, 2009). This resistant effect is mainly caused due to an overuse and misuse of antibiotics through time (Ventola, 2015). Another approach is needed to avoid biofilm formation.

Preventing the biofilm formation

A novel, and more convenient approach consists in preventing the biofilm's formation instead of trying to remove it after it has formed. The **first strategy** is to use anti-adhesive molecules, such as polyethylene glycol (PEG; also called PEO depending on their molar mass) to make non-fouling materials. These molecules do not kill bacteria or inhibit microbial function but they prevent the adherence of cells or proteins to the surface (Neoh et al., 2015).
The **second strategy** is to let bacteria adhere to the surface and then kill them. Killing bacteria at contact can be performed using anti-microbial peptides (AMPs). These are naturally occurring molecules that are produced as a first line of defence by all multicellular organisms. They can posses the activity to directly kill bacteria by either rupturing the bacterial membrane or by inhibiting intracellular function resulting in cell lysis (L. Zhang et al., 2016).
Despite their general effectiveness, both methods have flaws. Once bacteria adhere on the non-fouling surfaces, a biofilm will form because of the absence of bactericidal activities. On the other hand, the active killing surface that kills adhered bacteria suffers from the accumulation of dead bacteria on the surface, resulting in a decrease of bactericidal activity. To this end, a new method was developed called the *"kill-release"* method. Bacteria are killed when they adhere to the surface and in function of a specific stimuli (T, pH, etc), they are released to obtain a clean surface again resulting in a long-term antimicrobial activity. These dual antibacterial surfaces are usually prepared by incorporating biocides into non-fouling materials via covalent binding or layer-by-layer deposition. (Wei et al., 2017).

Unfortunately, prosthetic failure is not only caused by bacteria. Sometimes, the prosthesis can not be integrated well inside of the patient's bone due to a lack of osseointegration. This will be discussed in the next subsection.

1.4 Aseptic loosening

As stated in Subsection 1.1, another main reason for prosthesis failure is aseptic loosening, defined in Table 1. Having a good interaction between bone and prosthesis is of crucial importance to guarantee a successful, long-term implant. As explained before, the term osseointegration (OI) is only used for cementless prostheses.

Osseointegration was first defined by Professor Per-Ingvar Brånmark who studied blood flow in rabbit bone using titanium implant chambers. He discovered that the bone had integrated completely with the titanium implant and that the chamber could not be removed. He called this phenomenon *Osseointegration* (Brånmark, 1959). Osseointegration was first defined as *"direct contact on the light microscope level between living bone tissue and the implant"* (McCutchen et al., 1990) to evolve later on to a more specific definition being *"A direct structural and functional connection between ordered, living bone and the surface of a load-carrying implant"* (Parithimarkalaignan et al., 2013b). The key to osseointegration is a dynamic bone tissue where growth and differentiation factors are released by activated blood cells at the bone-prosthesis interface. These initiate a series of biological events that start the bone formation process at the interface. A fibrin matrix is first formed which acts as a scaffold for osteoblasts. When this process is done well, the interface is almost entirely filled with bone (Figure 5a). On the other hand, when the osseointegration process fails, the interface between prosthesis and bone is filled with a fibrous tissue resulting in low strength and loosening of the implant (Figure 5b) (Apostu et al., 2017). Osseointegration on a porous and coated surface 6 months after surgery can be seen on Figure 6.

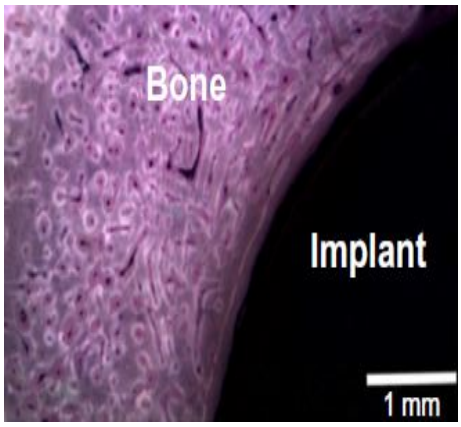

(a) Successful osseointegration showing bone and implant interface

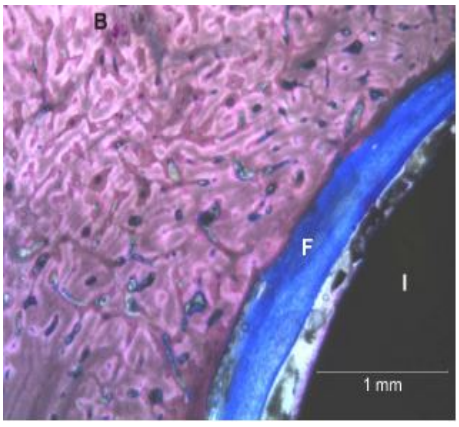

(b) Failed osseointegration: (I) implant, (B) bone tissue, (F) fibrous capsule

Figure 5: Cross sections of bone-implant for (a) a successful osseointegration and (b) a failed osseointegration (Isaacson et al., 2014)

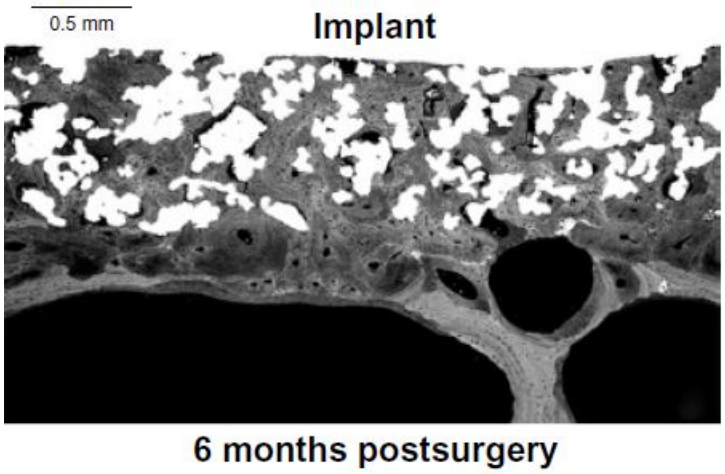

Figure 6: New bone tissue into porous, coated prosthesis after 6 months showing: (black) marrow cellular components, (grey) bone and (white) porous coating (Isaacson et al., 2014)

Parameters influencing osseointegration

Several factors can influence osseointegration. The **implant's surface** plays a major role in OI, and this on different levels. As mentioned in Subsection 1.2, the material of the prosthesis can be of different nature (cobalt chromium, tantalum, stainless steel, titanium and its alloys, etc). The choice of material is important with regard to several factors like *biocompatibility* and *corrosion resistance*. Corrosion can affect OI in a major way because released metal ions to the surrounding tissues will promote local inflammations. These will lead to excessive fibrous tissue formation that is typical for failed OI (note that ion release may also cause systemic damage. e.g.: aluminium might cause neurological pathologies, vanadium can cause cellular mutations (Apostu et al., 2017)). The surface's *roughness* and *porosity* are also important as it was showed that skeletal fixation on the prosthesis is most effective when using porous implants ($\sim 600\mu$m) with a porosity higher than 40% (Apostu et al., 2017). Surface energy is also believed to play a major role in OI, research reported that biofilm formation (Subsection 1.3) is more likely to form on hydrophobic surfaces. In these cases, osteoblasts can not adhere to the surface. The optimum range of hydrophobicity of the implant has yet to be determined (Apostu et al., 2017).

The second category of parameters belong to the **patients** themselves. Two main factors affect OI. First, patients having a body mass index (BMI) higher than 35 kg/m^2 are two times more susceptible to have aseptic loosening of their hip prosthesis (Kremers et al., 2016). Second is that smokers are reported to increase the risk of aseptic loosening three-fold (Teng et al., 2014).

Lastly, the **surgeon's experience** has also a big impact on OI. Inexperienced surgeons ($<$ 30 THA/year) have a four-fold higher failure rate than experienced surgeons ($>$ 60 THA/year) (Apostu et al., 2017). The type of surgery also impacts OI as it was found that excessive drilling or rasping to have a proper fit of the prosthesis in the bone may mechanically or thermally damage the bone resulting in necrosis of the cells responsible for bone repair.

A temperature of 47°C during one minute was measured to be critical for cells (Parithimarkalaignan et al., 2013a). Lastly, the surgeon must place the prosthesis in close contact with bone as it was shown that gaps bigger than 50-150 μm between bone and prosthesis may lead to fibrous tissue formation resulting in a failed OI. Also, micromotion of the implant with regard to the bone must be restricted to a maximal motion of 30 μm (Apostu et al., 2017; Isaacson et al., 2014).

To decrease or prevent PJI and promote osseointegration, several techniques can be used. The next subsection will be introducing the aspect of surface modifications that could be implemented to resolve these two problems.

1.5 Surface properties and modifications

Before talking about surface properties and modification, it is interesting to first look at what a surface really represents. A surface is defined as the outer part of a solid. If we consider that any solid is systematically placed in a given environment, in contact with another medium, the surface must rather be considered as an interface, in our case it is a solid-liquid interface. This is the part of the material that will wear out and corrode. It is therefore its visible part that gives it its appearance, morphology, roughness and colour. Something important to keep in mind is that the properties and composition of the surface and of the bulk material are different. This can be explained because, on the surface, the number of closest neighbours of an atom is different from what it is in the bulk material (Figure 7). In order to restore the balance of the force fields to which the surface atoms are subjected, they tend to exchange new bonds with the underlying atoms and/or molecules of the surrounding environment. This results in a reorganisation and high reactivity of the surface atoms (Audisio et al., 1998).

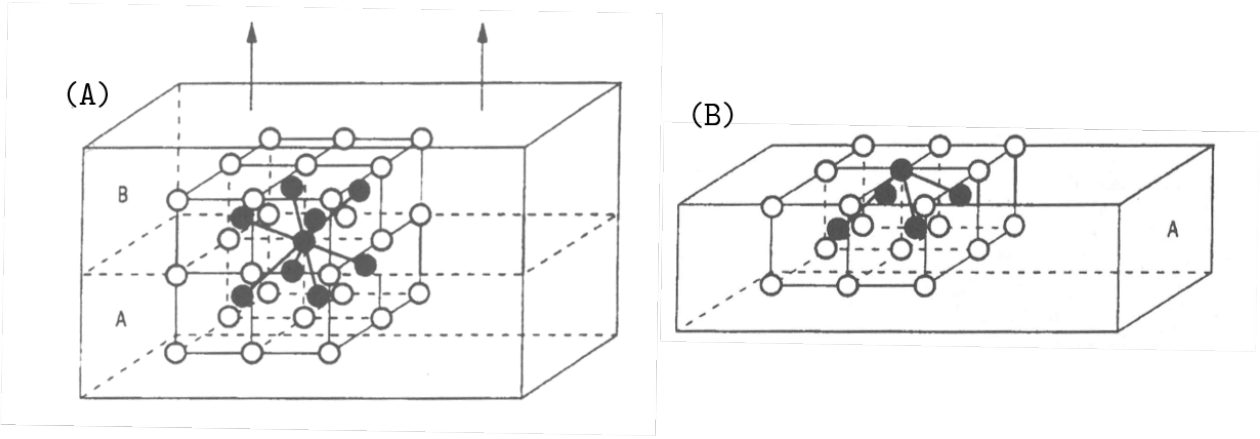

Figure 7: Closest neighbouring atoms in (A) the bulk material and (B) on the surface (Audisio et al., 1998)

The interactions of a material with its surrounding are characterised by the surface properties. Examples of such properties are wettability, surface morphology, corrosion resistance, adhesion properties (resistance to bacterial adhesion) and so on. While the Young's modulus, density, thermal expansion coefficient or conductivity are properties specific to the bulk material.

It is known that titanium forms a passive oxide layer on its surface, TiO_2, called anatase or rutile depending on which form is formed on the surface (Pouilleau et al., 1996). At normal temperatures, anatase is the primary crystalline structure of titanium oxide (Hamilton et al., 2013). This layer is created rapidly when the substrate comes in contact with air and when removed or damaged, it renews itself immediately. This passive oxide layer has a thickness of a few nanometers (< 10nm; Hamilton et al., 2013).

The major benefit of this layer is that it protects titanium, which is very active, from interacting with the surrounding environment that would result in corrosion of titanium (Spilker et al., n.d.). Materials used for hip prostheses are chosen because their bulk properties are close to those of bone. The need of surface modification comes from the fact that the surface properties of these materials are often inadequate for their utilisation. Because the surface is directly in contact with the physiological environment it has to respond in the same way as human tissues would. For this, the surface must be modified prior to use in order to obtain the desired interaction with the environment.

Surface modifications can either be seen as chemical or physical. There are many surface modification techniques that are more or less better than others and can be used under different conditions. An example of the use of such methods is to increase the contact area compared to the geometric area. This was for example done by Zhang in 2015 who created nano-pillars on a surface that considerably increased the contact surface. They used different techniques to do this (coatings, anodizing, electroplating, photoresist layer) (G. Zhang, 2015). It is also possible to create surface roughness using for example sand blasting or plasma spraying (Piatteli, 2017). Other examples can be seen on Figure 8.

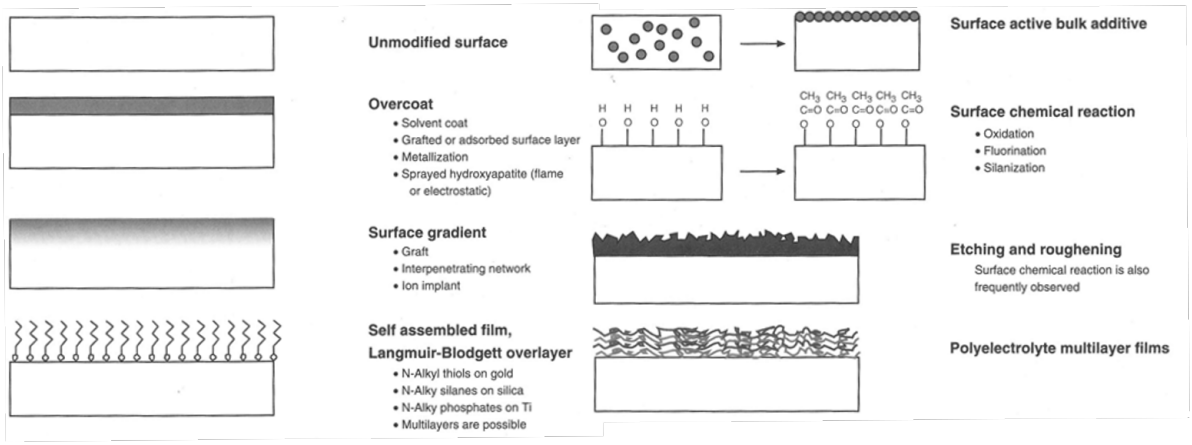

Figure 8: Schematic representation of different methods to modify surfaces (Allen, 1996)

Layer-by-Layer self assembly technique

Treating the two aforementioned problems (subsection 1.3 Prosthetic Joint Infections and 1.4 Aseptic Loosening) could be possible by modifying the surface of titanium prostheses to make them bacteria repellent or bacteria killing as well as osteoinductive. In this thesis, we will focus on a specific technique called **Layer-by-Layer** (LbL) assembly to modify the prosthesis' surface. This technique allows to make nano-films on the top of a surface. LbL is an easy technique and is quite straightforward. To use this kind of technique, the only needed materials are polyelectrolytes. Polyelectrolytes are polymers that have charges all along their backbone.

The process of LbL assembly is depicted on Figure 9 for a polycation (green, positively charged polyelectrolyte) and polyanion (red, negatively charged polyelectrolyte). This technique uses the strong electrostatic attraction between a charged surface and an oppositely charged molecule in solution. On figure 9 it can be seen that the whole process starts with a cleaned titanium (Ti-6Al-4V ELI) substrate having a negatively charged surface that is first immersed in a solution containing polycations (Fig.9.A). These will adhere to the surface by electrostatic interactions as mentioned above. The consequences of this first adsorption are dual. First, groups that are also charged positively will be repelled. This works as a self-regulating mechanism allowing the formation of only one layer. Second is the ability to now adsorb oppositely charged polyelectrolytes and allowing the formation of multilayers (Decher, 1997).

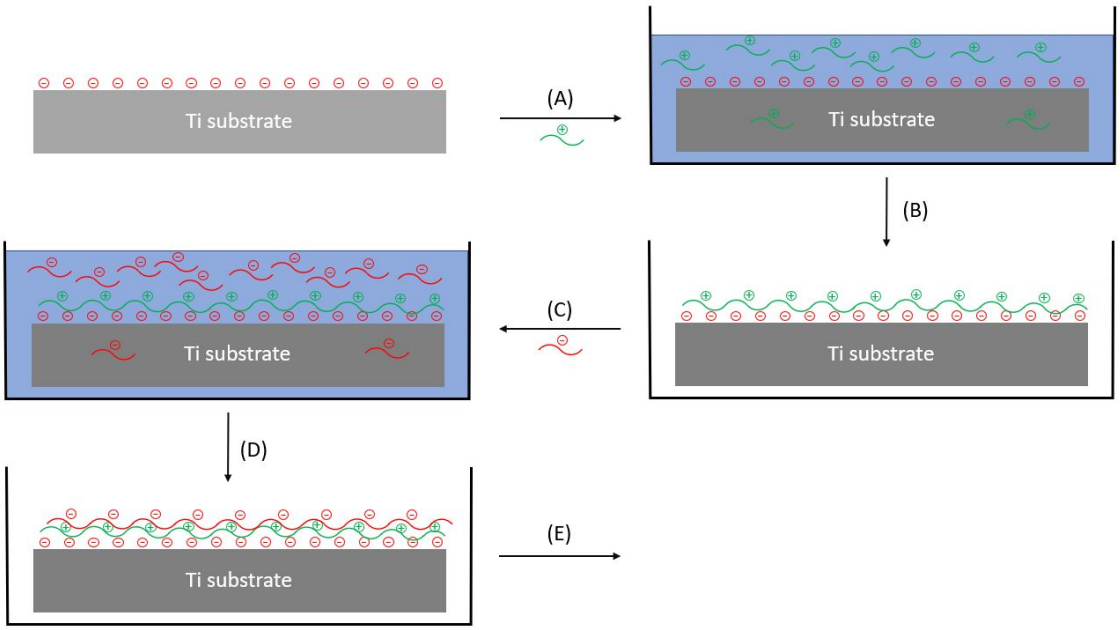

Figure 9: Layer-by-Layer method: A titanium sample is cleaned and has a negatively charged surface. (A) The substrate is immersed in a polycationic solution (B) and then washed (C) the substrate is then immersed in polyanionic solution (D) and washed again (E) repeat steps A-B-C-D according to the wanted layer setup

The next step is to wash the titanium substrates (Fig.9.B) that now contains a single layer of polycation on top of it. This is done to avoid contamination of the next used solution. Because the surface is now positively charged, the substrate can be immersed in a solution containing polyanions (Fig.9.C). The same process will take place and a single layer of polyanions will form on the polycation layer, forming a bilayer. Again, after this step, the substrate must be washed accordingly (Fig.9.D). In function of the desired layer architecture, these steps can be repeated as many times as wanted (Fig.9.E).

In the past, other preexisting techniques such as the *Langmuir-Blodget* technique were used to fabricate nano-structured films but they had too many restrictions (requires special equipment and had severe limitation on substrate size and topology). Because of this, a new method had to be invented. Decher et al. discovered the LbL in the early 90s and it rapidly increased in importance in the nanofabrication sector for several reasons. First because it is an easy method and the layer formation is independent of the nature, size and topology of the substrate (Decher, 1997). Other advantages of the LbL assembly are that the nature of solvent (water) is eco-friendly compared to other techniques using dangerous solvents and there are no complex chemical reactions to do before using the method. Also, it is possible to incorporate other materials inside the layers such as colloids, antibiotics or metal ions. This method can also be automated.

The main parameters affecting the layers' growth and structure are physiochemical properties such as pH and ionic strength. According to Lundin et al. in 2011 that made multilayers with heparin and chitosan, increasing the ionic strength at a fixed pH increases the adsorbed mass on a surface. The same effect was witnessed when increasing the pH for a fixed ionic strength (Lundin et al., 2011). This could be explained by the fact that at higher pH, chitosan is less charged. The electrostatic repulsion between charged groups of the same polymer is then lower resulting in a less rod-like shaped polymer. Because of this, more chitosan polymers could adhere to the surface, forming a thicker layer. Increasing the ionic strength has a screening effect on chitosan at low pH that would result in the same effect a higher pH has on chitosan polymer.

1.6 Objectives and strategy

The objective of this thesis is to develop a coating for titanium prostheses that will attract osteoblasts and repel bacteria. This will be done using two polysaccharides, heparin and chitosan, that each possess one of these activities. This work will be divided in two main parts, the first one will describe the characterisation of the bio-films made on the titanium substrates, and the second one will describe cell behaviour on the different layer setups.

The titanium substrate that is used to make the experiments has the same composition as the prosthesis of the research (Ti-6Al-4V ELI, grade 23 titanium). To make the bio-interfaces, heparin and chitosan are adsorbed alternately according to different arrangements with a method called *Layer-by-Layer* assembly. The different layer conditions that were used in this master thesis are depicted in Figure 10. The only sample that is not made using the LbL assembly technique is the CHI+HEP condition. Here, heparin and chitosan were allowed to form complexes before adhesion of these on the titanium surface. This was done to obtain information on how complexes form layers on the titanium substrate.
Different layer conditions are assumed to have a different impact on cells (viability, proliferation, differentiation). Therefore, in Section 2: *"Surface characterisation"*, it is first explained how the different setups are made followed by which characterisation techniques are used to obtain information on the layers' properties. Cell adhesion is directly influenced by the hydrophobic or hydrophilic behaviour of the surface (Ban et al., 2015). This property was measured using a static water contact angle technique. The film thickness is also expected to influence cellular behaviour and was measured using the ellipsometer as well as the quartz-crystal microbalance. The chemical composition of different layers was obtained using X-ray photoelectric spectroscopy. And finally, to visualise the sample's topography, atomic force microscopy in tapping mode was used.

After characterising the different samples, we wanted to know if these layers would be viable *in-situ*. To do so, in Section 3: *"Study of cellular behaviour"*, cell viability was investigated. This Section explains how the cell culture was done and in which conditions the cells were maintained. To find out if the different samples were cytotoxic for the chosen cells (mouse cells, MC3T3-E1), an AlamarBlue assay was performed at day 1, day 4 and day 7 after seeding the samples with cells. Then, to measure cell proliferation, a CyQUANT assay was performed at day 7. Finally, to observe the cells on the different surfaces, immunofluorescent staining using FAK 100 was performed.

Before entering Section 2, the choice of polyelectrolytes used to make the multilayers will first be explained.

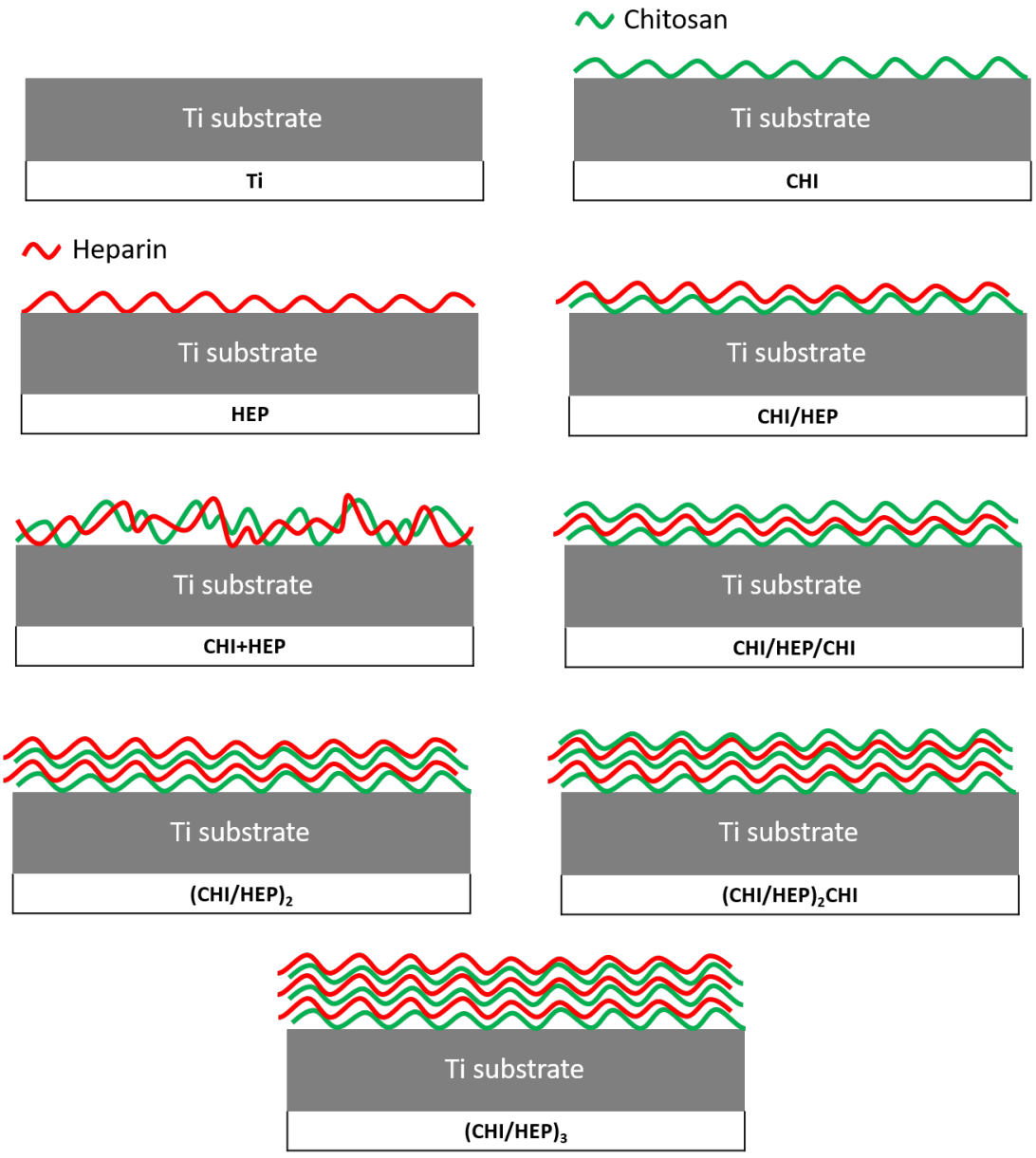

Figure 10: Different layer setups used in this thesis

1.7 Polyelectrolytes

A polyelectrolyte is defined as *"any macromolecular material that has repeating units and dissociates into a highly charged polymeric molecule upon being placed in any ionising solvent (e.g. H_2O) forming either a positively or negatively charged polymeric chain"* (Venkata et al., 2017). Polyelectrolytes can be natural (pectin, alginate, heparin, chitin, etc), semi-synthetic (chitosan, (partly) deacetylated chitin) or synthetic (polyacrylic acid, polystyrene sulfonate, polyallylamine,...) (Polymerdatabase, 2015). Polyelectrolytes have the dual character of polymers (high molecular weight compound) and electrolytes (salts). Thus, properties of polyelectrolytes are similar to both electrolytes and polymers, they are electrically conductive and the viscosity depends on the molecular weight and polymer concentration (Polymerdatabase, 2015). Similarly to bases and acids, they can be divided into strong and weak compounds. A weak (poly)electrolyte has a dissociation that is pH-dependent, while a strong (poly)electrolyte is totally dissociated over a very wide pH range (Hassan et al., 2012).
The conformation of such macromolecules depends on their charge. When uncharged, they behave like uncharged macromolecules. But when the dissociation of ionic group happens, electrostatic repulsion between these groups takes place and the random coil conformation of the uncharged macromolecule straightens (the end-to-end distance increases, Polymerdatabase, 2015) and the polymer properties could change according to the conformation change (viscosity, solubility, ionisation constant or ionic strength (Venkata et al., 2017)).

In this thesis, two polyelectrolytes are used; heparin (HEP) and chitosan (CHI) and will now be presented.

1.7.1 Heparin

Heparin (HEP) is a naturally occurring polysaccharide belonging to the family of glycosaminoglycans (GAG) ubiquitously present in mast cells. Before the year 2000 and the bovine spongiform enchephalopathy (BSE) epidemy (commonly known as the *mad cow* disease), heparin was mostly obtained by purification of animal tissue, more precisely from porcine small intestine mucosa. Since then, suspicion grew about all derivatives of animal origin. The need to provide heparin of other origin increased and bioengineered heparin was produced.

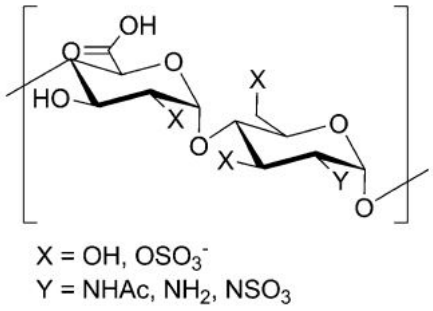

Figure 11: Heparin constitutive unit (From Boddohi et al., 2009)

Heparin is known as the most widely used anticoagulant drug in the world. It was discovered in 1916 by McLean and Howell and was first used for clinical use in 1936 (Lim, 2017; Oduah et al., 2016). This mechanism can be seen in Appendix A on Figure 45.

Heparin acts indirectly as anticoagulant by binding with antithrombin III (AT) that can bind to the factor Xa (Figure 45 path A) or to thrombin directly (chains longer than 17 disaccharide units, Figure 45 path B) to inhibit clot formation (Oduah et al., 2016).
Heparin is a strong polyelectrolyte (polyanion) and as can be seen on Figure 11, it contains three sulfonate groups, one carboxyl group, two alcohol groups and a primary amine per monomer unit. Heparin is a strong polyelectrolyte that is always fully charged, which means that there are 4 negatively charged groups per monomer at all pH values. Also, heparin is very soluble in water (Drugbank, 2018).

Knowing that the average molar mass of the repeating unit ($(C_{12}H_{15}NO_{19}S_3)Na_4$) is 665 $\frac{g}{mol}$ and that most commercial heparin sodium preparations have an average molar mass comprised between 12 and 15 $\frac{g}{mol}$, the heparin chains are, in average, 18 to 22 units long.

Heparin is chosen here because it enhances the activity of Bone Morphogenetic Proteins (BMP) and consequently increases BMP-induced osteoblast differentiation from mesenchymal stem cells (Ban et al., 2015). Remember that one of the wanted functions of the multilayer coating is to promote osseointegration, enhancing osteoblast differentiation could be a strong lead already. More research is however needed on this subject.

1.7.2 Chitosan

Chitosan (CHI) is a linear, natural polysaccharide that is derived from chitin. Chitin is the second most abundant natural biopolymer found in nature, after cellulose, and can be found in the exoskeleton of arthropods, in some algae, in the cell wall of some fungi and in the exoskeleton of many insects (Tolaimate et al., 2000). If the example of crustacean is taken (shrimps, lobster,...), then chitin is part of a complex network along with proteins with calcium carbonate deposits on it that, together, form their rigid shell (exoskeleton). To isolate the chitin, the other two main components must be removed using a process of deproteinisation (in a hot basic solution, usually sodium or potassium hydroxide) and demineralisation (with diluted acid) for the proteins and calcium carbonate respectively (Raafat et al., 2009). This deproteinisation process is very important and must be done to an extreme extent considering that a non-negligible percentage of the population is allergic to shellfish and that these proteins are the reason of the allergy. Pigments and lipids can also be removed along these processes to obtain pure, white chitin after treatment. Obtaining purified chitin is realised either with a chemical process or an enzymatic process. The first one is an industrialised process that has some drawbacks; it harms the physico-chemical properties of chitin and leads to a decrease in the molar mass of chitin (deproteinisation is done with chemicals that also depolymerise the biopolymer) and water effluents of this process contain some harmful chemicals. The enzymatic process, inversely, is a biological process that preserves the structure of chitin, has high reproducibility and is easy to perform (Arbia et al., 2013). However this method is still limited to the laboratory scale studies (Younes et al., 2015).

Chitosan production

Chitosan is obtained by (partial) deacetylation of chitin and forms a random copolymer of molar fraction DA (Degree of Acetylation) of β-(1→4)-N-acetyl-d-glucosamine and molar fraction DDA (Degree of DeAcetylation, DDA = 1 - DA) of β-(1→4)-d-glucosamine. The reaction is shown on figure 12. In fact, chitosan is a deacetylated form of chitin to a certain extent and if the degree of acetylation is lower than 50%, chitin is called chitosan. During this process, acetyl groups are removed and there is also a (partial) depolymerization reaction. Again, there exist various processes to obtain chitosan from chitin that can either be chemical or enzymatic. The chemical process is the industrialised one because of the low cost and the ability of mass production (Younes et al., 2015).

Chitosan properties

Chitosan is a weak polycationic polyelectrolyte with a pKa equal to 6,3 (Rinaudo et al., 1999). It is also a natural, biocompatible and biodegradable (through natural enzymes) polymer, hence it is widely studied and is already used in a lot of applications in sectors such as the food industry or for biomedical applications (Follmann et al., 2016; Zhang et al., 2018; Fu et al., 2005).

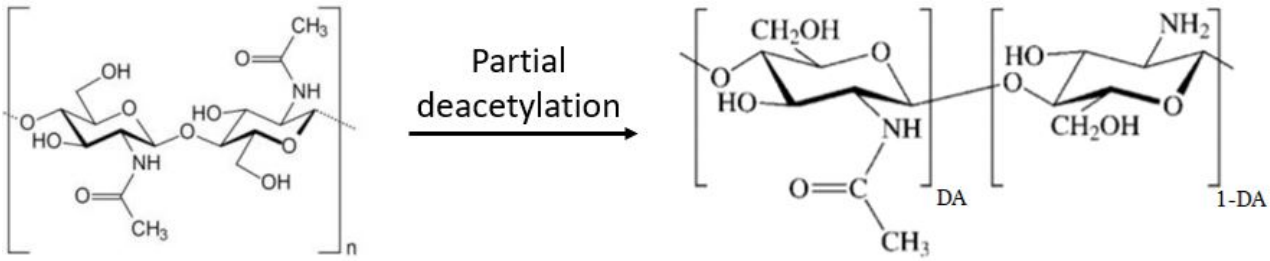

Figure 12: Partial deacetylation of chitin into chitosan (left; chitin, right; chitosan) (Modified from (Younes et al., 2015; Hudson et al., 2001)

But what makes chitosan so interesting in the application of this thesis is that it has an antibacterial or antimicrobial activity. This was first established in the 90s by Muzzarelli et al. and since then, chitosan has gained in general interest by researchers. Chitosan is active against filamentous fungi, yeasts and bacteria (higher attraction to Gram-positive bacteria than Gram-negative bacteria) and has a bacteriostatic activity (growth-inhibitory). The interaction with the bacterial cell surface is believed to be the interaction with and the disruption of the cell envelope. Chitosan has positively charged NH_3^+ groups along its backbone. These are the groups that interact with the negatively charged surface components of fungi and bacteria. This is thought to cause cell surface alterations, leakage of intracellular substances and finally, impairing them of vital bacterial activities (Fu et al., 2005).

The factors influencing the antibacterial activity of chitosan are multiple and still not all understood. What is certain is that the molecular weight of chitosan has to be higher than 10 kDa, no real activity variation was measured above that. Also, the degree of deacetylation is important because it is mainly the protonated amine groups that will attach the bacterial cell wall. Other factors influencing bacterial activity are viscosity of chitosan, concentration, pH, ionic strength, bacterial culture medium, etc (Raafat et al., 2009).

2 Surface characterisation

This second chapter will explain how the titanium substrates were prepared and how the different layers of heparin and chitosan were adsorbed to it. After that, the different layer setups will be analysed and characterised using different techniques. The obtained results will be presented and discussed.

2.1 Titanium substrates preparation

A titanium plate was purchased from President Titanium (MA, USA), with a thickness of 1 mm. A hydraulic shearing machine was used to cut the titanium plate in small coupons of 1cm x 1cm (Figure 13). These coupons being greasy, they were first washed by hand with ethanol and acetone. After that, three coupons were put together by hot mounting (LaborPress-3, Struers) using a *multi-fast* (Bakelite MultiFast 40100064, Struers) type resin with following parameters: 6 minutes heating at 180°C and 3 minutes cooling (Figure 14), the diameter of hot mounting cylinder is: $\phi = 25.4$mm. This was done to decrease the processing time of the next steps.

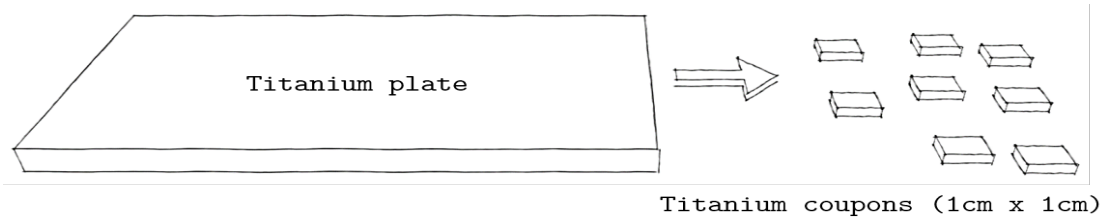

Figure 13: Sketch of the preparation of titanium coupons

Because a uniform surface for all samples was required, the next step was to grind and polish the titanium coupons. This was divided in two parts; first, the surfaces were ground using a grinder (Buehler, Metaserv 2000 Grinder/Polisher 95-2829) with silicon carbide grinding paper of different grit numbers to remove scratches and smoothen the surface. The second part was to finish the polishing using a diamond spray with a polishing machine (Struers, Pedemin DAP-7). All the steps are listed below.

- 1 min: SiC 320 (Struers, US#280)
- 1 min: SiC 800 (Struers, US#400)
- 1 min: SiC 1200 (Struers, US#600)
- 5 min: Diamond spray 9 μm (DP Spray-P 9 μm, Struers)

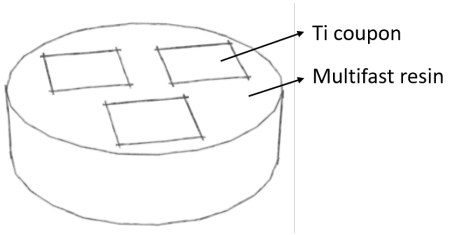

Figure 14: Sketch of the resin with three titanium coupons on top of it

Once all the coupons were polished, they were detached from the resin and kept safe for further use.

2.2 Construction of the bio-interfaces

Cleaning the titanium coupons

Once the titanium coupons are made, the different layers of heparin and chitosan can be constructed on top of it. But before doing so, the substrates must be thoroughly cleaned. This is done by first washing the coupons by hand with a tissue soaked in ethanol (Prolabo, VWR, Louvain, Belgium). Then, each coupon is sonicated using an ultrasonic bath (Branson 2510MT, Sigma-Aldrich, Saint-Louis, USA). This was first done in ethanol 2 times for 10 minutes. The coupons are then dried using gaseous nitrogen and then again sonicated 2 times for 10 minutes with acetone (Prolabo, VWR, Louvain, Belgium).
After being dried using gaseous nitrogen, the last cleaning step is performed. The coupons are put inside of the UV-O_3 cleaner (UVO-Cleaner® 42-220, Jelight Company Inc., Irvine, Californie, USA) during 15 minutes to remove contamination on the surface and to obtain an ultraclean surface.

Preparation of the polyelectrolyte solutions

Once the titanium coupons are cleaned and ready to use, the chitosan and the heparin solution need to be prepared. The parameters used for these will be critical for the layers growth and structure as mentioned in Subsection 1.5. The chosen parameters for both solutions are the following:

$$\text{pH} = 5.4 \qquad \text{I} = 150 \text{ mM} \qquad \text{c} = 0{,}5 \text{ g/L}$$

The pH value of 5.4 was chosen because chitosan is only soluble at pH values below 6.5 (pKa value of chitosan). To be sure that chitosan would be fully soluble, pH 5.4 was chosen. The ionic strength of 150 mM was chosen according to research done by Lundin et al. in 2011 that showed that with this ionic strength the thickest layers were formed. Also, this ionic strength is close to physiological conditions. A concentration in the range of the g/L was found to be more than enough to reach the plateau of the adsorption isotherm. This also allows us to ensure that the solutions would not be depleted in polymers while the adsorption step takes place (Decher, 1997).

Heparin solution: To attain the aforementioned conditions for 50 mL of heparin solution, 1 mL of sodium heparin (B. Braun, Diegem, Belgium, 5000IU/mL) was pipetted into an Erlenmeyer because this heparin is known to contain 200 IU/mg and that the wanted concentration is 0,5 g/L (25 mg/50 mL). To obtain an ionic strength of 150 mM, 750 μL of hydrogen chloride, HCl 10 M (Prolabo, VWR, Leuven, Belgium) and 750 μL of sodium hydroxide, NaOH 10 M (Sigma-Aldrich, Overijse, Belgium) were added together with 47,5 mL of ultrapure water at pH 5.4 (Elga Purelab Ultra Device, 18,2 MΩ·cm, Veolia, United Kingdom). The final pH was measured with a pH meter (PHM82 Standard pH Meter, Radiometer, Copenhagen, Denmark) and the solution was kept in the fridge at 4°C until further use.

Chitosan solution: Because chitosan is insoluble at normal pH, an additional step was performed to obtain a soluble chitosan solution with the above-mentioned parameters. First, 25 mg of 95% deacetylated chitosan (Heppe Medical Chitosan GmbH, Halle, Germany, Molecular weight comprised between 10 and 50 kDa) was mixed up with 25 mL ultrapure water and 750 μL of HCl. This solution was heated up at 60°C for one hour and mixed from time to time to solubilise chitosan. After cooling down, 750 μL of NaOH was added with ultrapure water to reach the 50 mL mark.
The obtained solution was then filtered with a cellulose filter 5 μm (VWR, Leuven, Belgium) and a second filter of polyether sulfonate 0.2 μm (VWR, Leuven, Belgium). The solution was filtered to remove non solubilised particles. Again, the pH of the solution was measured using the same pH meter and the chitosan solution was kept in the fridge at 4°C until further use.

Chitosan + heparin solution A third solution was made in the early stage of this thesis were chitosan and heparin were mixed together according to the same conditions as mentioned above. This was done to see how complexes of CHI+HEP would behave when deposited on the titanium surface. To make this solution, 4.9 mL of the aforementioned chitosan solution was transferred to an Erlenmeyer and 100 μL of heparin sodium was added. Doing so, the imposed parameters (concentration, ionic strength, pH) are met.

Construction of the multilayers

As mentioned in Subsection 1.5, the layers of polyelectrolytes are constructed using a technique called *Layer-by-Layer* self assembly.
The cleaned titanium coupons are put in a 24 well-plate (Greiner Bio-one, 662160) and they are then submerged during 25 minutes per adsorption step in the heparin or chitosan solution. In between each adsorption phase, a washing step is performed where 80% of the volume in each well is removed (to prevent the films from drying out) and replaced with ultrapure water for 1 minute. In the meantime, the well-plate is gently mixed. This washing step is performed three times. The third time, 100% of the volume in each well is removed and the next polyelectrolyte solution is added in the wells. According to the wanted layer setup, the order of deposition can be changed. After all the layers are made, the samples are washed 7 times during 30 seconds and then put under the fume hood to dry. Once dry, the samples are placed again in a 24 well-plate inside of a desiccator to separate the samples from ambient humidity. The range of samples used through the master thesis is illustrated on Figure 10.

The complete protocol for the formation of $(CHI/HEP)_3$ (three bi-layers) can be found in Appendix B, Figure 46.

2.3 Characterisation techniques

Once the layers are made on top of the titanium substrates, they need to be analysed and characterised. The methods that were used allow to characterise the physicochemical properties of the freshly made layers. The following part of this Section will summarise the principle of the characterisation methods.

2.3.1 Water Contact Angle

The Water Contact Angle (WCA) is a method that quantifies the wettability of a solid surface using a liquid, in this case ultrapure water. The hydrophobic or hydrophilic character of the substrate is thus examined. To do so, a water droplet is deposited on the surface of the sample to be tested and the contact angle (θ) is measured. θ is the angle between the surface and the deposited droplet, at the gas-water-solid interface (Figure 15.a). A surface is defined as hydrophobic (water repellent) if $\theta > 90°$ and as hydrophilic if $\theta < 90°$ (Figure 15.b).

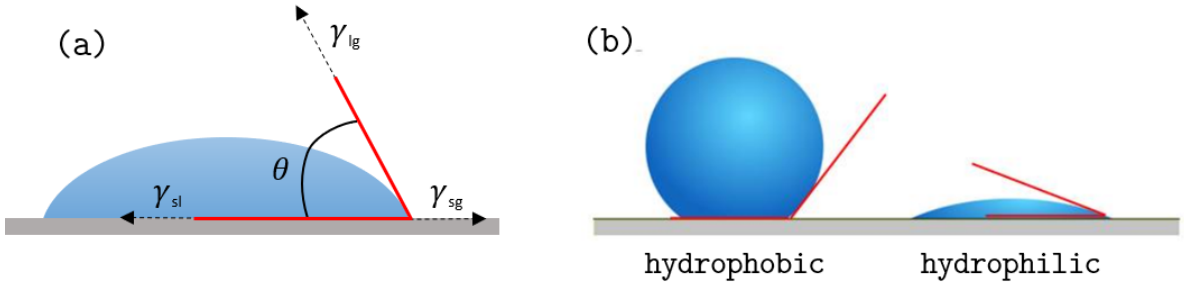

Figure 15: (a) Schematic representation of the gas-liquid-solid interface (b) Difference between hydropobic and hydrophilic surface (modified from FMPS, n.d.)

The wettability was quantified by Young with the following equation:

$$\gamma_{sg} - \gamma_{sl} = \gamma_{lg} \cdot \cos(\theta)$$

Where γ_{sg}, γ_{lg} and γ_{sl} represent respectively the interfacial energy between the solid and gas, the liquid and gas and the solid and liquid. These parameters are the link between the macroscopic (contact angle) and microscopic (γ_{sg}, γ_{lg} and γ_{sl}) properties of the tested samples (Demoustier & Dupont, 2018).

WCA is particularly interesting in this study because the wettability of a surface has a big impact on cellular and bacterial adhesion as it is maybe the most important property governing biocompatibility of a material. Many studies have been done regarding the effect of wettability on protein and bacterial adhesion. Zhang et al. showed in 2013 that bacteria adhered effectively to polymer surfaces having a static contact angle comprised between 40 and 70° but these values are not found in all research papers because the contact angle is only one of many parameters influencing bacterial

adhesion (others are surface charge, roughness or environmental pH).
For example, Dou et al. found in 2014 that the highest level of bacterial peptidoglycan adhesion was on surfaces having a static contact angle comprised between 54 and 130°.
Finally, Lee et al. studied in 1998 the effect of cell adhesion on a surface having a contact angle gradient on its whole length. According to their study, cells adhere best to surfaces having a static contact angle between 43 and 65°.
To summarise what was said above, it could be said that bacteria adhere well to surfaces having a contact angle comprised between 40 and 130° while cells adhere best to surfaces with contact angles between 43 and 65°. Because these two intervals overlap, the importance of having a bi-functional coating is even higher. The contact angle of our coating should be comprised between 43 and 65° to improve cellular adhesion. Because bacteria adhere well in this range too, our layers should be able to repel or kill bacteria.

It should be noted, however, that the relationship between the wettability of the surface and cell adhesion is not direct; it involves the action of proteins. When cells are cultured, for example in culture flasks, they are immersed in culture medium containing non-adhesive proteins like albumin. These proteins tend to adsorb more on surfaces that are hydrophobic. By doing so, they reduce the available surface for adhesive proteins secreted by the cells that are used to adsorb to the surface. Hydrophobic surfaces thus indirectly reduce cell adsorption.

To measure the contact angle under static conditions, a drop of 0.3 μL of ultrapure water is deposited on the surface of the samples using a micro syringe. A camera connected to a computer provides an image on which the contact angle is shown. The measurements are taken 5 seconds after the drop deposition on the surface. For statistical analysis, four measurements are performed per sample. Measurements were executed at day 1, day 5 and after 3 weeks following sample preparation. Doing this, information was retrieved about the influence of the layers as well as the time-dependency of the contact angle of the different samples.

2.3.2 Ellipsometry

The ellipsometer is a non-destructive optical technique used to analyse surfaces and has several applications such as analysing the thickness of thin films on top of the substrate, crystalline nature of the surface, roughness or to measure the refractive index of materials (Demoustier & Dupont, 2018). In this work, the ellipsometer is used to measure the thickness of the deposited polyelectrolyte layers. The principle of the ellipsometer consists in *"measuring and interpreting the change of amplitude and polarisation state that occurs when a polarised light beam is reflected at non-normal incidence from a sample surface"* (Theeten, 1981). The incident light is characterised by the amplitude and phase of s- and p-polarised light (**s**enkrecht (i.e. perpendicular in German) and **p**arallel to the plane of incidence). The change in polarisation of the incident light is due to characteristics specific to the

used substrate and the thin layers on top of it.
The incident light that is reflected on the substrate passes through a polarisation state analyser and is then caught in the photo detector. The measured values are the angles Ψ and Δ corresponding to the difference in amplitude and phase of the two reflections respectively. The obtained values are then modelled in order to extract the desired properties. The model can then, for example, compute the thickness of the layers given some extra information such as the refractive index of the substrate and film.

The type of ellipsometer used in this work is called *Nulling ellipsometer*. It uses a camera as a detector to obtain a real-time visualisation of the sample. To obtain information about the layer on top of the substrate, the analyser and polariser (Figure 16) are adjusted so that no light from the substrate reaches the detector.

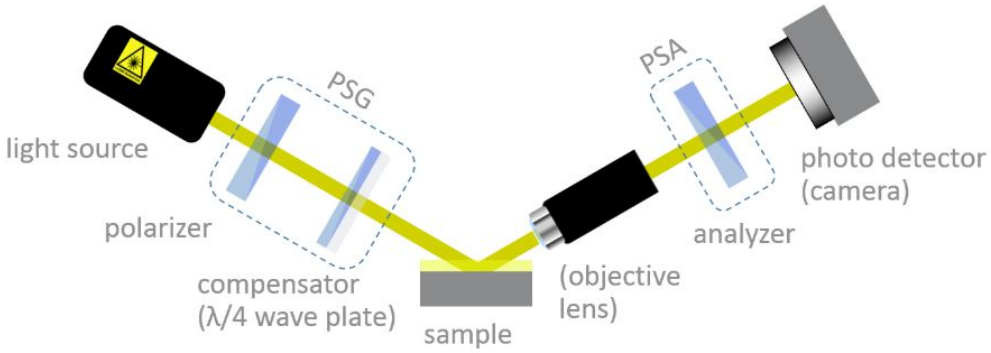

Figure 16: Schematic representation of the setup of the ellipsometer. PSG: polarisation state generator; PSA: polarisation state analyser (Accurion, 2019)

Several hypotheses are made when using the ellipsometer that can have a strong impact on the interpretation of the obtained results. First it is supposed that the thin layer is homogeneous on the whole substrate. Also, the layers formed by successive adsorption of heparin and chitosan are seen as a single layer, having the same refraction index (n = 1.46; Lundin et al., 2011).

The film thickness is found using the following method: the titanium coupons are washed and layers are constructed according to the wanted setups. These were made 24 hours before tests were performed. The samples are then put in the device. The first coupon to be tested is the control, bare titanium coupon. According to the obtained data, a model can be chosen. Once this is found, the other samples can be tested and the film thickness can directly be recovered from the ellipsometer.
The ellipsometer used in this work is the *NanoFilm_EP4* (Accurion GmbH, Goettingen, Germany) and the wavelength of the incident light is 658 nm. The refraction index for titanium was taken from the database of the device.

2.3.3 Atomic Force Microscopy

Atomic Force Microscopy (AFM) is a well-known technique that allows the user to obtain information about the surface's morphology and topology of a sample but it can also be used to measure inter-molecular forces, electrical forces, magnetic forces and so on of the surface. In this work it was used to map the topography of the prepared samples and to compare them.

The principle of the AFM technique is based on the tip-cantilever assembly (probe) that interacts in different ways with the surface. The probe makes a raster-like motion (Figure 17.A) on the sample to obtain information over the whole imaged part of the sample. This motion is monitored by a *position sensitive photo-detector* (PSPD, also called a split photodiode) through a laser beam reflected on the back of the cantilever. The force is not measured directly but is calculated by measuring the deflection of the cantilever, knowing its stiffness constant k and using Hooke's law: $F = -kz$ (NanoSurf, n.d.)

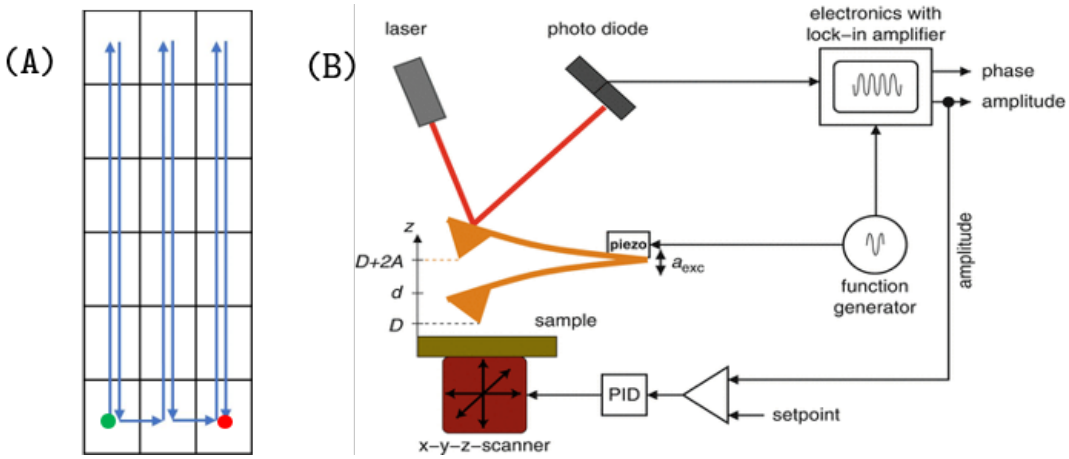

Figure 17: (A) Representation of raster scanning (green = begin, red = end) (B) Setup of a tapping-AFM: the deflected laser is detected by the split photo diode. The cantilever vibration is caused by piezo element (Hölscher, 2012)

Three different modes can be used when using the AFM: contact, non-contact and tapping.
In **contact mode**, the tip on top of the cantilever is in continuous contact with the sample while a raster scan is performed. Most of the time in contact mode, the applied force of the cantilever is kept constant but it can also be used in a constant-height mode (Bruker Nano Surfaces, 2012).
In the **non-contact mode**, the tip is raster scanned close to the surface (several Angstroms) while vibrating with a specific amplitude and a frequency close to its resonance frequency.
The image is constructed from the measured long distance (attractive) forces between sample and probe (NanoWerk, n.d.). The last AFM mode is the one used in this master thesis. In **tapping mode** (Figure 17.B), the cantilever also oscillates at (or close to) its resonance frequency using a small piezo-element on which the cantilever is mounted.

The frequency and amplitude of its movement are kept constant. The probe will attach and detach from the surface during each oscillating cycle. When approaching the surface, forces like Van der waals, dipole-dipole or electrostatic interactions will impact the amplitude of the cantilever (monitored through the PSPD). According to this variation, the z-position of the sample is changed. Doing so, the measured intermittent forces allow to map the topography of the sample (Hölscher, 2012). This mode has the advantage to damage less the samples and the probe tip. It is also more adequate to analyse soft materials such as polymers on top of stiffer substrates (Sicard, 2013).

The AFM used in this thesis is the Nanoscope Multimode V (Brucker, Santa Barbara, USA) and the used tip is made of silicon (Veeco, Camarillo, Canada). The used cantilever has a resonance frequency comprised between 200 and 500 kHz.

2.3.4 X-ray Photoelectron Spectroscopy

X-Ray Photoelectron Spectroscopy (XPS) is a technique that characterises the chemical composition of a surface. This technique is based on the photoelectric effect. The XPS spectra are obtained by irradiating the samples with X-rays of known energy. An atom that is irradiated by X-rays will emit electrons that are proper to the atom itself as well as its surrounding (neighbouring atoms) (Genet et al., 2008). The kinetic energy of the expelled electrons is measured and the binding energy of the electron can be found using:

$$E_{binding} = E_{photon} - E_{kinetic} - \phi$$

Where E_{photon} is the energy of the used X-rays, $E_{binding}$ is the binding energy of the electron and ϕ is added due to an offset of the XPS setup. The kinetic energy of the electrons is measured using a detector put at the end of the electron energy analyser (EEA, Figure 18) that also allows to count the amount of electrons (peaks intensity). From the measured binding energy and intensity of a peak on the spectrum it is possible to obtain the elemental identity, chemical state and quantity of the involved atoms (Oswald, 2013; Physical Electronics, 2019).

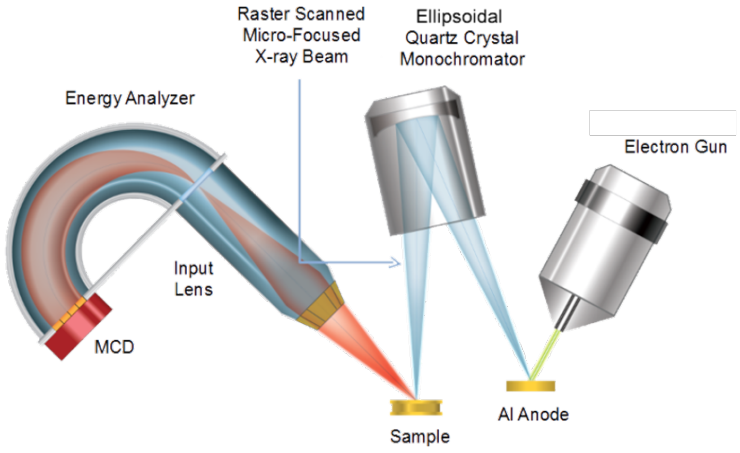

Figure 18: Schematic representation of the XPS

Using the XPS, information can be obtained about the first 10 nm of the sample. Atoms located deep in the sample bulk can also release electrons but these will collide with other particles preventing them from leaving the sample's surface. Electrons located at an intermediate depth will leave the sample's surface, with a decreased energy due to collisions with other atoms. They will contribute to the spectra under the form of a background signal. Also, the detection limit of an element lies between 0.1 and 0.5% (Oswald, 2013).
The analyses were performed on a SSX 100/206 photoelectron spectrometer from Surface Science Instruments (USA) equipped with a monochromatised micro focused Al X-ray source (powered at 20 mA and 10kV). The pressure in the analysis chamber was around 10^{-6} Pa and the analysed area was approximately 1.4 mm^2. To treat the obtained data, CasaXPS was used (Casa Software LTD, UK) and the C-(C,H) component of the C1s peak of carbon was fixed at 284,8 eV to correct the binding energy scale.

2.3.5 Quartz Crystal Microbalance with Dissipation

Quartz Crystal Microbalance with Dissipation (QCM-d or QCM) is an extremely sensitive technique that can measure mass changes in the order of the nanogram to microgram. The QCM-d can be used for different applications such as monitoring the buildup of polymer films, measure the amount of molecule-surface interactions, biosensor applications, etc. The QCM's principle is based on the piezoelectric effect of the quartz crystals (Figure 19.A). When piezoelectric materials are under stress, they produce an internal electric charge. This process is also reversible and the reversed piezoelectric effect is used here. When a voltage is applied to the quartz crystal, it will oscillate with a certain frequency (Figure 19.B). The voltage is chosen such that the quartz oscillates at its resonance frequency or its overtones (NanoScience, n.d.). This frequency will change (Δf) with the adsorbed mass as can be seen on Figure 19.C. The frequency variation, Δf, given by Sauerbrey's equation (Reviakine et al., 2011):

$$\Delta f = \frac{-n}{C} \cdot \Delta m$$

Where Δm is the change of mass per unit area, n represents the overtone number and C is a constant that depends on the property of the used crystal. Because here the QCM is used under liquid conditions, several hypothesis are made to be able to use Sauerbrey's equation. First, the added mass is small compared to the crystal's mass. Second, the added mass is rigidly adsorbed. Third, the mass is evenly distributed over the active area of the crystal (NanoScience, n.d.). To control these hypotheses, the QCM-D measures also the dissipation (red curve on Figure 19.C). The dissipation is defined as *the energy loss per oscillation cycle, divided by the total energy of the system* and this correlates to the softness of layers on the crystals' surface (Pettersson, 2019). This dissipation measurement allows us to obtain information on the model that must be used to analyse the QCM-D data. If the deposited layer behaves as a rigid film, Sauersbrey's equation can be used.

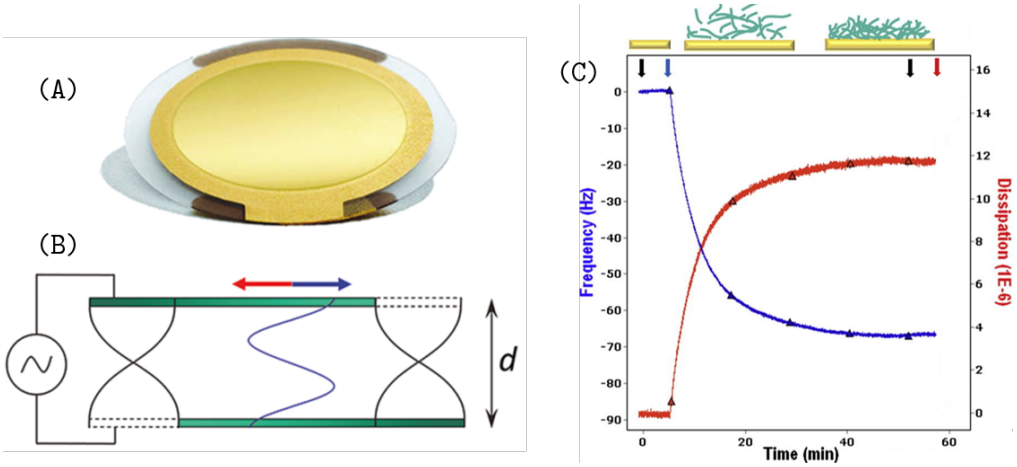

Figure 19: (A) Quartz crystal used in the QCM, here with gold electrodes (yellow). (B) Application of oscillatory voltage to the crystal resulting in cyclical deformation. Top and bottom surfaces move in an antiparallel way. (C) Representation of frequency shift (blue) and dissipation (red) when Δm increases (Reviakine et al., 2011; Oh et al., 2015)

The QCM-D is thus of real value in this work, it allows to have real time measurements on how the polyelectrolytes adsorb to the surfaces. The film thickness can also be retrieved and results can be compared with the ones obtained with ellipsometry. It could also show us how the formed layers would interact in different media. Ethanol for example must be put on the samples before performing *in vitro* tests in order to sterilise them. The QCM could be used to monitor the behaviour of the multilayers in such media.

The Quartz Crystal Microbalance used in this work is the Q-Sense E4 system (Gothenburg, Sweden). The used crystals are AT-cut 5 MHz crystals coated with 100 nm of gold from Q-Sense (Gothenburg, Sweden). Before use, they were washed in piranha solution (H_2O_2 30% (Prolabo, VWR, Leuven, Belgium)/H_2SO_4 95% (Prolabo, VWR, Leuven, Belgium) 1:2) during 2 minutes and then thoroughly rinsed with ultrapure water.
Gold coated crystals were used instead of titanium ones because data was already obtained with the titanium crystals by Cédric Vranckx. This experiment was done to compare the obtained results of adhered layers on different substrates.

The first part of Section 2 explained how the surface characterisation techniques work and why they are useful in this master thesis. The second part of this section aims to treat, analyse and discuss the results obtained with the previously discussed techniques.

2.4 Results and discussion

In this subsection all the obtained results will be presented. The order of used techniques follows the general strategy of this work. After that, the results will be discussed.

2.4.1 Wettability of the samples

The first characterisation technique used in this work is the water contact angle measurements. The WCA allows us to find the hydrophobic or hydrophilic character of the different samples. This was the first test performed because it is easy, the data interpretation is straightforward and the results are obtained in real time. It also gives confirmation that layers are effectively built on top of the substrates.

As mentioned above, the titanium coupons are cleaned before the layers are constructed on top of them. The different layer conditions that were used for the WCA technique are depicted on Figure 20. These are the conditions used in most of the experiments. If other conditions are added or removed, it will be mentioned.

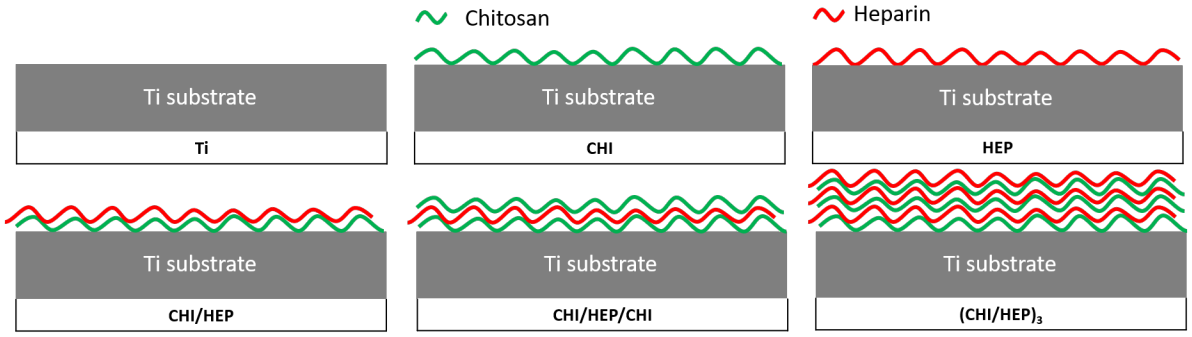

Figure 20: Different layer conditions used for the water contact angle measurements

The samples were prepared in the same way as explained in Subsection 2.2, which means that the polyelectrolyte solutions are made at a pH of 5.4, with an ionic strength of 150 mM and a concentration of 0.5 g/L with an adsorption time of 25 minutes for the polyelectrolyte solutions. For each condition, three samples were made (n = 3).

Once the data retrieved, a single factor ANOVA test was performed to see if the obtained values for the different samples having the same condition could be pooled together. The null hypothesis, H_0, of the ANOVA test states that $\mu_1 = \mu_2 = \mu_3$. For all the different conditions, it was found that the null hypothesis could not be rejected with a confidence level of 95% ($\alpha = 0.05$). The obtained values are therefore presented as coming from one single sample. The measured contact angles can be seen on Figure 21 representing the mean ± standard deviation for the different conditions. Also, measurements were performed after 1 day, 5 days and 3 weeks to obtain an evolution of the water contact angle with time.

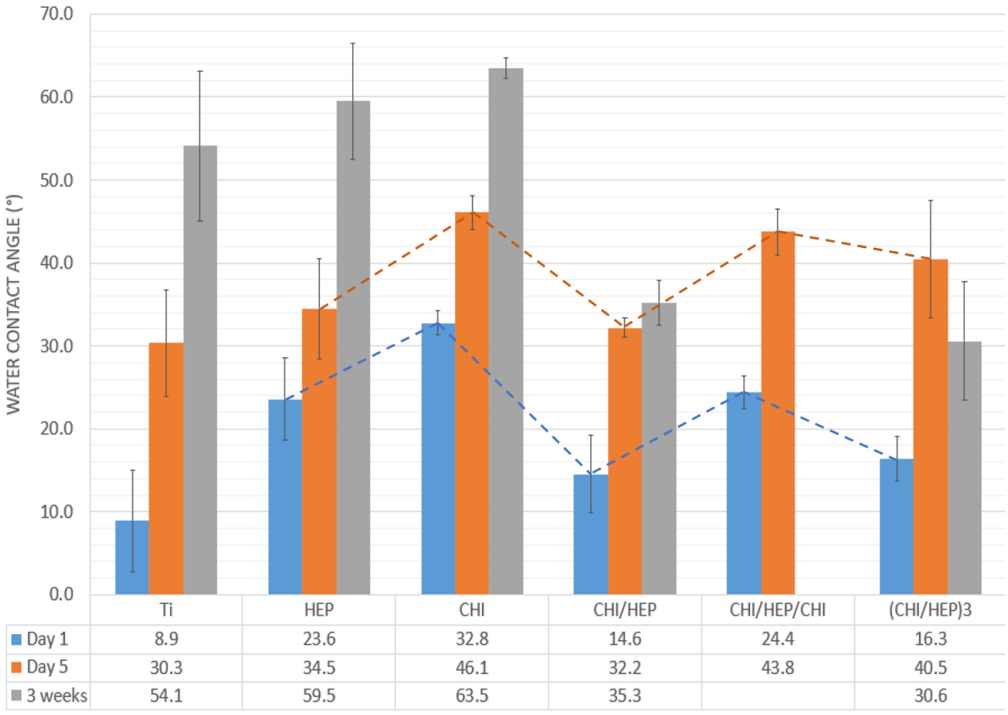

	Ti	HEP	CHI	CHI/HEP	CHI/HEP/CHI	(CHI/HEP)3
Day 1	8.9	23.6	32.8	14.6	24.4	16.3
Day 5	30.3	34.5	46.1	32.2	43.8	40.5
3 weeks	54.1	59.5	63.5	35.3		30.6

Figure 21: Water contact angle (°) for the different conditions

A lot of information can be retrieved by looking at the obtained data. The first element to be mentioned is that the cleaning of the titanium surfaces according to the aforementioned protocol was optimal. Bare titanium surfaces have the most hydrophilic surfaces thus proving that contamination of the surfaces disappeared with the cleaning.

A first major trend that can be seen on Figure 21 is that the contact angle of the different conditions increases with time. There is a drastic increase for the conditions Ti, HEP and CHI between the 3 measurements, while the increase for CHI/HEP and $(CHI/HEP)_3$ is not considered significant (p-value > 0.05) between 5 days and 3 weeks. The contact angle is known to increase when contamination of the surface occurs. The reason why this is not the case for these two samples may be because the multilayers protect the surface from contaminants and thus preventing an increase of the water contact angle. Another explanation could be that the surface of these samples does not behave in the same way anymore. Indeed, if the surface becomes a *non-ideal rough surface*, the Young's equation does not apply anymore and other models have to be used. The two main models used for such cases are called the model of Wenzel and the model of Cassie (Figure 22).

The **Wenzel model** applies for homogeneous surfaces where the droplet used to measure the contact angle penetrates the rough surface, resulting in a high adhesion force. The contact angle is given by: $\cos(\theta^*) = \mathbf{r} \cdot \cos(\theta_Y)$ Where r is the ratio between the true area of the solid and the apparent area, θ_Y is the contact angle defined on an ideal surface and θ^* is the apparent contact angle. Two cases arise to us; (1) the ideal surface is measured as hydrophobic ($\theta_Y > 90°$) and then $\theta^* > \theta_Y$ or, (2) the ideal surface is hydrophilic ($\theta_Y < 90°$) and then $\theta^* < \theta_Y$ (Marmur, 2003).

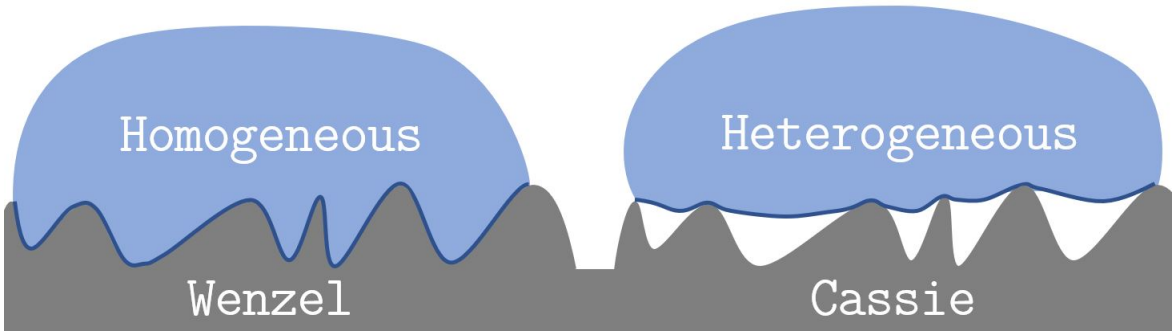

Figure 22: Schematic representation of the model of Wenzel and of Cassie

Cassie's model is used to describe heterogeneous surfaces and gives us the contact angle when the water droplet is in contact with various surfaces. On Figure 22, the water droplet is in contact with the surface and with air because it does not enter in the rough surface. The apparent contact angle, θ^*, is then given by $\cos(\theta^*) = \sum_{i=1}^{N} \sigma_i \cdot \cos(\theta_i)$ Where σ_i represents the fraction of the surface made up of i and θ_i is the contact angle on an ideal surface made entirely of species i. This equation is generalised for N different chemical species (Swain et al., 1998). The model of Cassie could be used if the polyelectrolytes adhere to the sample by forming little islands, without covering the whole surface. Unfortunately, with the available data, it is not possible to know which model should be used here.

The second identified trend is the saw-tooth trend seen when increasing the amount of layers (dotted lines on Figure 21). These are consistent with data found in the literature (Lundin et al., 2011). This confirms that layers are constructed on top of each other because both polyelectrolytes have a different hydrophobic character. Indeed, when heparin is the outermost layer, the measured contact angle is lower than when chitosan is the outermost layer.
Also, it seems that the measured contact angle values tend to an intermediate value between chitosan and heparin when increasing the number of layers. Yoo et al. found in 1998 that sequentially adsorbed layers could interact. Chains segments from the underlying layer can penetrate the layer on top of it. This could explain why the contact angle of the condition $(CHI/HEP)_3$ lies in between that of heparin and chitosan.

2.4.2 Thickness of the film

The information that we wanted to retrieve after knowing that layers were effectively deposited on the titanium substrates, was the film thickness. To do so, the ellipsometer was used. As mentioned in Subsection 2.3.2, the first test done was with a cleaned titanium surface, without layers adhered to it. This would tell us which model to use for the analysis of the other samples. Two models were compared when fitting the obtained data and this fit can be seen on Figure 23. The blue dots represent the obtained data while the blue curve represents the used model to which data will be

fitted. The titanium model (left) fits the data perfectly while the model of titanium oxide on top of titanium (right) does not fit the obtained data at all. When using the modelling tool, *EP4 model*, of the ellipsometer, it is possible to modify the oxide layer thickness manually to find a proper fit of the obtained data with the model. When doing so, a fit was obtained for a layer thickness of 0 nm and for all multiples of 120 nm.

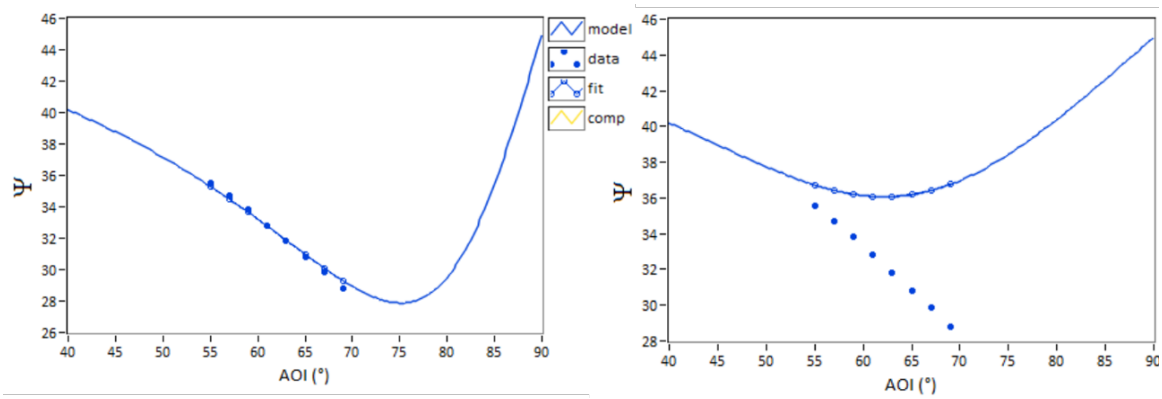

Figure 23: Data obtained with the ellipsometer for bare titanium surfaces. Comparison of two models: (left) titanium and (right) titanium oxide (10 nm) on top of titanium

Thus, the following experiments were all performed using a model without titanium oxide. To be sure, the measured layer thicknesses were also retrieved using the model of Ti + TiO_2 because using only titanium seemed counter-intuitive. In Subsection 1.5, we learned that a passive oxide layer, TiO_2, forms on top of titanium and that it renews itself rapidly. Also, this oxide layer should be smaller than 10 nm. Thus, an oxide layer thickness of 120 nm exceeds the expected values. A layer thickness of 120 nm is only achievable by annealing the sample for 5 hours at 600°C (Hamilton et al., 2013). When using the Ti + TiO_2 model, the measured layer thickness of the constructed films were always smaller than when using the Ti model. Also, the measurement errors were 2 to 3 times higher. Because of this, these results are not shown in this master thesis.

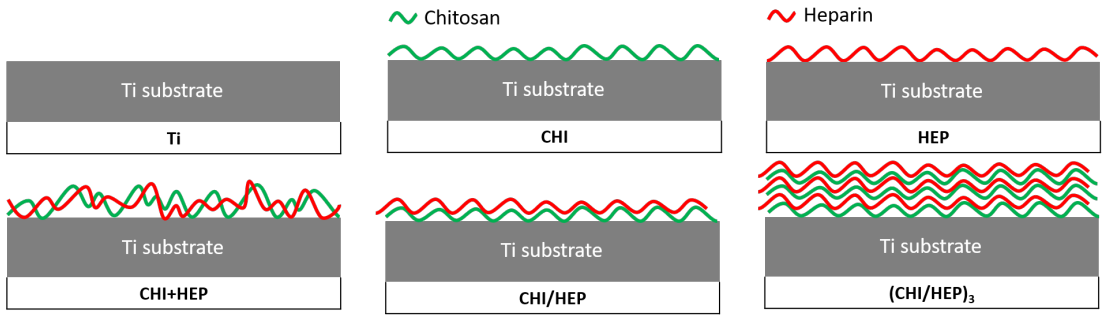

Figure 24: Different layer conditions used for ellipsometry measurements

Two samples were made for each condition (n = 2). Measurements were performed after 1 day and after 3 weeks of layer deposition. The conditions were slightly changed compared to the ones investigated in Subsection 2.4.1 as can be seen on Figure 24.
The results obtained with the ellipsometer can be seen on Figure 25. The first element to see is that measured values for the conditions CHI and HEP equal 0 nm. Then, something very small is measured for the conditions CHI+HEP and CHI/HEP and the three bi-layers, $(CHI/HEP)_3$, have an average thickness of 4.05 nm at day 1. The difference between CHI+HEP and CHI/HEP is statistically not significant while the values for $(CHI/HEP)_3$ are considered statistically significantly different from the other measured conditions. Also, ageing time had no statistical influence on film thickness.

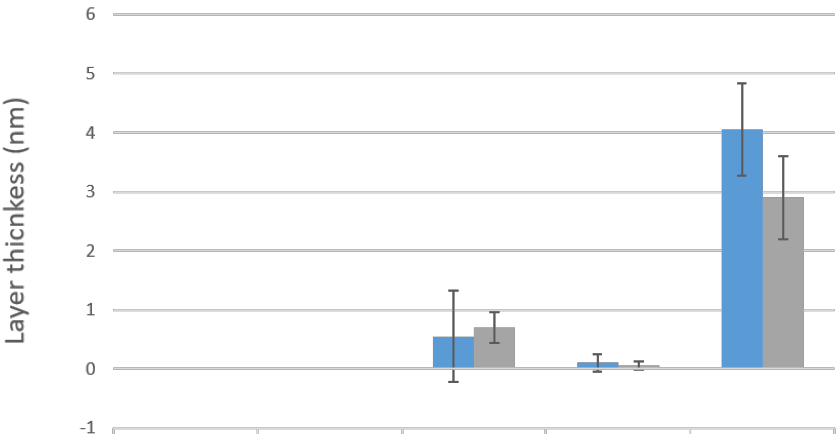

	CHI	HEP	CHI+HEP	CHI/HEP	(CHI/HEP)3
1 Day	0	0	0,55	0,1	4,05
3 Weeks	0	0	0,7	0,05	2,9

Figure 25: Values obtained with the ellipsometer using a titanium model

The obtained values are quite below what was expected when comparing with values from the literature (Lundin et al., 2011), and are rather unexpected with regards to the WCA analysis. In Subsection 2.4.1, the alternating construction of layers could clearly be seen by the saw-tooth trend (Figure 21). The reason why these results are discouraging may be the fact that the hypotheses made (homogeneous, single layer with one refraction index) to extract data by modelling may not be in line with the physico-chemical properties of the systems.

To investigate if the assumptions made were correct or not and to learn more about the elaborated films, the topography of the different samples was examined using Atomic Force Microscopy.

2.4.3 Topography of the layers

To study the topography and morphology of the films, the AFM was used. The AFM could also help us control the hypotheses made when using the ellipsometer (homogeneous, single layer with one refraction index).

Two samples (n = 2) were made for each condition and 2 images are taken per sample. The most representative images of each sample were kept. The same layer conditions are used as for ellipsometry (Figure 24). The obtained images are first processed by a flattening step (*NanoScope* program) to eliminate low-frequency noise and other distortions. *Nanoscope* also allows to modify the Z-axis of the images and the vertical scale used was set from -70 nm to +70 nm on all images except the one where complexes of chitosan and heparin are adsorbed on the surface (Figure 27.C). White parts of these figures must be read as higher parts than the darker ones.

Figure 26 is obtained from the bare titanium surface. It can be seen here that a lot of nano-scratches are present on the surface and that the roughness is high. This may be caused by the polishing of the surfaces in the early stage of this work.

The images obtained for all the different conditions are shown in Figure 27. There are no striking differences between all the samples, the scratches are a bit more faded when layers are constructed but the visible differences remain small and are sometimes hard to catch.

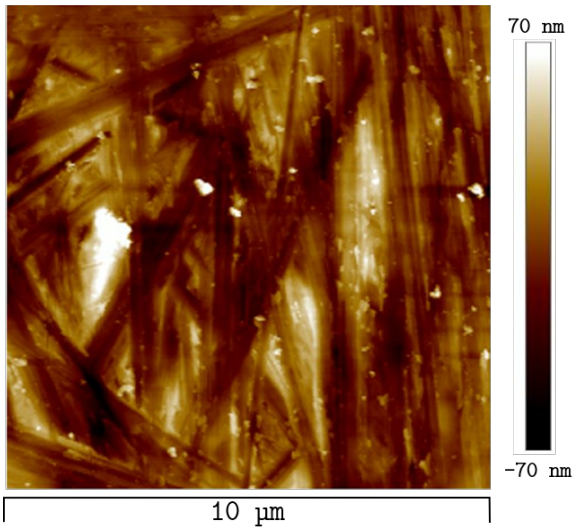

Figure 26: AFM image obtained from bare titanium surfaces

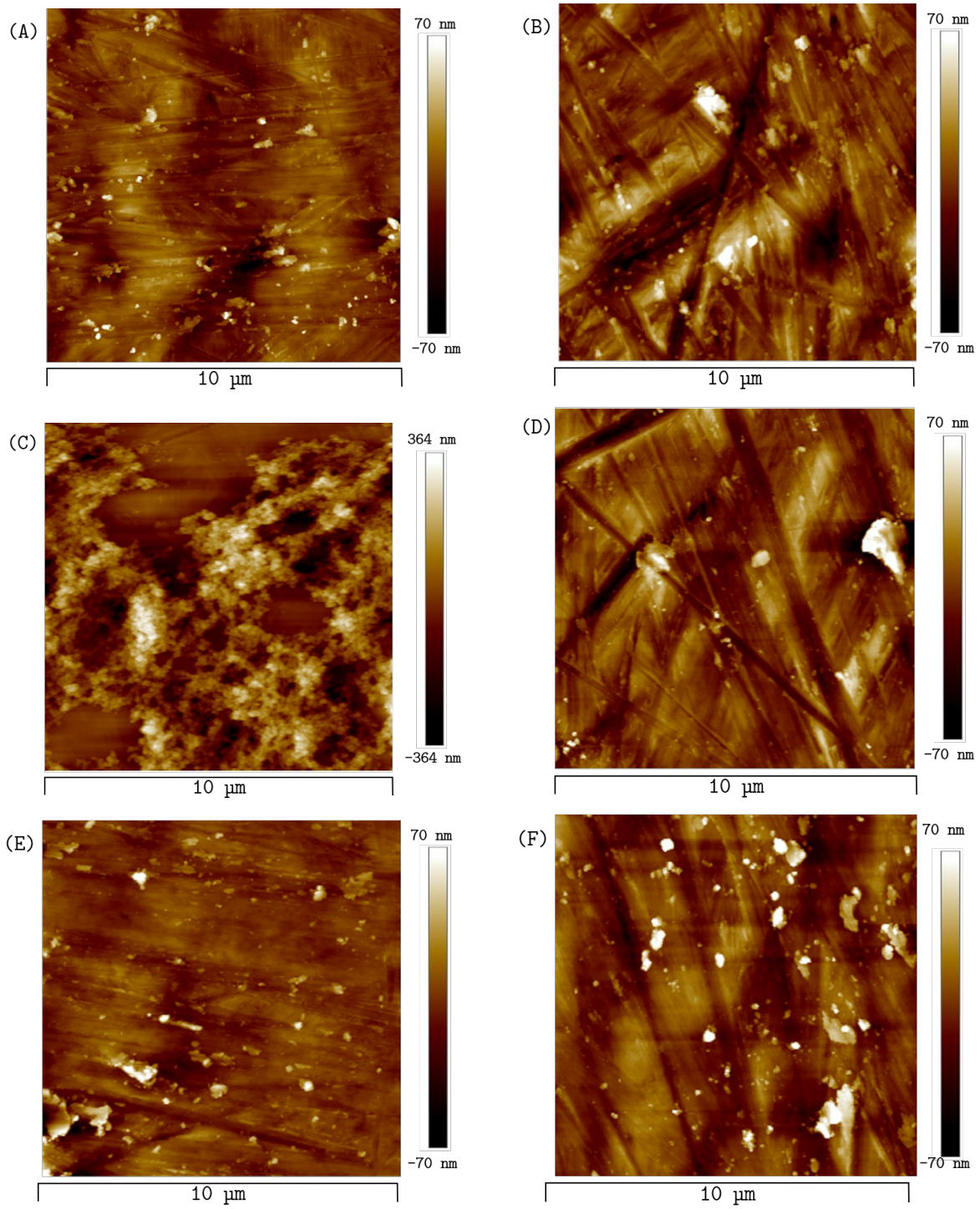

Figure 27: AFM images obtained from different conditions; (A) CHI (B) HEP (C) CHI+HEP on an aggregate (note that the scale is different) (D) CHI+HEP not on an aggregate (E) CHI/HEP (F) $(CHI/HEP)_3$

Considering no real visible differences were detected, the sample's roughness was investigated. The root mean square average values, Rq, of the height profiles are shown in Table 3. The decreasing roughness with increasing layers seems quite logical regarding the initial rough surfaces. Nonetheless, the measured difference is quite small.

The only striking difference is seen on the sample of CHI+HEP on Figure 27.C where aggregates of chitosan and heparin complexes adhered to the surface. They can clearly be seen on this image. Note that the Z-scale is different on this image. Figure 27.D is taken on the same sample but on a spot where these aggregates did not form. Also, the Rq value of Figure 27.C is 100 nm while that for Figure 27.D is 17.6 nm which is really close to that of the control surface. These observations accord with what was mentioned just above, allowing us to think that the CHI+HEP solution only formed aggregates on the titanium surface.
Because homogeneity is a mandatory feature for our coating, the CHI+HEP condition was discarded from further study.

Table 3: Root mean square average (Rq) of the height profile for the different tested conditions

Condition	Ti	CHI	HEP	CHI/HEP	$(CHI/HEP)_3$
Rq (nm)	17.3	13.4	15	12.75	12

The hypotheses made for ellipsometry in Subsection 2.3.2 can finally be discussed. First, we assumed that the surfaces were smooth. This is clearly not the case when inspecting Figure 26 and Figure 27. Also, the measured layer thicknesses in Subsection 2.4.2 are in the order of the nanometers while the measured height of features found on titanium can go up to 140 nm. Using this information, it can be concluded that the technique of ellipsometry was not adequate in this study because the roughness of the sample is much more important than the thickness of the formed layers.

To investigate further the layer deposition and thickness, XPS and QCM were used.

2.4.4 Chemical composition of the samples

To obtain the chemical composition of the samples, XPS was used. The chosen samples for this experiment are depicted on Figure 28, the CHI+HEP condition was replaced by CHI/HEP/CHI. Also, no control sample was used for the reason that XPS analysis was already performed on the polished and washed Ti coupons by Cédric Vranckx as part of his PhD thesis.

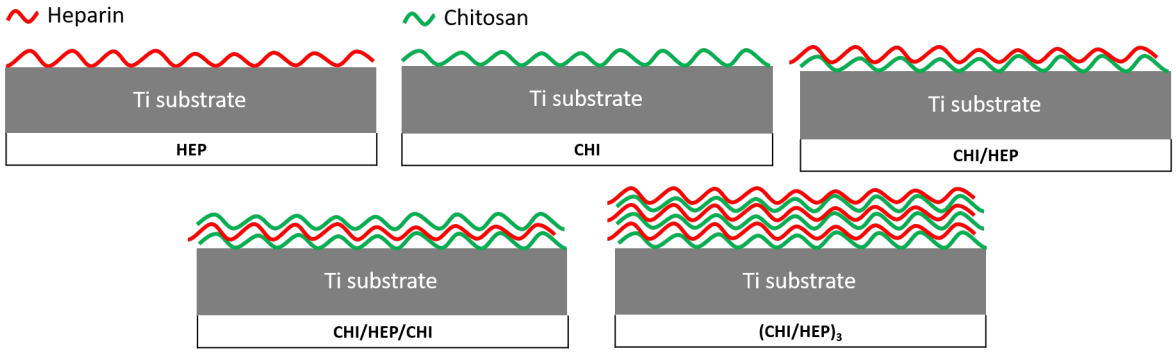

Figure 28: Layer conditions used for XPS measurements

Before looking at the obtained spectra, our attention should first be focused on the two used polymers in this work (Figure 11; Figure 12). They both present a lot of C–O bonds and the main difference between both is the presence of sulfonate groups in heparin.

Table 4: General composition of tested samples (in %), Ti was obtained from Cédric Vranckx
bdl means *below detection limit* and "/" means that no measure was

Element (%)	Ti	C	O	N	Al	S
Ti	10.0	46.9	40.8	bdl	2.3	/
CHI	9.8	45.2	41.9	1.9	1.2	/
HEP	11.6	33.6	48.7	1.6	1.3	0.9
CHI/HEP	9.1	33.7	51.3	3.0	1.6	1.3
CHI/HEP/CHI	6.1	38	49.6	4.4	1.1	0.8
$(CHI/HEP)_3$	2.4	42.8	47.1	4.7	0.5	2.4

The chemical composition of the surface for the different samples are presented in Table 4. First, It can be seen that the amount of measured titanium decreases when adding more layers on top of the substrate. The same can be said for aluminium. The carbon percentage decreases first when adding layers and increases again for CHI/HEP/CHI and $(CHI/HEP)_3$. Nitrogen on the other hand increases steadily with additional layers as nitrogen detected on the bare titanium was below the detection limit and for $(CHI/HEP)_3$ it represents almost 5% of surface composition.

Figure 29 presents the high resolution analysis of the spectra of carbon (C1s) and titanium (Ti 2p) for the above mentioned samples. The analysis of these will be done below.

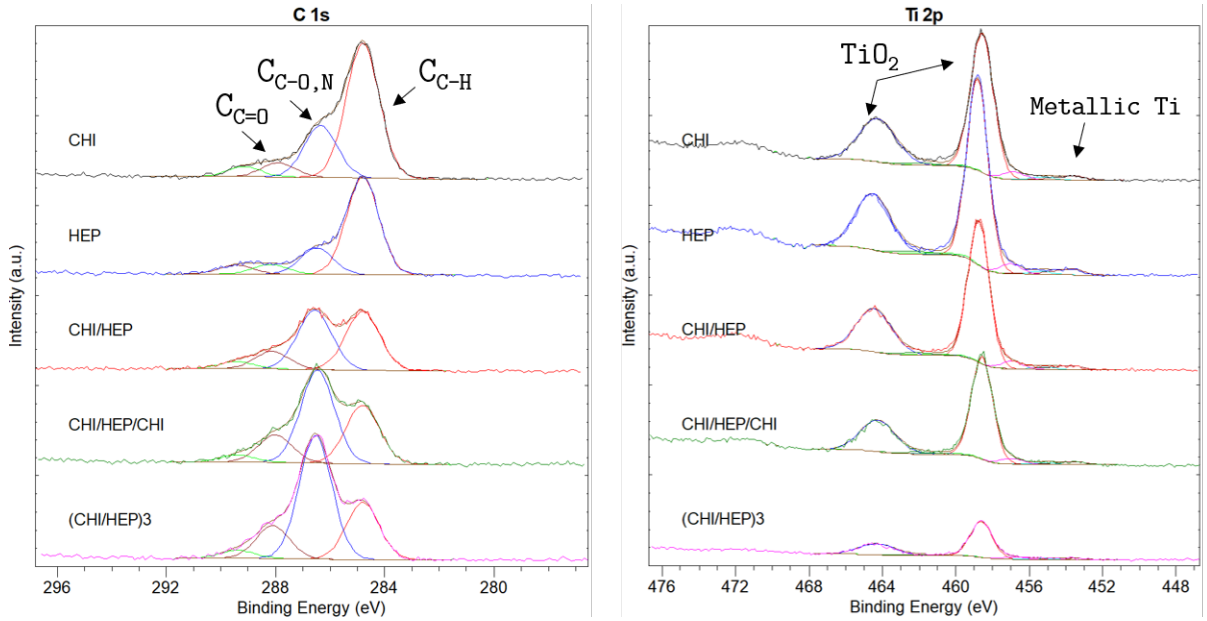

Figure 29: Obtained spectra for the peaks of C1s and Ti 2p for the different layer setups

Carbon spectra interpretation

It can be seen on Figure 29 that the carbon spectrum is divided into 3 main peaks. Most samples that have been exposed to the atmosphere will have a detectable quantity of carbon contamination. This contamination is represented here by the $C_{C\text{-}H}$ peak located at 284.8 eV. This peak decreases in intensity when additional layers are added showing us that the titanium surface is progressively covered by the layers. The second peak is that of $C_{C\text{-}O,N}$ located at 286.5 eV. By analysing Figures 11 and 12, it can be seen that a lot of C-O bonds are presents in both constitutive units. By adding additional layers on the samples, an increase in intensity should be witnessed for the $C_{C\text{-}O,N}$ peak. By comparing the conditions HEP and CHI/HEP, this increase can clearly be witnessed. For the conditions CHI/HEP/CHI and $(CHI/HEP)_3$, the intensity of the $C_{C\text{-}O,N}$ peak is higher than that of $C_{C\text{-}H}$.

The general trend seen when inspecting the spectra of carbon for the different samples is that the peak of contamination decreases while the other two peaks increase, when putting additional layers on the surfaces. This is in accordance with what was measured using the WCA (Subsection 2.4.1) and proves that chitosan and heparin are effectively alternately adhered on the titanium samples.

Titanium spectra interpretation

The titanium spectrum is here composed of two main peaks, both representing titanium oxide (Ti^{4+} doublet). At 454.1 eV a really small peak can be seen that represents metallic titanium. Because the metallic titanium peak is so small, it shows that in the first 5 to 10 nm of the samples, almost only titanium oxide is present. This again, allows to reject the obtained results with the ellipsometer. The general trend seen for the titanium oxide doublet is the same as what was seen when looking at the $C_{C\text{-}H}$ peak before; the intensity of titanium oxide decreases when additional layers are put on the titanium substrate, showing that the substrate is progressively covered by the layers. The same can be seen when inspecting the spectra of aluminium and vanadium (not shown here).

A question that could be asked now is; how do the layers form on the titanium coupons? It can be seen in Table 4 that the measured titanium decreases when adding additional layers and that the intensity of the $C_{C\text{-}O,N}$ peak increases. Two possible hypotheses can be made for the partial screening effect of the substrate; (1) The formed layers are thin and homogeneous (Figure 30.A) and we can still measure titanium through it or (2) the layers are discontinuous and form small islands (Figure 30.B). With the available information it is however not possible to make a conclusion now. To gain further insight on this subject, other tests have to be made such as angle-resolved XPS where the test sample is tilted.

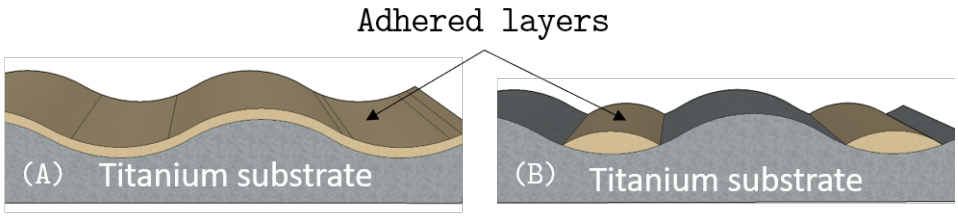

Figure 30: Schematic representation of how the multilayers could form on top of the titanium coupons. (A) The layers form homogeneously or (B) the layers fill the holes of the coupons

2.4.5 Adsorbed mass and film thickness

Since the study of film thickness by ellipsometry did not give a precise idea of the thickness of the layers, the QCM-d was used. Using the QCM-d to monitor mass changes, 3 bilayers of chitosan and heparin were adsorbed on the crystals to obtain $(CHI/HEP)_3$. Doing so, information about all the other layer setups could also be retrieved. The adsorption time of each solution was set to 30 minutes for this experiment and the flow rate was equal to 20 μL/min. The adsorption time was increased from 25 minutes to 30 minutes to be sure that the adsorption plateau of the isotherm was reached. In between each polyelectrolyte solution, ultrapure water was passed in the system during 15 minutes. Four crystals were used for this test (n = 4).

Figure 31 shows the adsorbed mass per adsorption step for the above mentioned process. An increase of adsorbed mass is seen every time the crystals are in contact with the polyelectrolyte solutions while a small decrease is seen when water is added. This can be explained by the fact that the viscosity and density of the heparin and chitosan solutions are different than that of ultrapure water. Indeed, when comparing data with the QCM-d, the values extracted between two baselines in water are of interest. Also, the ultrapure water could wash away polymers that did not adhere well to the surface.

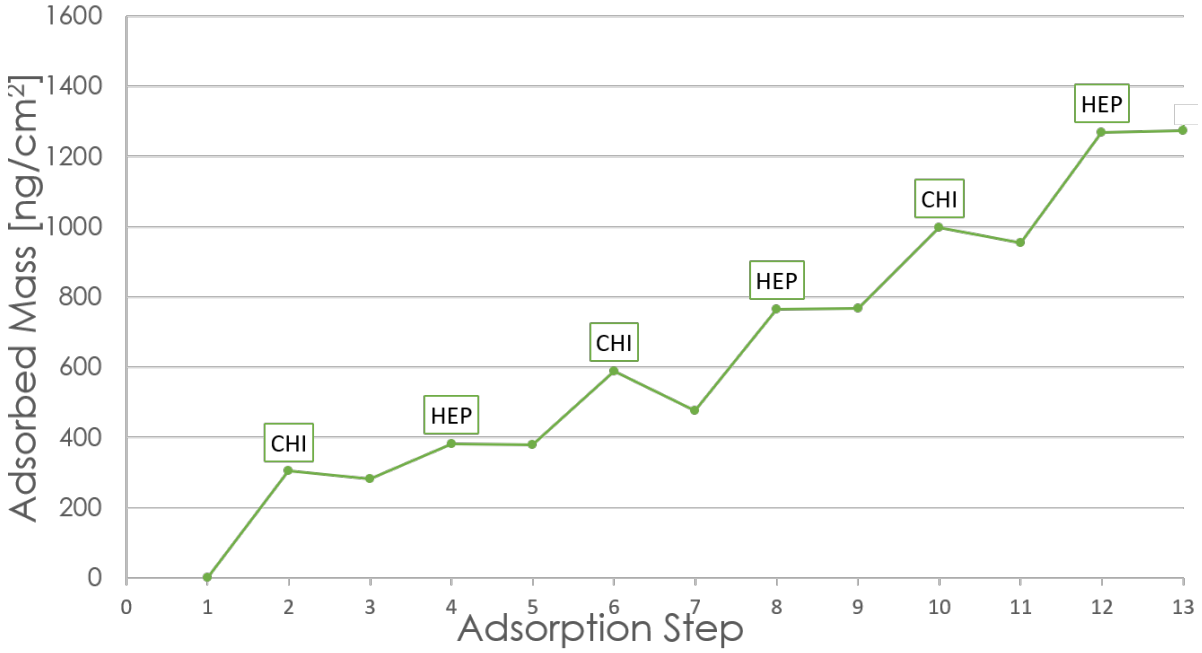

Figure 31: Adsorbed mass after each adsorption step

With the gained information about adsorbed mass, the layer thickness can be computed. Knowing that $\Delta m = \rho \cdot h$ where h is the thickness of the layer, Δm the variation in adsorbed mass and ρ is the density of the layer and is assumed equal to 1 in soft matter. Figure 32 shows the layer thickness after each adsorption step.

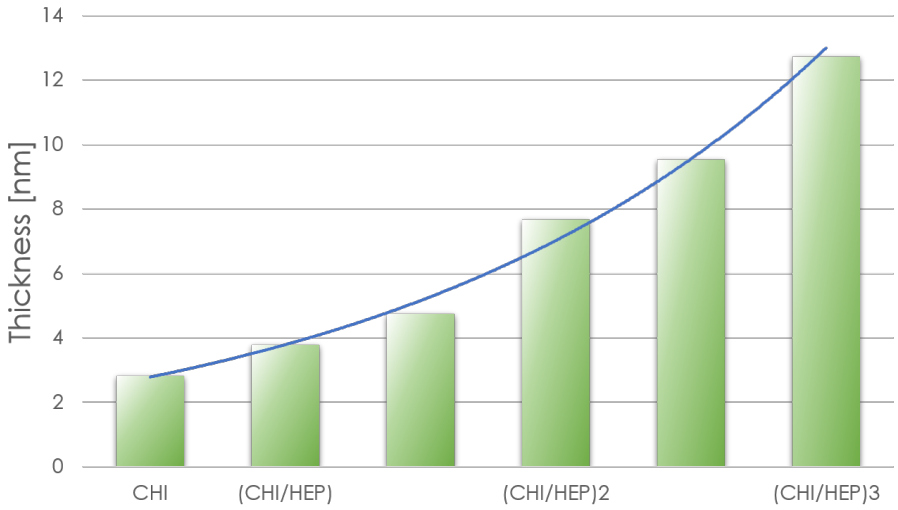

Figure 32: Layer thickness computed after each adsorption step

The first element to notice on Figure 32 is that the measured thickness is way above what was measured with the ellipsometer. It is supposed that the main difference between both analyses is that the surface roughness of the titanium coupons was too high in order to use the ellipsometer. Note also that with the ellipsometer, the layer thickness is measured in a dry state, while with the QCM-d we measure it in a wet state. Another difference is that here the polysaccharides adhere to gold and not titanium. But as mentioned before, data was also retrieved by Cédric Vranckx using titanium crystals. In Table 5, the layer thickness of both crystal types (gold and titanium) are displayed.
The second information gained by analysing Figure 32 is that the layer's thickness increases exponentially (blue curve).

Table 5: Measured layer thickness (in nm) for titanium crystals (retrieved by Cédric Vranckx using the QCM-d) and gold crystals

Adhesion step	Au crystals	Ti crystals
CHI	2.8	0.9
CHI/HEP	3.7	1.8
CHI/HEP/CHI	4.7	3.1
$(CHI/HEP)_2$	7.6	4.7
$(CHI/HEP)_2/CHI$	9.5	6.1
$(CHI/HEP)_3$	12.7	8.6

Comparing Table 5 with the results obtained in Subsection 2.4.2 shows us that the assumption made about surface roughness being the critical factor for the ellipsometry measurements is true because the measured thickness on the titanium crystals using the QCM-d is still much higher than the results obtained from the ellipsometry.
What is also seen in this Table is that the layer thickness is higher when gold crystals are used.

The QCM was also used to investigate how the next step of this work, cellular analysis, would influence the layers of chitosan and heparin. The intended purpose of the layers is to work in a physiological environment, and in particular to perform in vitro tests. First, ethanol 70% was added because when performing *in vitro* tests with cells, the samples need to be sterilised. Then, PBS and cellular medium (MEM-α) were added to the QCM-d to investigate if the layers would behave normally. Ethanol (70%) was added during 30 minutes. Then, PBS was added to the QCM during 15 hours. PBS is a solution in which the osmolarity and ion concentration match that of the human body. Finally, MEM-α was added during 6 hours because when doing cell culture on the titanium substrates, the cells are kept in this solution so that they can grow adequately. During these steps, the adsorbed mass was monitored and the measured values of the adsorbed mass are showed on Figure 33.

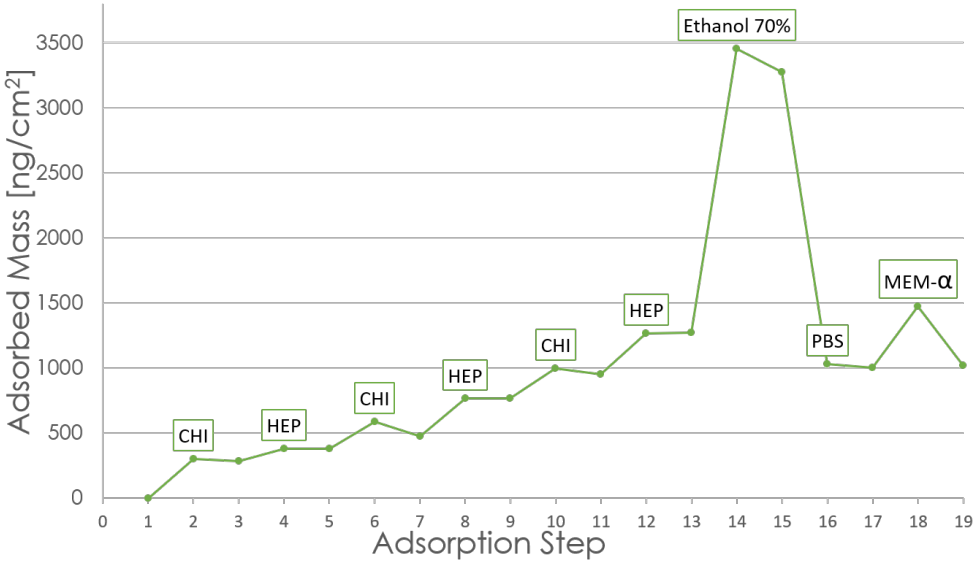

Figure 33: Adsorbed mass after each adsorption step including ethanol, PBS and MEM-α

It can be seen that there is a big adsorption peak when ethanol is added. This can be explained by the fact that, when using the QCM, the frequency and dissipation shifts are both proportional to the square root of the product of liquid viscosity and density. Since the QCM is sensitive to the properties of the bulk liquid, a reference measurement is performed before the experiment starts (Reviakine et al., 2011). Here, this was done with ultrapure water. Because ethanol has a different density and viscosity than water, the increased adsorbed mass may not be taken into account as these values are not comparable with the other obtained values. It can also be seen that when other solutions are added afterwards, the adsorbed mass comes back to values before adding ethanol. When adding PBS and MEM-α, after rinsing, the layers seem not to have changed as the adsorbed mass remains the same. These measurements show us that there is good hope that the layers will not be removed when used for cell culture.

2.5 General discussion on surface characterisation

Surface analysis and characterisation allowed to collect information about the tested samples and the different layer's conditions. With all this information, differences between the different layers could be witnessed. The most important results will be listed below.

The wettability of the different layers was first tested. Differences between the conditions were seen and a saw-tooth trend was identified when alternately adding chitosan and heparin, which highlights the succes of assembly. The measured contact angles for the final condition, $(CHI/HEP)_3$, is in the wanted range for efficient cell adhesion (Lee et al., 1998). It was also seen that with passing time, the contact angle measurements increased. This was not the case when enough layers were adhered to the titanium substrate. This may lead us to believe that the layers protect the substrate from contamination from the surrounding.

To measure the film thickness, the ellipsometer was first used. Because the hypotheses made when using this device were not investigated beforehand, the obtained results were disappointing. To verify these assumptions, the Atomic Force Microscopy was used. This allowed us to obtain a visual representation of the surface's morphology and topography. Thanks to the AFM, we could see that the initial titanium surface was rough and that the assumptions made for the ellipsometer had to be rejected. The AFM also allowed us to measure the surface roughness using the root mean square average, Rq. It was then seen that with increasing the amount of layers, the surface roughness tend to decrease; however, the deposited layers are very thin compared to the substrate's roughness and their visualisation by AFM is almost impossible.

After that, the chemical composition of the surfaces were investigated. The general conclusion is in accordance with the WCA measurements. The chemical signature of chitosan and heparin is well identified after their deposition on titanium. After analysing the surface chemistry, one question remains about how the layers form on top of the titanium coupons. Further tests are required to answer this question.

Finally, with the QCM, the adsorbed mass and the layer's thickness could be measured and computed using gold crystals. The obtained values were compared to the data obtained with titanium crystals. After forming three bilayers, the layer thickness of $(CHI/HEP)_3$ equals approximately 13 nm. It was also found that the layer's thickness increases exponentially.
Also, with the next steps of this master thesis in sight, the crystals with the layers on top of it were put in contact with ethanol 70%, PBS and MEM-α to see how the layers would behave in such media. They were shown to be stable in such conditions.

3 Study of cell behaviour

The last chapter of this thesis is dedicated to the study of cell behaviour on the previously characterised surfaces. To this end, cells will be cultivated on the chitosan and heparin films while cell adhesion, viability and proliferation will be studied.
The first part of this Section will explain which materials and methods were used for cell culture. Then, the tests that were performed to measure cell viability, proliferation as well as adhesion will be explained. Finally, the obtained results will be presented and discussed.

3.1 Choice of cells

The first thing to do before analysing cell behaviour is to choose the type of cell that will be used in this work. In the context of human bone cell analysis there are three types of cells that are most often used; MG-63 – MC3T3-E1 – SaOs2.

MG-63 is a human osteosarcoma cell line derived from a 14 year old male. These are cancerous cells and they produce immature bone (Shriver, 2012; Merck, 2019a).
SaOs2 is also a human osteosarcoma cell line derived from an 11 year old Caucasian girl (Merck, 2019a). These cells posses several human osteoblast (HOb) like features which justify why they are often chosen for HOb-like analyses (Rodan et al., 1987).
The last cell line that was investigated is **MC3T3-E1**. These are preosteoblasts coming from mice calvaria. Subclones 14 of MC3T3-E1 was selected because of its high osteoblastic differentiation (ATCC, 2016).

The main purpose of this Section is to analyse cell viability and proliferation of the potentially chosen cells on the previously made multilayers. Because the ultimate goal of this work is to use the prosthesis with its coating inside of the human body, the chosen cell line should act in a similar way as HOb for the tested properties. Czekanska et al. studied these three cell lines in 2013 and compared their responses to those of HOb. Their final conclusion can be seen in Table 6.

Table 6: Comparison of three cell lines (MG-63, SaOs2 and MC3T3-E1) with human osteoblasts (HOb). (Modified from Czekanska et al., 2013)

Cell line	Proliferation	Gene expression	ALP activity	Mineral deposition
MG-63	–	–	–	–
SaOs2	–	++	++	+
MC3T3-E1	++	–	++	++

As said before, what is of interest here are cell proliferation and viability. The only cell line that has a similar proliferation rate compared to HOb is MC3T3-E1.

It was shown by Pautke et al. in 2004 who compared MG-63 and SaOS2 to HOb that osteosarcoma cell lines revealed a 2 to 3-fold greater mean doubling-time and a 15 to 20-fold higher saturation density than HOb. Czekanska et al. also showed that after 7 days, a significant difference was measured when comparing the proliferation of SaOs2 and HOb. For MG-63, the difference was already significant after 2 days. Both have a larger proliferation rate than HOb. For MC3T3-E1 cells, cell proliferation stays consistent with HOb up to 10 days (maximum analysed time). Because of the studied discrepancies between HOb and both MG-63 and SaOs2, both cell lines have been discarded in this study.

Because a cell proliferation like that of HOb is the most important factor, the chosen cells are MC3T3-E1 (ATCC, MC3T3-E1 subclone 14, CRL-2594^{TM}, ATCC). The bought cell vial contained approximately 1 mL of solution with $8.8 \cdot 10^5$ cells. Also, the cells came in passage 15, in this work this will be referred as "P". For example, after passaging cells two times they will be named as "P+2".

3.2 Cell culture

Before using the cells for analysis, several steps need to be taken such as: thawing the newly bought cells as well as culturing and passaging them to ensure that enough cells are available for the experiments. Cell culture requires sterile conditions to avoid any form of contamination (bacteria, etc). Therefore the steps explained below were all executed under a sterile hood with vertical laminar flow.

Thawing process of the cells

The MC3T3-E1 cells were acquired frozen in a cryogenic tube and were kept in a liquid nitrogen tank ($<$ – 130°C). Before freezing the cells, a cryoprotectant is added that protects cells from dying during the freezing process. In this case DMSO was used to reduce the ice formation during freezing. Because the cryoprotectant is toxic for the cells, it must be removed quickly after the thawing process. Thus, before using the cells we must thaw them and remove the DMSO.

Once the cells were removed from the liquid nitrogen tank, thawing must be done quickly to prevent cell damage. The cells were directly put in a water bath at 37°C until the ice crystals in the cryogenic tube were almost gone. The solution containing the cells was then transferred into a Falcon tube and 5 mL of cold culture medium was added. In the meantime, the temperature of the centrifuge (Eppendorf, 5810R) was set at 4°C. Once the required temperature was reached, the cells were centrifuged. Then the supernatant, containing DMSO, was decanted and the sediment in the Falcon only contained MC3T3-E1 cells. Then, 6 mL of culture medium at 37°C was added drop by drop so as to not shock the cells. This solution was then mixed thoroughly using a pipette and transferred

into a cell culture flask (Corning Incorporated, Corning, USA) of 25 cm^2 made of polystyrene (TCPS; tissue culture grade polystyrene). The flask was then put inside of the incubator (Thermo Scientific, Direct Heat CO_2 Incubator, 311 S/N) at 37°C and 5% CO_2.

Cell culture

To allow cells to proliferate, they must be cultured within an adequate culture medium. In this study, the culture medium is mainly made of MEM-α (Gibco, A10490-01). MEM-α stands for Minimum Essential Medium and contains L-glutamine, ribonucleosides and deoxyribonucleosides.
MEM-α contains no proteins, lipids, or growth factors. Therefore, additional solutions must be added so that the cells can proliferate normally. First, Fetal Bovine Serum (FBS; Merck, Darmstadt, Germany. F7524) is added (10%). FBS provides nutrients, growth and attachment factors and protects cells from oxidative damage and apoptosis by mechanisms that are difficult to reproduce in serum-free media (SFM) systems (Merck, 2019a). Then, penicillin-streptomycin (ThermoFisher, 15140-122) is added (1%) to prevent bacterial contamination of cell cultures due to their effective combined action against gram-positive and gram-negative bacteria. Lastly, sodium pyruvate (Merck, Darmstadt, Germany. S8636) is added (1%) as a carbon source in addition to glucose. Note that phenol red is contained in the MEM-α medium to identify changes of pH. The intial pH of MEM-α is the physiological pH ($\sim$ 7.4). When the red colour turns to yellow, the pH lies below 6.8 while when the colour turns to purple, the pH lies above 8.2. The pH should remain around 7.4.
The cells are cultured in polystyrene culture flasks of 25 cm^2 or 75 cm^2 (Corning Incorporated, Corning, USA) in function of how many cells are seeded in it and each flask contains 6 or 18 mL (respectively) of the above mentioned culture medium.
The culture medium was changed every 2 to 3 days.

Cell passage

When the cells are confluent, or close to confluence ($> 80\%$), they need to be passaged. To do so, the cells that adhered to the surface of the flask need to be detached. First, the cell medium is removed from the culture flask and 1 mL of preheated trypsin (Lonza 17-161E, 1:125 Cell Culture Reagent) at 37°C is added (3 mL for 75 cm^2 culture flasks). Trypsin allows to dissociate cells from themselves and from the flask by breaking down adhesion proteins and extracellular matrix. The flask, containing 1 mL of trypsin, is then inserted 5 minutes in the incubator at 37°C and 5% CO_2. After that, the detachment of the cells is controlled by using the optical microscope. If less than 90% of the cells are detached, we can hit the culture flask to detach the remaining cells. In the case of flasks of 25 cm^2, 3 mL of culture medium is then added to deactivate the trypsin (8 mL for 75 cm^2 culture flasks). The whole solution containing the detached cells is transferred to a Falcon tube and is then centrifuged. Again, the supernatant is decanted and the sediment, containing the cells, remains. These are finally resuspended in culture medium and seeded in a new culture flask. To know in how many culture flasks the cells must be divided, the amount of cells can be counted using the counting technique of

Bürker. This technique is explained below. Generally, after counting, $7.5 \cdot 10^5$ cell were seeded in a 25 cm^2 culture flask and $2 \cdot 10^6$ cells in a 75 cm^2 culture flask.

Cell counting

Knowing how many cells are present in a given volume is required before starting the experiments. To this end, the counting technique of Bürker was used.
Counting cells is done after the cells reached confluency in the culture flask. The cells are first detached using trypsin in the same way as explained above, and then resuspended in culture medium. Thereafter, 20 μL of this solution is transferred into a small tube together with 20 μL of trypan blue (Merck, Darmstadt, Germany. T8154). This solution is thoroughly mixed and brought to the Bürker cells. The Bürker cell is composed of two counting squares, one on each side of the slide. On Figure 34, one of these two counting cells is represented. It is composed of one big square that is divided in 9 smaller squares of 1 mm^2 each, all separated by triple lines. Each of these are again subdivided into 16 smaller squares of 0.04 mm^2, separated by double lines, as can be seen on the right image of Figure 34. To evaluate the amount of cells in a given volume, the user has to visually count the number of cells in the 4 green squares on Figure 34, located in the corners. The cells are visible thanks to the trypan blue.

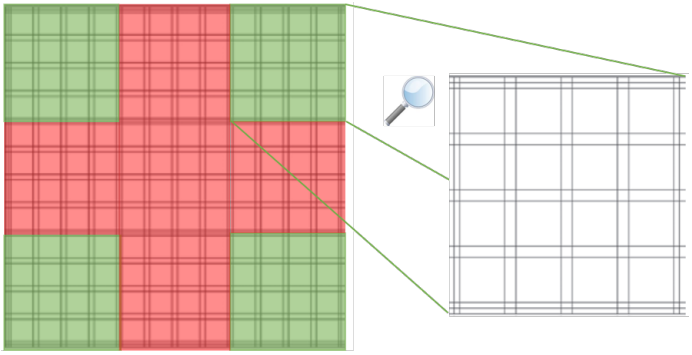

Figure 34: Counting cell of Bürker (modified from Brand, n.d.)

Note that this method gives an estimate of the total amount of cells in a given volume. The user can make counting mistakes and the solution used in the Bürker cells can not be fully homogeneous if not mixed correctly.
Once the amount of cells is counted in the 4 corner squares of both counting cells, the mean of those 8 values is taken and the following formula is used to find the amount of cells per mL:

$$\#\text{ of cells per mL} = \frac{\text{Counted cells} \cdot F}{10^{-4}}$$

Where F is the dilution factor and equals 2 in this case because the tested solution contains 20 μL of both trypan blue and culture medium. The value of 10^{-4} equals the counting surface times the depth of the counting cell: 1 $mm^2 \cdot 0.1$ mm $= 0.1$ $mm^3 = 10^{-4}$ mL.

To obtain the amount of cells in the initial solution, the value found per mL is then multiplied by the volumine in mL from which the cells were initially taken.

This counting technique is very useful when cells have to be frozen or passaged. It allows to adequately control the amount of cells that are placed in the cryogenic tubes or in the culture flasks.

Cell freezing

After counting the cells, it is possible to freeze a certain amount of them. In this work, this was done at passages P+1, P+2 and P+3. Choosing to freeze cells is judicious because it ensures a supply of cells adapted to the timing of the experiments as well as a backup when an experiment fails. It is then possible to repeat the experiment with cells in the same passage as first tested.
The protocol to freeze cells is the same as the one described by the provider (ATCC). This means that when the cells with culture medium are centrifuged, after reaching confluency, and that they are kept at the bottom of the Falcon tube, culture medium containing 10% DMSO (Merck, Darmstadt, Germany. 276855) is added drop by drop. Remember that DMSO protects cell from dying when freezing but is also toxic for cells at ambient temperature. This step is thus done on ice to reduce the temperature at which the cells are in contact with DMSO.
Considering that the cells were counted before freezing, the total amount of cells in the sediment before adding culture medium containing DMSO is known. When freezing, it is recommended to place $5 \cdot 10^5$ cells per cryogenic tube. These tubes can contain 1 mL volumes. Thus, if for example $2 \cdot 10^6$ cells were counted, then 4 mL of medium + DMSO will be added to the tube. This solution is then mixed thoroughly to obtain an homogeneous solution and 1 mL is pipetted in each cryogenic tube. These tubes are then put in a freezer at – 80°C (Eppendorf, Ultra low temperature freezer U101 Innova) for 1 day and then in the liquid nitrogen tank (Taylor-Warton, 4800 RS series).

Cell passage in this master thesis

As mentioned before, the cells are passaged to have enough cells for the tests and to be sure to have a backup of cells when something unexpected happens. In this work, the following was performed: at every passage, some cells were frozen and the remaining cells were further passaged. The experiments were started when the cells arrived at passage P+3 (remember that P is the initial passage at which the cells were retrieved, P = 15) we started the experiments. The whole cell handling is represented in Figure 35. Icons of a freezer implies that the cells were frozen, a 24 well-plate means that these cells were used for experiments and a garbage bin represents the fact that the excess of cells was thrown away. Also, the small culture flasks are flasks of 25 cm^2 and the big one is of 75 cm^2.

After reaching P+3, the cells were passaged without freezing anymore. This was done to ensure that unfrozen, living cells were available if needed. Because this was not the case, after reaching P+5 they were thrown away.

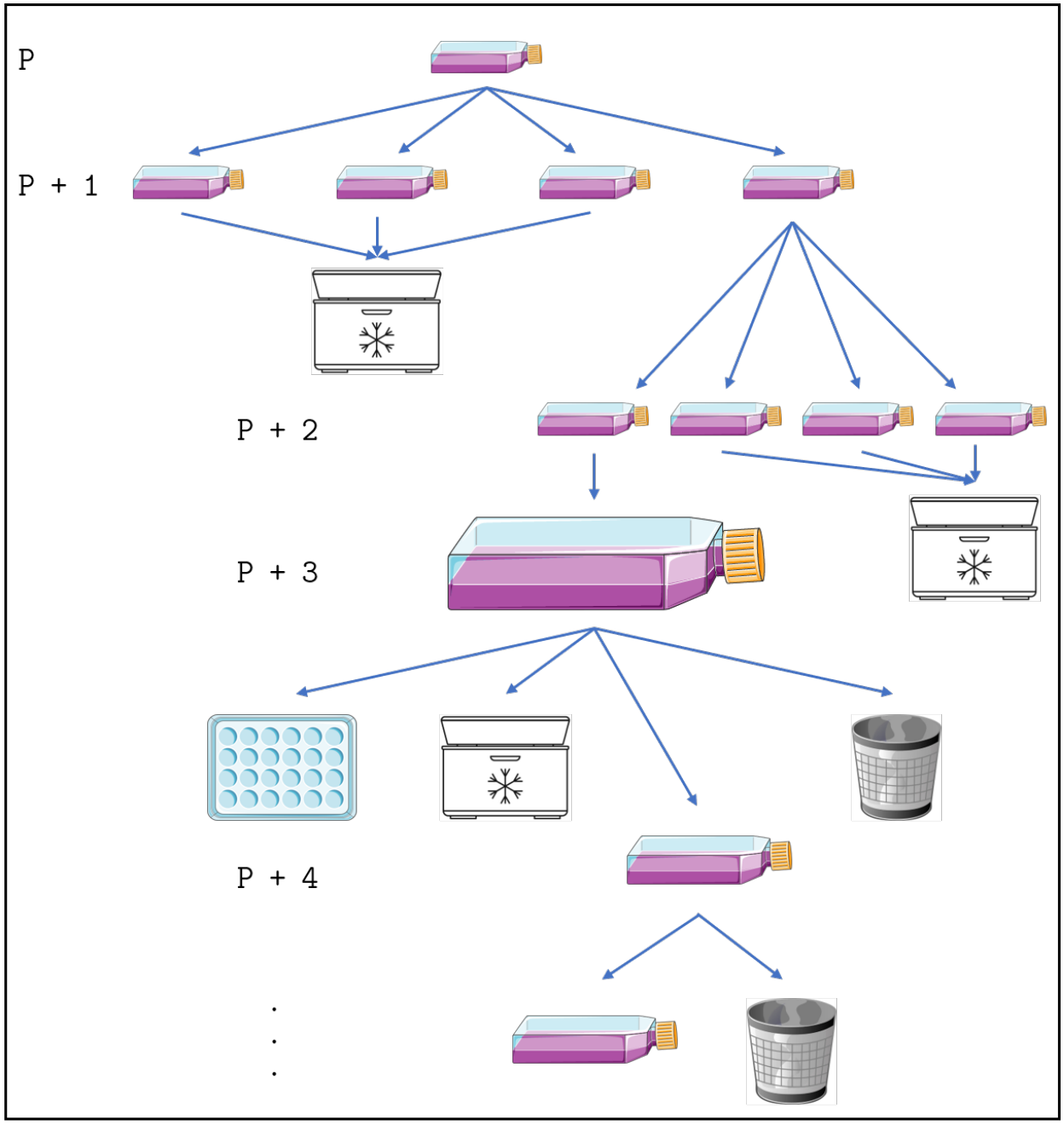

Figure 35: Tree diagram representing the passage, cell freezing and cells chosen for the experiments in this work

3.3 Preparation of samples for cell analysis

After understanding how cell culture works, we will first look at which samples were used to study cell behaviour.
As mentioned before, this work fits into a wider research work. Because other conditions were more favourable in Cédric Vranckx's PhD thesis for the formation of chitosan and heparin LbL multilayers, the conditions will be changed for this Section as well. In his thesis, functional proteins of interest in orthopaedy are adhered on "a cushion" made of three bilayers of chitosan and heparin, $(CHI/HEP)_3$. In that work, the pH used is of 3.5 because the cushion formation is optimal at that pH. Therefore, for cell-based experiments the pH of construction of the LbL films will be changed to 3.5.

When analysing cell behaviour, a negative control and a positive control are required. The negative control here will be bare titanium while for the positive control two different samples are used. MC3T3-E1 cells are known to grow well on TCPS and glass. Both surfaces are often used in the literature for these cells. Because the opinions were divided, we chose to use both as positive samples. TCPS is the material from which the multiwells are made, there is thus no preparation required for this condition. The glass samples have a diameter of 15 mm and fit exactly in the wells having a diameter of 15.6 mm.
All the conditions are depicted on Figure 36. Again, the layer setups changed with the thesis' work in mind. The condition CHI/HEP/CHI was kept because it was used throughout the whole study, $(CHI/HEP)_3$ is also kept because it is the most important condition. A new condition is added, $(CHI/HEP)_2CHI$ to obtain information about the influence of the last layer of the film on cell behaviour.

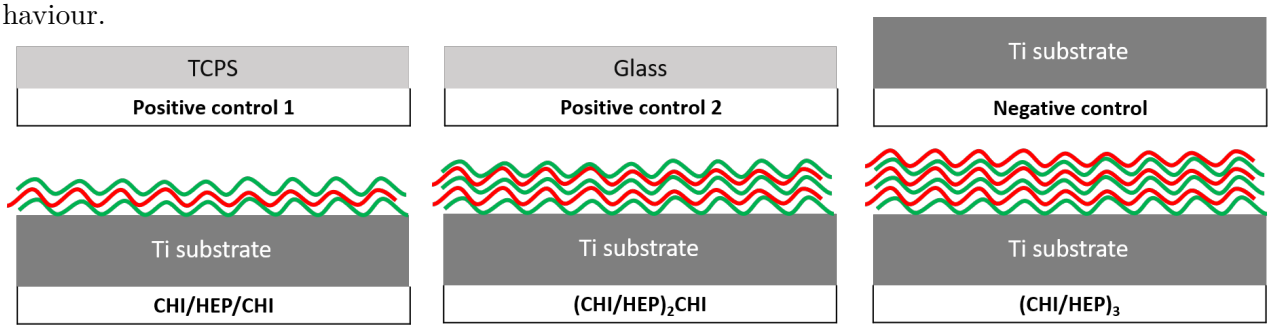

Figure 36: Different samples used for cell analysis

These samples were prepared as was explained in Subsection 2.2 except that the layers are constructed at pH 3.5. Once they are ready, the titanium coupons are transferred into a 24 well-plate. The wells for the condition TCPS are empty and a glass coupon is put into the wells of condition "Glass". Before using these samples for cell culture, it is first required to sterilise them. This was done by submerging all the samples in ethanol 70% during 30 minutes under the sterile hood. Then, ethanol was removed from the wells and the samples were let to dry. Once the samples were dry, they were seeded with cells (20000 cells/well) together with 1 mL of culture medium.

3.4 Study of cell behaviour

The last step of this master thesis is to analyse cell behaviour on the above-mentioned samples. To do so, three techniques will be used; AlamarBlue, CyQUANT and FAK100. The first one will allow us to obtain information about cell viability on the different samples while CyQUANT is a cell proliferation assay that quantifies the DNA of the cells. Lastly, using the FAK100 which is a kit for fluorescence staining, it will be possible to obtain images of the cells grown on the different samples.

3.4.1 Cell viability assay - AlamarBlue

The AlamarBlue assay allows us to quantitatively measure cell viability and activity. It contains an oxidation-reduction reagent, resazurin, that works as a cell health indicator. Upon entering cells, resazurin undergoes a colorimetric change in response to cellular metabolic reduction because viable cells maintain a reducing environment within their cytoplasm (ThermoScience, 2012). The reduced form of resazurin is called resorufin and is highly fluorescent (red). This assay is very convenient because resazurin is non-toxic, cell-permeable and is weakly fluorescent (blue). (Merck, 2019a).
Thus, changes in cell viability can be monitored using either an absorbance or fluorescent based plate reader. In this work, it was decided to measure the changes using a fluorescent based plate reader (Tecan, Infinite 200Pro) to obtain a better signal. The fluorescence was monitored using an excitation wavelength at 560 nm and emission wavelength at 590 nm.

Because the AlamarBlue assay (ThermoFisher, DAL1100) is non-destructive, measurements can be performed at different time steps on the same sample. Here, this was done at day 1, day 4 and day 7 after seeding the samples with cells. For statistical analysis, 4 samples were prepared for each condition (n = 4).

To measure cell viability on the samples, the substrates with cells on were first washed once with PBS (ThermoFisher, 18912014). In the meantime, freshly made culture medium was preheated at 37°C and the AlamarBlue (ThermoFisher, DAL1100) reactant was filtered. Thereafter, the filtered reactant was added to the warm culture medium to obtain a concentration of 5% (v/v). Each sample was then submerged in 1 mL of this solution. This step had to be very precise and a pipette, P1000 (Gilson, F123602), was used. The well-plate containing the samples submerged in the AlamarBlue solution was then put 4 hours in the incubator at 37°C and 5% CO_2.
After 4 hours, 3 times 100 μL were withdrawn from each well and put in a black 96 well-plate (Greiner Bio-One, 655076). The samples are then put again in the incubator and the 96 well-plate is read using the fluorescent reading machine. If there are no problems with the obtained results, the cells are washed 2 times with PBS and culture medium is transferred in each well before putting the plate back in the incubator.

Note that because the AlamarBlue assay quantifies cell metabolism, the obtained values can be interpreted in several ways. We could for example obtain the same values for two samples that have: (1) many cells with a low metabolism or (2) fewer cells with a high metabolism.

To be able to make a distinction between those two cases, the CyQUANT proliferation assay was conducted.

3.4.2 Cell proliferation assay - CyQUANT

To quantify cell proliferation and cell density, the CyQUANT (ThermoFisher, CyQUANT Cell Proliferation Assay Kit) assay was used. The difference with the AlamarBlue assay is that CyQUANT does not rely on metabolic activity of the cells but it depends directly on the quantity of DNA. Indeed, the used dye in this assay, CyQUANT GR dye, exhibits strong fluorescence enhancement when bound to cellular nucleic acids. It allows the user to directly quantify the entire cell population within a broad linear detection range. This assay allows to measure cell quantity from 50 up to 50000 cells using a pre-established standard curve.
The fluorescence is here also read with a fluorescent microplate reader (Tecan, Infinite 200Pro). The excitation wavelength was set at 480 nm and the emission wavelength at 520 nm.

Creating the standard curve

A standard curve is established to allow fluorescence measurements to be converted into a number of cells. To make this curve, a concentrated cell suspension containing 10^6 cells in 1 mL of culture medium was prepared. After centrifuging this solution, the supernatant was discarded and the cells were frozen at –70°C without additional treatment.

The reagent for all the CyQUANT experiments is then prepared and contains ultrapure water in which cell-lysis buffer (1x20) and the CyQUANT GR dye (1x400) are diluted. The volume of this solution was chosen knowing that each well requires 200 μL of solution.

To start the experiment, the cells are thawed at room temperature. Then, 200 μL of reagent is added to the thawed cells and a dilution series is performed in the wells of the microplate. This was done so that in each well a specific amount of cells was present. The specific amount of cells per well is represented below:

50000 – 25000 – 12500 – 6250 – 3125 – 1560 – 780 – 390 – 195 – 98 – 49 – Control

This was performed 3 times (n = 3) for statistical analysis. Also, reagent was added in each well to obtain a total volume of 200 μL per well.

Protocol followed for the proliferation assay

At the same time as creating the standard curve, we performed the proliferation measurements on the different samples. This was a bit more tricky than expected because the cells had first to be detached from their respective surface. To do so, 600 μL of trypsin solution was added in each well. After 5 minutes in the incubator, the cells are normally detached from the samples. To be sure that as many cells as possible are detached from the different surfaces, we scraped the surfaces of the samples with the tips of the pipette. For each sample, the totality of trypsin solution containing the cells was then transferred in an Eppendorf. These were centrifuged and the supernatant was discarded. Again, to ensure that the totality of cells was transferred to the Eppendorf, the different samples were washed two times with 600 μL of PBS according to the same process as explained above. After discarding the supernatant of the Eppendorf after the last washing step, the cells were frozen at –70°C.

When all the cells from the different samples were acquired, the proliferation assay could be performed. The steps followed are the same steps as for the standard curve. After thawing the cells at ambient temperature, 200 μL of the reagent were added in each Eppendorf. After thoroughly mixing the solutions contained in the Eppendorf tubes, they were transferred in a black 96 well-plate and were read using the fluorescent microplate reader.
For statistical analysis, 3 samples were made for each condition (n = 3). The measurements were performed 7 days after seeding the samples with cells.

3.4.3 Immunofluorescent staining - FAK 100

The immunofluorescent staining kit (actin cytoskeleton/focal adhesion staining kit. Merck, Darmstadt, Germany. FAK100) is used to obtain images of the cells on the different samples. This kit contains vinculin monoclonal antibodies, TRITC-conjugated phalloidin and DAPI.
The **vinculin monoclonal antibodies** will be used to image the focal adhesion and adherent junctions that serve for actin filaments. Focal adhesions consist of integrin-type receptors that are attached to the extracellular matrix and are intracellularly associated with protein complexes containing vinculin, talin, α-actin, etc (Merck, 2019b). The visualisation of focal adhesion is made possible using a green fluorescent-labeled anti-mouse secondary antibody (Millipore, FITC conjugated, AP124F) that will attach to the vinculin antibodies.
TRITC-conjugated phalloidin is used to image the actin cytoskeleton. Actin's function is to mediate a variety of essential biological functions in eukaryotic cells, including intra- and extra-cellular movement and structural support (Merck, 2019b). To do so, the organisation of the actin filaments is highly regulated. Phalloidin is used here to map the local orientation of actin filaments within cells and shows high red fluorescence.
The last component used for fluorescent staining is **DAPI** (vectashield, antifade Mounting Medium with DAPI). DAPI is a fluorescent blue stain that binds strongly to DNA regions that are rich in adenine-thymine. It will allow to see the nucleus of cells stained in blue.

Sample preparation for fluorescence imaging

Before staining our different samples, several solutions were prepared and are listed below:

- Fixative solution: 4% paraformaldehyde
- Wash buffer: 1x PBS containing 0.05% Tween-20
- Blocking solution: 1% BSA in 1x PBS
- Permeabilising reagent: 0.1% Triton X-100
- Anti-vinculin: monoclonal vinculin antibody 175x in the blocking solution
- TRITC-conjugated phalloidin solution: 100x TRITC in PBS

Before staining the different parts of the cells, several steps have to be taken. First, we need to fix the cells. Fixation of cells allows to preserve cells in a “life-like state” (Rolls, n.d.) and to stain them for later microscopic visualisation. This was done using the fixative solution of 4% paraformaldehyde. The samples were submerged during 30 minutes at ambient temperature in this solution and washed two times using the wash buffer thereafter.
After fixation of the cells, the cells were permeabilised with the permeabilising reagent. This was done because when fixating the cells, the plasma membrane is still intact, making intracellular targets inaccessible. The permeabilising reagent removes different molecules from the cellular membrane, making various pore sizes in the membrane and allowing the passage to intracellular staining (Ken, 2017). The samples were submerged 5 minutes in 200 μL of this solution and were again washed two times with the wash buffer.
The samples were then submerged during 1 hour in 400 μL of blocking solution. This has for effect to "block" the sample in order to reduce non-specific binding, preventing the dyes to link to inappropriate structures (Held, 2015).
The anti-vinculin solution is then used to attach the focal adhesion sites. For this, 200 μL of solution is put on each sample during 1 hour at ambient temperature. Thereafter, the samples are washed 3 times with the wash buffer.
The TRITC-conjugated phalloidin solution is then applied to the samples to mark the actin filaments in red. This solution also contained the secondary antibodies that will attach to the vinculin antibodies and dye the focal adhesion green. Again, 200 μL were used during 1 hour at ambient temperature and the samples were washed 3 times with the wash buffer.

The glass sample and the titanium coupons were then clamped between two microscope slides using Patafix (UHU, Patafix) as can be seen on Figure 37. Before closing this structure with the second microscope slide, 20 μL of the vectashield solution was deposited on each sample.

These constructions were then stored at 4°C, away from light. Once that all the samples were prepared, it was possible to visualise the stained parts of the cells using epifluorescence microscopy. *Epi* means that the samples are illuminated from the same side that as the user of the microscope sees. This had to be done because titanium coupons are opaque. The images were obtained 7 days after seeding the samples with cells and the microscope that was used for this is the Olympus IX71.

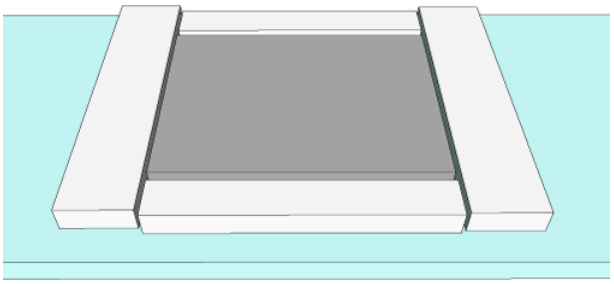

Figure 37: Sketch of how the samples were clamped between two slides. Light blue is the slide, white is the Patafix and grey is the sample. The second slide is deposited on this construction to close the whole structure.

3.5 Results and discussion

In this Subsection, the results obtained with the previously explained techniques will be presented and discussed.

3.5.1 Comparison of cell viability

Cell viability was monitored through the AlamarBlue assay. As stated above, measurements were performed at day 1, day 4 and day 7 after seeding the samples with cells. The obtained results can be seen on Figure 38 for day 1 and on Figure 39 for day 4 and 7. Three measurements were performed for each sample and four samples were prepared per condition. These two figures represent mean ± standard deviation of the measured fluorescence for the different conditions. Two Figures had to be drawn because the arbitrary units do not have the same meaning on day 1 vs day 4 and day 7, as the gain of the spectrometer was not kept constant. The results in Figure 38 were indeed obtained with a gain of 103 while the ones of Figure 39 were obtained with a gain of 91 and no link was found between the gain and the measured fluorescence.

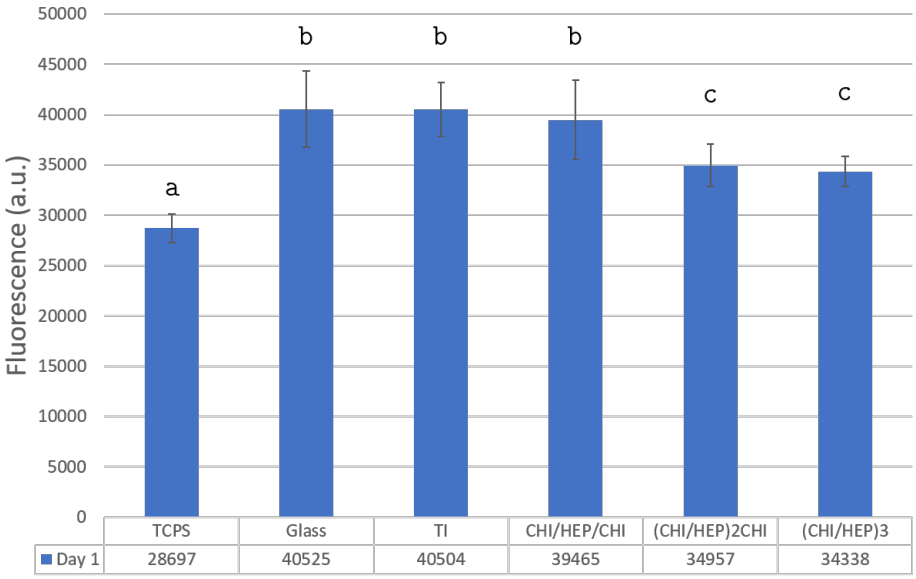

Figure 38: Fluorescence measured with the AlamarBlue assay for the different conditions after 1 day - statistically equal measurements are represented by the same letter

Remember that TCPS and glass were taken as positive controls and the condition Ti was the negative control. Also, 20000 cells were seeded on each sample.
By inspecting Figure 38 it can be seen that the measured fluorescence seems quite equal for all the samples except for TCPS. Indeed, using the Student's T-test ($\alpha = 0.01$), it was found that the measured fluorescence for the condition TCPS is statistically different ($p < 0.01$) from the other samples as its measured fluorescence lies way below the other conditions. The values having the letter *"b"* above them are computed as statistically equal. This means that after 1 day, no significant difference is measured between the conditions Glass, Ti and CHI/HEP/CHI.

The same can be said for the samples having the letter *"c"*, $(CHI/HEP)_2$ and $(CHI/HEP)_3$.
The values are thus slightly lower for these two latter samples, but still higher than the one recorded on TCPS.

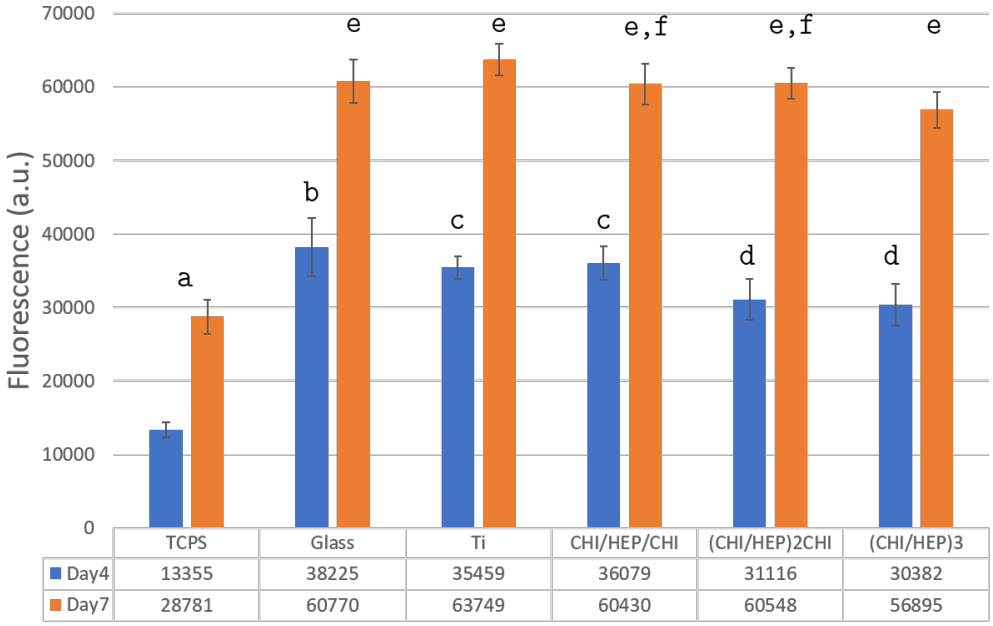

	TCPS	Glass	Ti	CHI/HEP/CHI	(CHI/HEP)2CHI	(CHI/HEP)3
Day4	13355	38225	35459	36079	31116	30382
Day7	28781	60770	63749	60430	60548	56895

Figure 39: Fluorescence measured with the AlamarBlue assay for the different conditions after 4 days and 7 days - statistically equal measures are represented by the same letter

By looking at Figure 39 it can be seen that the trend present at day 1 is still there at day 4 and 7. Indeed, the fluorescence of TCPS at day 4 and day 7 is still way below the other conditions. The other conditions still seem quite equal.

Day 4

Doing the same statistical analysis as before, it was computed that the difference between Ti and CHI/HEP/CHI was not statistically different. The same was perceived for $(CHI/HEP)_2$CHI and $(CHI/HEP)_3$. It seems that after 4 days, the condition "Glass" is the most adequate for cellular viability. Then comes Ti and CHI/HEP/CHI and finally $(CHI/HEP)_2$CHI and $(CHI/HEP)_3$.

Day 7

After 7 days, all the samples were statistically equal to the glass condition (*"e"*), except TCPS. Also, the difference between CHI/HEP/CHI and $(CHI/HEP)_2$CHI was not statistically significant showing that the last deposited layer of a multilayer produces a similar response for cell activity.

The first conclusion that can be made is that TCPS can not be used as a positive control sample for MC3T3-E1 cells. Glass on the other hand is appropriate.

By comparing the measured fluorescence after 4 days of our samples with that of glass, it seems that glass is a better surface for cell viability as the difference is statistically significant ($p < 0.01$).
After 7 days though, the difference between glass and the other conditions is not statistically significant anymore ($p > 0.01$). It thus seems that after 7 days, cell viability on the tested surfaces is as good as on the positive control. These results are encouraging since the coatings do not have a cytotoxic effect as revealed by the test.

3.5.2 Proliferation on different samples

Cell proliferation was monitored through the CyQUANT assay. As mentioned before, the measurements are performed 7 days after 20000 cells were seeded on the different samples.

Once the data retrieved with the fluorescence plate reader, the standard curve was established. Normally the standard curve should give us a linear regime to detect cells from 50 to 50000, above that we enter a non-linear regime and cell number can not be retrieved with this liner standard curve. The device used for the fluorescence readings was a different one than for other experiments (Thermo Scientific, Varioskan Flash). The results of the calibration curve are depicted on Figure 40. As shown there, the curve goes only up to 25000 cells because the obtained values for 50000 cells diverged too much from each other. Also, one measured value of 25000 cells was also discarded for the same reason. The reasons for these discrepancies will be explained afterwards.

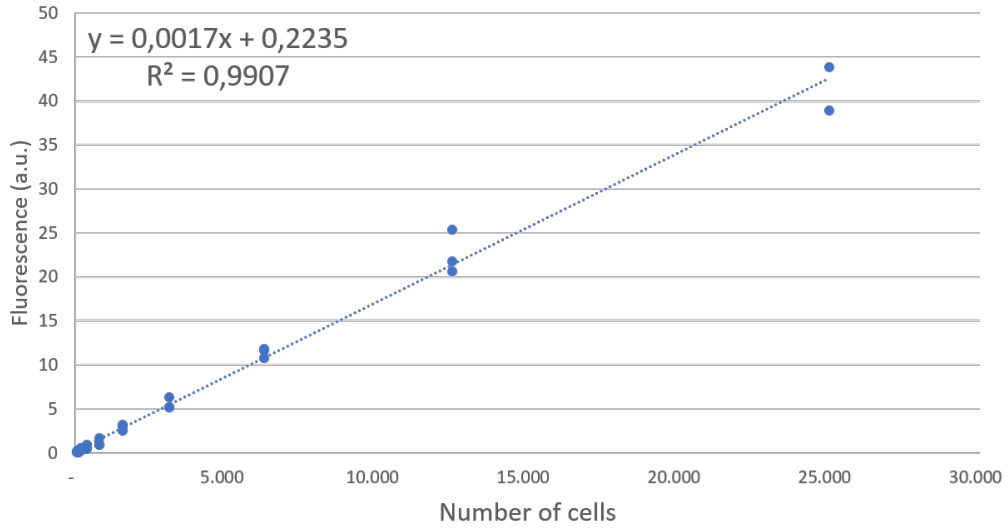

Figure 40: Standard curve for the CyQUANT assay representing the number of cells in function of the measured fluorescence

Once the standard curve retrieved with its equation, it is possible to know how many cells are present in each well after measuring their fluorescence. Table 7 displays the obtained fluorescence with the computed amount of cells with the standard curve. Knowing the equation of the standard curve, finding the number of cells for a given fluorescence measurement is straightforward using the equation:

$$\#\text{Cells} = \frac{\text{Fluorescence} - 0.2235}{0.0017}$$

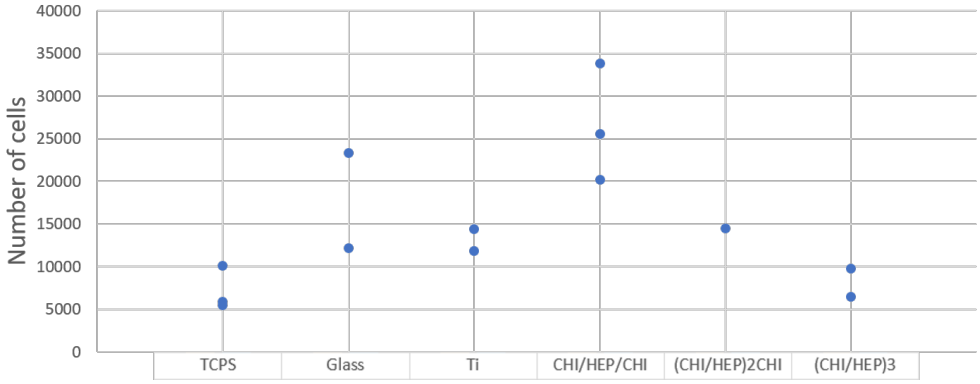

Figure 41: Number of cells per sample computed using the standard curve and the CyQUANT assay

Looking at the obtained data on Figure 41, several informations can be retrieved. First, it can be seen that the amount of cells present in the wells after one week is particularly low knowing that the wells were seeded initially with 20000 cells each. The second element of concern is that the reproducibility of this experiment seems quite low as the measured values for different samples of the same conditions are very different. Three measurements were performed for each sample, if less than 3 dots are shown on Figure 41 it means that the measured fluorescence was out of range using the standard curve (complete data can be found in Table 7 in Appendix C). Finally, no trend is seen between the different conditions when analysing the data.

Seeing these inconsistent results, it can be assumed that an error appeared somewhere. This error can have several origins. The first possible error could be when collecting the cells from the samples. Because this was a tricky step and it was not possible to control if all the cells were collected, the error margin can be big. Then, the second cause of error could be due to the used fluorescence reader which was an older device compared to the one used for other tests. Nevertheless, the standard curve does not seem too bad and this hypothesis is discarded. Finally, the amount of cells that were initially seeded on the surfaces was maybe too high. A high number of cells were used to seed the surfaces to be sure that enough cell would adhere to the samples. A too high initial amount of cells can lead to a high cell mortality in the early stage of the tests because cells could not be able to adhere well on the surface. This is a parameter that should be tuned by repeating this experiments several times.
To gain further insight on this, the epifluorescence microscope was used.

3.5.3 Cell epifluorescence

Cell visualisation was made possible using immunofluorescent staining. As mentioned in Subsection 3.4.3, the different samples are visualised using a fluorescence microscope. The obtained images are seen on Figure 42 and 43 below and are taken 7 days after seeding the samples with cells.

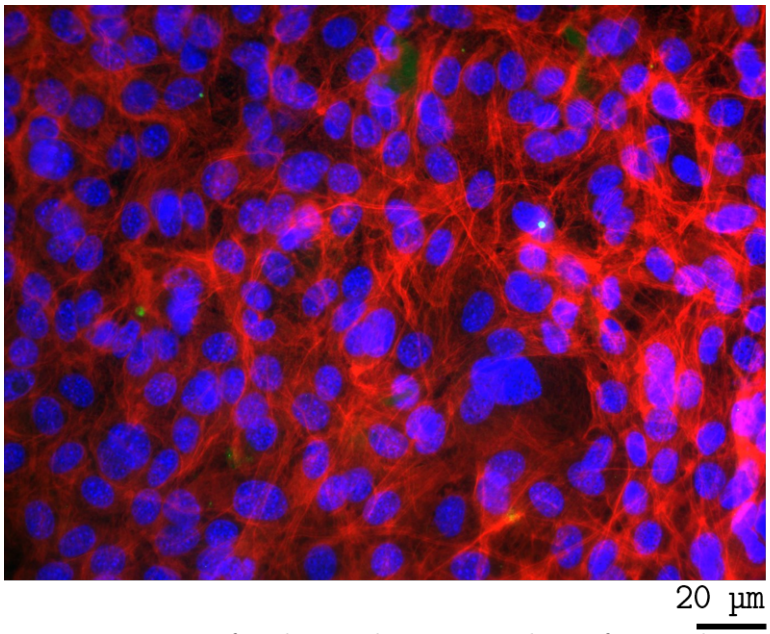

Figure 42: Fluorescence microscopy for the condition Ti, 7 days after seeding the samples with cells

On Figure 42, the microscopy image obtained from the condition Ti is shown. It can be seen that the cell density is really high as the whole substrate is fully recovered by cells. As mentioned in section 3.4.3, the red parts seen on this Figure (and on Figure 43) represent the actin filaments and the sections coloured in blue are cell nuclei. Remember that we used a green dye to reveal the focal adhesions. This green dye is known to be very weakly represented on imaged cells, this is the reason why they are not seen here. Note that all the different samples showed similar images. Another element that was seen on every sample is that the cell bed was peeled of in some places. This can be seen on Figure 43.A. On Figure 43.B, one cell remains after the cell bed was peeled off. The actin remnants can also be seen. On the other images of Figure 43, the other samples are shown. Again, it can be seen that the cell density is very high. This peeling off of the cellular bed could be the cause for the failed CyQUANT assay. If the cells detach from the samples, they could be discarded when the culture medium was changed during the 7 days before cell analysis, resulting in a huge decrease in cells on the different samples.

In the future, if these experiments were to be repeated, the samples should be seeded with less cells. Doing so, the results should be better and better conclusions could be made.

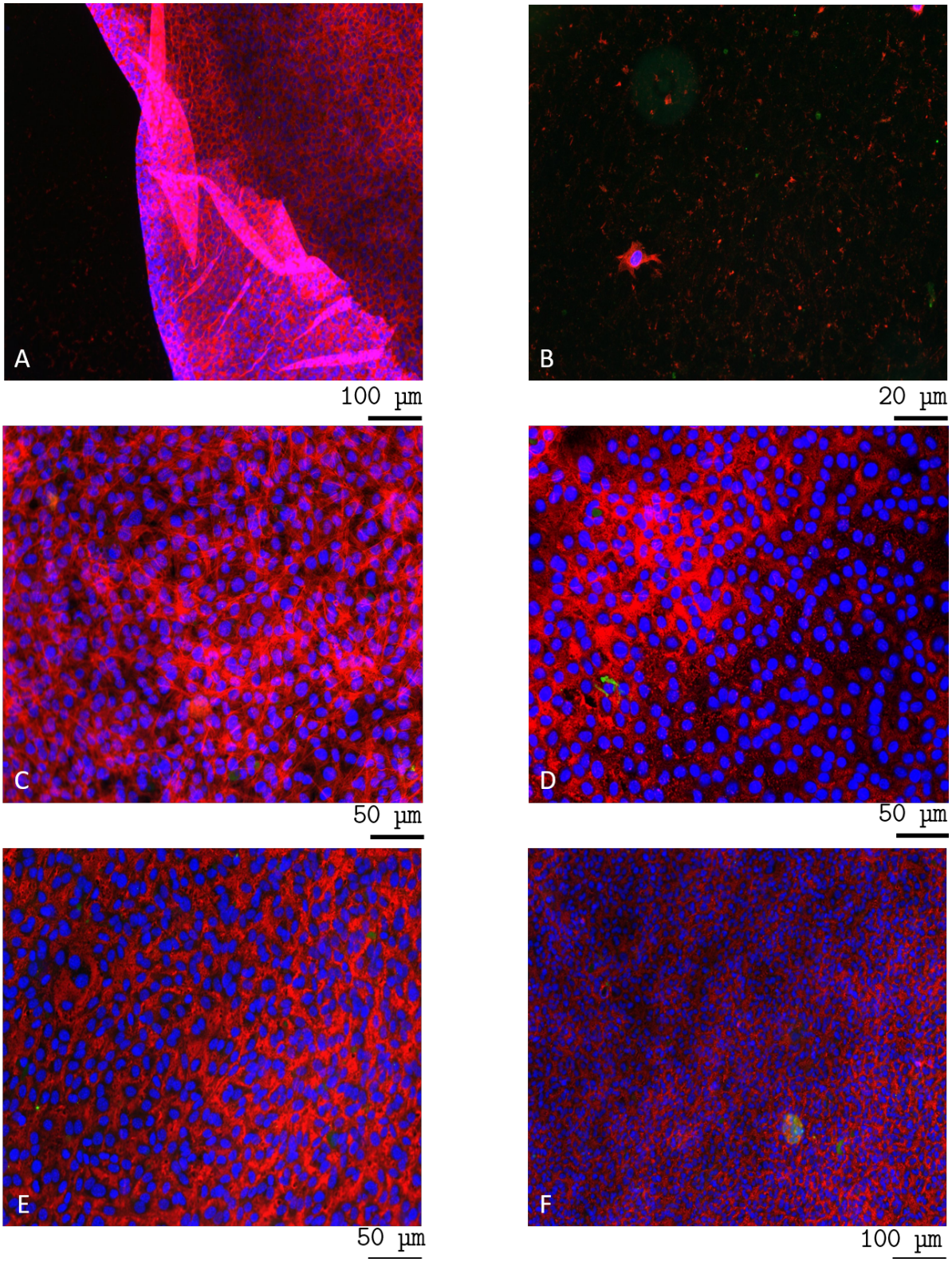

Figure 43: Images obtained 7 days after seeding the samples with cells using the epifluorescence microscope; (A) and (B) Titanium, (C) Glass, (D) CHI/HEP/CHI, (E) $(CHI/HEP)_2CHI$ and (F) $(CHI/HEP)_3$

3.6 General discussion

This last Section has allowed us to collect information on the impact of heparin and chitosan multilayers on cell viability and proliferation.

First, a cell type was chosen. MC3T3-E1 cell were selected because of their high resemblance to human osteoblasts for the investigated properties.

Then, cell viability was investigated. To do so, the AlamarBlue assay was performed. The main conclusion made after this assay is that the titanium coupons and their coatings are less good for cell viability after 1 day and 4 days compared to the glass positive control. After 7 days however, this tendency is reversed as all the samples were statistically equal to the positive control. It was also found that TCPS can not be used as positive control for MC3T3-E1 cells. The obtained results are encouraging and show that the developed coatings present no cytotoxicity, and can therefore serve as a basis for developing more complex coatings.

Then, cell proliferation was investigated on the different surfaces using the CyQUANT assay. Measurements were performed after 7 days but unfortunately the experimental error was very large, possibly related to the step where cells had to be retrieved from the different surfaces before analysis. The obtained results could not be analysed.

Finally, fluorescence microscopy was used to visualise the cells on the different samples. To do so, actin filaments were dyed red, the cell nuclei blue and focal adhesion in green. With this method, it could be seen that the initial cell seeding on the surface was too high. We saw that the cell bed detached from the surfaces and that this could be a possible cause to the failed CyQUANT assay. If these experiments are repeated in the future, the initial quantity of cells seeded on the samples should be decreased. The high fluorescence signal measured with CyQUANT and the high number of cells seen in epifluorescence microscopy shows that the coatings allow good cellular anchoring, which is really positive.

It should not be forgotten that results obtained for cellular behaviour are known to be extremely variable. Therefore, the conducted experiments should be done multiple times to measure the reliability of the obtained results. Unfortunately, due to lack of time, this could not be done in this master thesis but in future experiments this should be done.

4 Conclusion and future perspectives

To conclude this work, aimed at developing a coating for titanium prostheses that will be used to attract osteoblasts and repel bacteria, here are the main elements to remember.

The first part of this work consisted in the deposition of layers of chitosan and heparin onto titanium coupons using the layer-by-layer self assembly method. Both polyelectrolytes were chosen because of their specific properties to repel bacteria and attract cells respectively. Moreover, such multilayered films may serve as a basis to build more complex coatings, notabely by further incorporation of antibacterial peptides. Different layer compositions were prepared to analyse the influence of the composition on the layer properties. The layers were then characterised using various analytical methods. The second part of this work was dedicated to the study of cell behaviour on the previously characterised surfaces. For this, MC3T3-E1 cells were chosen because of their human osteoblast-like behaviour regarding the properties of interest.

In the first part of this work, water contact angle measurements revealed that the layers were successfully deposited, with a saw-tooth trend corresponding to the alternated deposition of chitosan and heparin. The measured contact angle of the final layer composition, $(CHI/HEP)_3$, was in the required interval for proper adsorption of the adhesion proteins secreted by cells, according to the literature. The chemical composition of the surfaces were then investigated by XPS and the chemical signature of chitosan and heparin was well identified on the titanium substrates. However, no conclusion could be reached on how the molecular organisation of the layers at the interface form on the surface. Finally, the layer thickness was measured by QCM and a value close to 13 nm was computed for the condition $(CHI/HEP)_3$ constructed on gold crystals.

The study of cell behaviour on the previously characterised layers provided information about cell viability and cell proliferation. When studying cell viability using the AlamarBlue assay, it was found that the different deposited layers showed a lower viability at day 1 and day 4 compared to glass taken as positive control. At day 7, however, no significant statistical difference was measured anymore between glass and heparin- and chitosan-based films. These results suggest that the developed coatings present no cytotoxicity and can therefore serve as a basis for developing more complex coatings. Cell proliferation was also investigated on the different samples. Unfortunately the data could not be used quantitatively but the high measured fluorescence signal measured shows that the coatings allow good cellular anchoring. This was also confirmed by direct observation of the cells using fluorescence microscopy.

In the future, $(CHI/HEP)_3$ multilayers could serve as a basis for more complex coatings. Research is already conducted in this regard. Cédric Vranckx is currently investigating the development of an anti-bacterial coating for orthopaedic prostheses where the multilayers $(CHI/HEP)_3$ are used as a "cushion" to further attach antimicrobial peptides on it. This work aims at developing a coating for hip prostheses but the coating could also be used for other type of metallic prostheses.

5 Appendix

Appendix A - Figures

Introduction

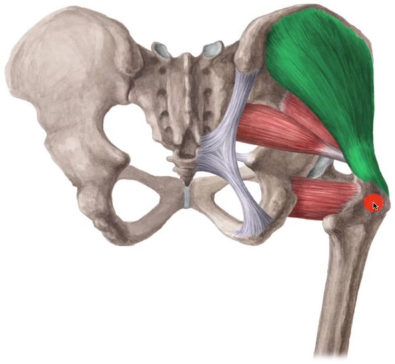

Figure 44: Anatomical localisation of the *gluteus medius* (green)(KenHub, n.d.)

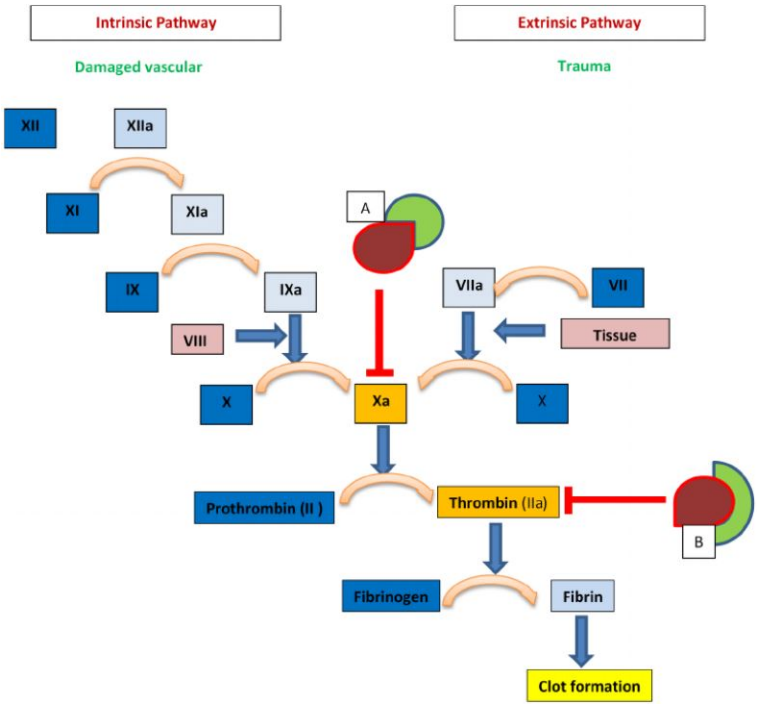

Figure 45: Heparin's (green) mechanisms within the coagulation cascade to prevent coagulation. Two pathways exist: (A) AT bound with heparin fragment of any length (B) AT bound to heparin with chain length $>$ 17 disaccharide units (Oduah et al., 2016)

Appendix B

Layer formation

Time (min)	Step
t < 0	Preparation step: - Make solutions of chitosan and heparin - Prepare a 24 well-plate - Prepare Milli-Q water at wanted pH - Wash the titanium coupons (day before) - Put 1 coupon per well
t = 0	In each well: - 1 mL of chitosan solution
t = 25-30	Washing step: - Remove 0,8 mL of each well - Add 0,8 mL of Milli-Q water - During 1 min, mix gently - Do this 3 times (remove water, add water) - Then, remove 1 mL of remaining medium
t = 30	In each well: - 1 mL of heparin solution
t = 55-60	Washing step
t = 60	In each well: - 1 mL of chitosan solution
t = 85-90	Washing step
t = 90	In each well: - 1 mL of heparin solution
t = 115-120	Washing step
t = 120	In each well: - 1 mL of chitosan solution
t = 145-150	Washing step
t = 150	In each well: - 1 mL of heparin solution
t = 175-190	Washing step: - Repeat the washing step 7 times
t = 190	Put the coupons with their layers to dry

Figure 46: Followed protocol to construct 3 bi-layers: $(CHI/HEP)_3$

Appendix C

CyQUANT data

Table 7: Data of the fluorescent measurements of the CyQUANT assay and the computed quantity of cells per sample using the standard curve

Condition	TCPS			Glass			Ti		
Sample	1	2	3	1	2	3	1	2	3
Fluorescence (a.u.)	9.53	10.24	17.45	20.98	127.46	39.87	20.33	169.34	24.72
Number of cells	5473	5889	10133	12208	/	23326	11825	/	14407

Condition	CHI/HEP/CHI			$(CHI/HEP)_2CHI$			$(CHI/HEP)_3$		
Sample	1	2	3	1	2	3	1	2	3
Fluorescence (a.u.)	43.73	57.80	34.60	24.85	289.83	147.59	16.832	11.254	162.87
Number of cells	25593	33868	20223	14488	/	/	9770	6488	/

Bibliography

Accurion (2019). *Ellipsometry*. URL: https://www.accurion.com/ellipsometry.

Allen, Geoffrey (1996). *Comprehensive polymer science*. Elsevier. Chap. 7.

Apostu, Dragos et al. (2017). "Current methods of preventing aseptic loosening and improving osseointegration of titanium implants in cementless total hip arthroplasty: a review". In: *Journal of International medical research* 46, pp. 2104–2116.

Arbia et al. (2013). "Chitin extraction from crustacean shells using biological methods - A review". In: *Food Technology and Biotechnology* 51, pp. 12–25.

Arciola, Carla, Davide Campoccia, and Lucio Montanaro (2018). "Implant infections: adhesion, biofilm, formation and immune evasion". In: *Microbiology* 16, pp. 397–409.

ASM Handbook (1990). *ASM Handbook, Volume 1: Properties and Selection: Irons, Steels, and High-Performance Alloys*. ASM International. Chap. 2, p. 1063.

ATCC (2016). *MC3T3-E1 Subclone 14 (ATCC CRL-2594)*. URL: https://www.lgcstandards-atcc.org/products/all/CRL-2594.aspx?geo_country=be#characteristics.

Audisio, Sylvain et al. (1998). *Revêtements et traitements de surface*. Formation Continue. Chap. 1.

Baetens, Kristof and Thomas Forment (2018). *Prothèse totale de la hanche*. URL: https://www.azdelta.be/fr/patient/quel-en-est-le-cout-pour-vous/estimations-de-prix/prothese-totale-de-la-hanche.

Ban, Ju Yeon, Sang Wook Kang, and Gyeong-Ju Park (2015). "Heparin increases the osteogenic effect of recombinant human bone morphogenetic protein-2 in the rabbit bone defect model". In: *Animal Cells and Systems* 19.5, pp. 312–320.

Belgica, Orthopride (2018). *The Orthopride Hip-Registry*. URL: https://orthobelgica.be/wp-content/uploads/2018/06/16.30-Scheerlinck-The-Orthopride-Hip-Registry-where-are-we.pdf.

Béthune, Xavier de and Katte Ackaert (2015). *24 ans d'analyses : l'étape suivante d'une collaboration transparente et équilibrée entre soignants et soignés et entre hôpitaux et mutualités*. URL: https://www.mc.be/media/Etude%5C%20MC%5C%20proth%5C%C3%5C%A8se%5C%20de%5C%20hanche-FR_DEF_tcm49-33191.pdf.

Boddohi et al. (2009). "Polysaccharide-Based polyelectrolyte complex nanoparticles from chitosan, heparin, and hyaluronan". In: *Biomacromolecules* 10, pp. 1402–1409.

Brand (n.d.). *Counting Chambers*.

Brånmark, Per-Ingvar (1959). *Vital microscopy of bone marrow in rabbit*.

Bruker Nano Surfaces (2012). "Fundamentals of Contact Mode and Tapping Mode Atome Force Microscopy". In:

Cedars-Sinai (2019). *Aseptic Loosening*. URL: https://www.cedars-sinai.edu/Patients/Programs-and-Services/Imaging-Center/For-Physicians/Musculoskeletal-Radiology/Exhibits-and-Presentations/Knee-Arthroplasty/Aseptic-Loosening.aspx.

Czekanska, E et al. (2013). "A phenotypic comparison of osteoblast cell lines versus human primary osteoblasts for biomaterials testing". In: *Journal of Biomedical Materials Research*, pp. 2636–2643.

Decher, Gero (1997). "Fuzzy Nanoassemblies: Toward Layered Polymeric Multicomposites". In: *Science* 227.

Drugbank (2018). *Heparin Disaccharide I-S*. URL: https://www.drugbank.ca/drugs/DB02322.

FMPS (n.d.). "Contact Angle platform". In: URL: https://fmps.fbk.eu/contact-angle-platform.

Follmann et al. (2016). "Advances fibroblast proliferation inhibition for biocompatible coating by elecrostatic layer-by-layer assemblies of heparin and chitosan derivatives". In: *Journal of colloid and interface science* 474, pp. 9–17.

Fu, Jinhong et al. (2005). "Construction of anti-adhesive and antibacterial multilayer films via layer-by-layer assembly of heparin and chitosan". In: *Biomaterials*, pp. 6684–66692.

Fu et al. (2005). "Construction of anti-adhesive and antibacterial multilayer films via layer-by-layer assembly of heparin and chitosan". In: *Biomaterials* 26, pp. 6684–6692.

Genet, Michel, Christine Dupont, and Paul Rouxhet (2008). *XPS analysis of biosystems and biomaterials*. Springer. Chap. 5, pp. 177–307.

Hamilton, M et al. (2013). "Anatase Phase, Hydrophilicity, and Thickness of Thermally Oxidized TiO_2 Layer on Titanium-V Alloy". In: *Journal of Undergraduate Research* 6, pp. 16–19.

Hanson, Brian (1995). *The Selection and Use of Titanium*, p. 44.

Hassan, P, Gunjan Verma, and R Ganguly (2012). *Soft Materials – Properties and Applications*. Elsevier. Chap. 1, pp. 1–59.

Held, Paul (2015). *Sample Preparation for Fluorescence Microscopy: An Introduction - Concepts and Tips for Better Fixed Sample Imaging Results*. URL: https://www.biotek.com/resources/white-papers/sample-preparation-for-fluorescence-microscopy-an-introduction-concepts-and-tips-for-better-fixed-sample-imaging-results/.

Hölscher, Hendrik (2012). "AFM, Tapping Mode". In: *Encyclopedia of Nanotechnology*. Springer Netherlands, pp. 99–99.

Hudson and Jenkins (2001). "Chitin and chitosan:" in: *Encyclopedia of polymer science and technology*.

Isaacson, Brad and Sujee Jeyapalina (2014). "Osseointegration: a review of the fundamentals for assuring cementless skeletal fixation". In: *Orthopedic Research and Reviews*, pp. 55–65.

John, Jaganathan, and Supriyanto (2016). "Surface modification of titanium and its alloys for the enhancement of osseointegration in orthopaedics". In: *Current Science*, pp. 1003–1015.

Ken, B (2017). *Successful Immunofluorescence: Fixation and Permeabilization*. URL: https://blog.cellsignal.com/successful-immunofluorescence-fixation-and-permeabilization.

KenHub (n.d.). *Gluteus medius and minimus muscles*. URL: https://www.kenhub.com/en/library/anatomy/gluteus-medius-and-minimus-muscles.

Klemm (1979). "Gentamicin-PMMA-beads in treating bone and soft tissue infections". In: *Zentralblatt fur Chirurgie* 104, pp. 934–942.

Klouche, S, E Sariali, and P Mamoudy (2009). "Analyse du coût des reprises des prothèses totales de hanche infectées". In: *Chirurgie Orthopedique* 96, pp. 167–175.

Kremers, Hilal et al. (2016). "Clinical Factors, Disease Parameters, and Molecular Therapies Affecting Osseointegration of Orthopedic Implants". In: *Current molecular biology reports*, pp. 123–132.

Lee, Jin et al. (1998). "Interaction of Different Types of Cells on Polymer Surfaces with Wettability Gradient". In: pp. 323–330.

Lim, Gregory (2017). *Discovery and purification of heparin*. URL: https://www.nature.com/articles/nrcardio.2017.171.

LMHHealt (2019). *Total Hip Arthroplasty*. URL: https://www.lmh.org/get-care/orthokansas/hip/total-hip-arthroplasty/.

Lundin, Maria et al. (2011). "Layer-by-Layer Assemblies of Chitosan and Heparin: Effect of Solution Ionic Strength and pH". In: *Langmuir*, pp. 7537–7548.

Marmur, Abraham (2003). "Wetting on Hydrophobic Rough Surfaces: To Be Heterogeneous or Not To Be?" In: *Langmuir* 19, pp. 8343–8348.

McCutchen, John, John Collier, and Micheal Mayor (1990). "Osseointegration of titanium implants in total hip arthroplasty". In: *Titanium implants in THA*, pp. 114–125.

Medacta International (2018). URL: https://www.medacta.com/EN/hip-replacement.

Merck (2019a). URL: https://www.sigmaaldrich.com.

— (2019b). *Actin Cytoskeleton / Focal Adhesion Staining Kit*. URL: http://www.merckmillipore.com/BE/fr/product/Actin-Cytoskeleton-Focal-Adhesion-Staining-Kit,MM_NF-FAK100?ReferrerURL=https%5C%3A%5C%2F%5C%2Fwww.google.com%5C%2F%5C#overview.

Micheal, B and MD Cross (2017). *Revision Total Hip Replacement*. URL: https://orthoinfo.aaos.org/en/treatment/revision-total-hip-replacement/.

Miller, Melissa and Bonnie Bassler (2001). "Quorum Sensing in Bacteria". In: *Annual Review of Microbiology* 55, pp. 165–199.

NanoScience (n.d.). "Quartz Crystal Microbalance (QCM)". In: *NanoScience Online*. URL: https://www.nanoscience.com/techniques/quartz-crystal-microbalance/.

NanoSurf (n.d.). *How does AFM work?* URL: https://www.nanosurf.com/en/how-afm-works/afm-operating-principle.

NanoWerk (n.d.). *Non-Contact Mode AFM vs. Tapping Mode AFM*. URL: https://www.nanowerk.com/nanocatalog/productimages/1441024751Non-Contact-AFM-vs.-Tapping-Mode-AFM.pdf.

Neoh, K, R Wang, and E Kang (2015). "Surface nanoengineering for combating biomaterials infections". In: *Biomaterials and Medical Device – Associated Infections*, pp. 133–161.

Oduah, Eziafa, Robert Linhardt, and Susan Sharfstein (2016). "Heparin: Past, Present and Future". In: *Pharmaceuticals (Basel)* 9, p. 38.

Oh, Sejin et al. (2015). "Optimal design for studying mucoadhesive polymers interaction with gastric mucin using a quartz crystal microbalance with dissipation (QCM-D): Comparison of two different mucin origins". In: *European Journal of Pharmaceutics and Biopharmaceutics* 96, pp. 477–483.

Orapiriyaku, W et al. (2018). "Antibacterial surface modification of titanium implants in orthopaedics". In: *Journal of Tissue Engineering*, pp. 1–16.

Orapiriyakul, Wich, Peter Young, and Laila Damiati (2018). "Antibacterial surface modification of titanium implants in orthopaedics". In: *Journal of Tissue Engineering* 9, pp. 1–16.

Orthopride (2017). *Annual Report: Belgian hip and knee arthroplasty registry 2015-2016*. Tech. rep. Chap. 3. URL: https://www.ehealth.fgov.be/file/view/7a77de8d3e1a4ae8dbd375898a32%203670?filename=orthopride_annual_report_2016_final.pdf.

Oswald, Steffen (2013). "X-ray Photoelectron Spectroscopy in Analysis of Surfaces". In: *Encyclopedia of Analyticl Chemistry*, p. 45.

Otto, Michael (2009). "Staphylococcus epidermidis - the 'accidental' pathogen". In: *Nature reviews. Microbiology* 7, pp. 555–567.

Parithimarkalaignan, S. and T. Padmanabhan (2013a). "Osseointegration: a review". In: *Indian Prosthodontic Society*, pp. 2–6.

— (2013b). "Osseointegration: An update". In: pp. 2–6.

Pettersson, Fredrik (2019). *What is the difference between QCM-D and traditional QCM?* URL: https://blog.biolinscientific.com/what-is-the-difference-between-qcm-d-and-traditional-qcm.

Physical Electronics (2019). *XPS / ESCA*. URL: https://www.phi.com/surface-analysis-techniques/xps-esca.html.

Piatteli, Adriano (2017). *Bone Response to Dental Implant Materials*. Elsevier. Chap. 4.

Polymerdatabase (2015). *POLYELECTROLYTES*. URL: https://polymerdatabase.com/polymer%5C%20classes/Polyelectrolyte%5C%20type.html.

Pouilleau, J et al. (1996). "Structure and composition of passie titanium oxide layers". In: *Materials Science and Engineering*, pp. 235–243.

Raafat, Dina and Hans-Georg Sahl (2009). "Chitosan and its antimicrobial potential - a critical literature survey". In: *Microbial Biotechnology* 2 (2), pp. 186–201.

Reviakine, Ilya, Diethelm Johannsmann, and Ralf Richter (2011). "Hearing what you cannot see and visualizing what you hear: Interpreting Quartz Crystal Microbalance Data from Solvated Interfaces". In: *Analytical Chemistry* 83, pp. 8838–8848.

Rinaudo, Pavlov, and Desbrières (1999). "Influence of acetic acid concentration on the solubilization of chitosan". In: *Polymer* 40, pp. 7029–7032.

Rodan, Sevgi et al. (1987). "Characterization of a Human Osteosarcoma Cell Line (Saos-2) with Osteoblastic Properties". In: *Cancer Research* 47, pp. 4961–4966.

Rolls, Geoffrey (n.d.). "Process of Fixation and the Nature of Fixatives". In: *Leica BioSystems*. URL: https://www.leicabiosystems.com/pathologyleaders/fixation-and-fixatives-1-the-process-of-fixation-and-the-nature-of-fixatives/.

Shiel, William C. (2018). *Medical Definition of Total hip replacement*. URL: https://www.medicinenet.com/script/main/art.asp?articlekey=18292.

Shriver, Liddy (2012). *Osteosarcoma: An Introduction*. URL: http://sarcomahelp.org/osteosarcoma.html.

Sicard, Delphine (2013). "Caractérisation par microscopie à force atomique des arrangements protéine/sucre impliquant la lectine PA-IL de la bactérie pseudomonas aeruginosa", p. 168.

Sood, Vivek (2014). *Cemented vs. Cementless Alternatives in Joint Replacement*. URL: https://www.arthritis-health.com/surgery/shoulder-surgery/cemented-vs-cementless-alternatives-joint-replacement.

Spilker, Hans, Gundula Jänsch-Kaiser, and N. Perez (n.d.). "A38 Titanium and titanium alloys". In:

Springer et al. (2004). "Systemic safety of high-dose antibiotic-loaded cement spacers after resection of an infected total knee arthroplasty". In: *Clinical orthopaedics and related research* 427, pp. 47–51.

Statbel (2019). *Structure of the Population*. Tech. rep. URL: https://statbel.fgov.be/en/themes/population/structure-population#figures.

Swain, Peter and Reinhard Lipowsky (1998). "Contact Angles on Heterogeneous Surfaces: A New Look at Cassie's and Wenzel's Laws". In: *Langmuir* 14, pp. 6772–6780.

Teng, Songsong et al. (2014). "Smoking and Risk of Prosthesis-Related Complications after Total Hip Arthroplasty: A Meta-Analysis of Cohort Studies". In: *PLoS ONE*.

Theeten, J. (1981). "Ellipsometry in thin film analysis". In: *Annual Review of Materials Research* 11, pp. 97–122.

ThermoScience (2012). "alamarBlue™ Cell Viability Assay Reagent". In:

Tolaimate et al. (2000). "On the influence of deacetylation process on the physiocochelmical characterics of chitosan from squid chitin". In: *Polymer* 41, pp. 2463–2469.

Vasconcellos, Leite, and Oliveira (2010). "Evaluation of bone ingrowth into porous titanium implant: histomorphometric analysis in rabbits". In: *Braz Oral Res*, pp. 399–405.

Veerachamy, Suganthan et al. (2014). "Bacterial adherence and biofilm formation on medical implants: A review". In: *Journal of Engineering in Medicine* 228, pp. 1083–1093.

Venkata et al. (2017). "A comprehensive review on polyelectrolyte complexes". In: *Drug Discovery Today* 22.11, pp. 1697–1706.

Ventola, Lee (2015). "The Antibiotic Resistance Crisis". In: *Pharmacy and Therapeutics*, pp. 277–283.

Wei, Ting et al. (2017). "Smart Antibacterial Surfaces with Switchable Bacteria-Killing and Bacteria-Releasing Capabilities". In: *ACS Applied Materials and Interfaces* 9 (43), pp. 37511–37523.

Werner, Brian and Thomas Brown (2018). "Instability after total hip arthroplasty". In: *World Journal of orthopedics*, pp. 122–130.

Younes, Yslem and Marguerite Rinaudo (2015). "Chitin and Chitosan Preparation from Marine Sources. Structure, Properties and Applications". In: *Marine Drugs* 13, pp. 1133–1174.

Zhang, Guigen (2015). *Nanoscale surface modification for enhanced biosensing*. Springer. Chap. 2.

Zhang, Ling and Richard Gallo (2016). "Antimicrobial peptides". In: *Current Biology* 26 (1), R14–R19.

Zhang et al. (2018). "Surface immobilization of heparin and chitosan on titanium to improve hemocompatibility and antibacterial activities". In: *Colloids and sufraces B: Biointerfaces* 172, pp. 338–345.

UNIVERSITÉ CATHOLIQUE DE LOUVAIN
École polytechnique de Louvain
Rue Archimède, 1 bte L6.11.01, 1348 Louvain-la-Neuve, Belgique | **www.uclouvain.be/epl**